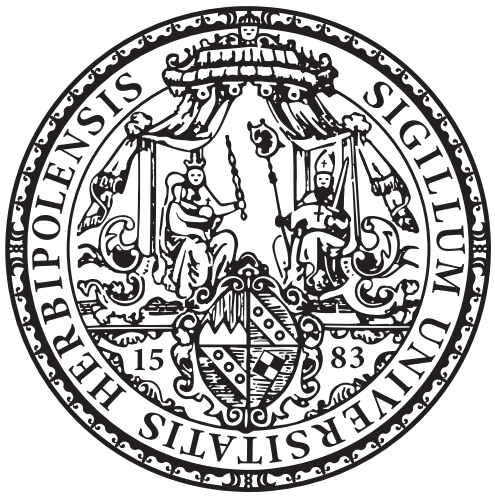

Regulation of MCMV immediate early gene expression by virally encoded miRNAs

Regulation der MCMV immediate early Genexpression durch viral kodierte miRNAs

Doctoral thesis for a medical doctoral degree

at the Graduate School of Life Sciences

Julius-Maximilians-Universität Würzburg

Section: Infection and immunity

submitted by

Stefanie Maria Herb

from Augsburg, Germany

Würzburg 2023

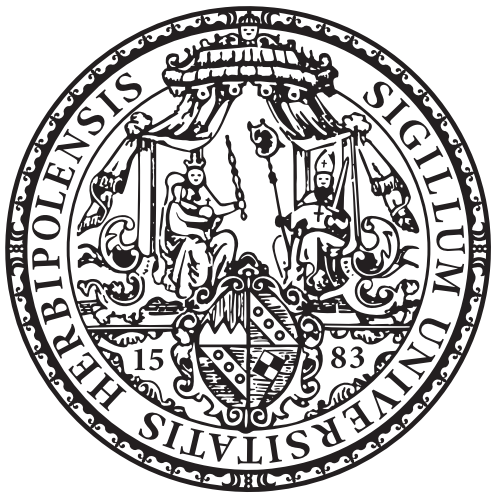

Regulation of MCMV immediate early gene expression by virally encoded miRNAs

Regulation der MCMV immediate early Genexpression durch viral kodierte miRNAs

Doctoral thesis for a medical doctoral degree

at the Graduate School of Life Sciences

Julius-Maximilians-Universität Würzburg

Section: Infection and immunity

submitted by

Stefanie Maria Herb

from Augsburg, Germany

Würzburg 2023

Submitted on:

.....

Office stamp

Members of the Thesis Committee

Chairperson:	Prof. Dr. Klaus Brehm
Primary Supervisor:	Prof. Dr. med. Lars Dölken
Supervisor (Second):	Prof. Dr. Florian Erhard
Supervisor (Third):	Prof. Dr. med. Nurcan Üceyler
Supervisor (Fourth):	PD Dr. med. Niklas Beyersdorf

Date of Public Defence: .....

Date of Receipt of Certificates: .....

Affidavit

I hereby declare that my thesis entitled **"Regulation of MCMV immediate early gene expression by virally encoded miRNAs"** is the result of my own work. I did not receive any help or support from commercial consultants. All sources and/or materials applied are listed and specified in the thesis.

Furthermore, I verify that this thesis has not yet been submitted as part of another examination process neither in identical nor similar form.

Leonberg, January 2023

_____

Stefanie Maria Herb

Eidesstattliche Erklärung

Hiermit erkläre ich an Eides statt, die Dissertation **"Regulation der MCMV immediate early Genexpression durch viral kodierte miRNAs"** eigenständig, d.h. insbesondere selbstständig und ohne Hilfe eines kommerziellen Promotionsberaters, angefertigt und keine anderen als die von mir angegebenen Quellen und Hilfsmittel verwendet zu haben.

Ich erkläre außerdem, dass die Dissertation weder in gleicher noch in ähnlicher Form bereits in einem anderen Prüfungsverfahren vorgelegen hat.

Leonberg, Januar 2023

_____

Stefanie Maria Herb

Contents

List of Figures

List of Tables

List of Abbreviations

°C	degree **C**elsius
△	deletion
AGO	**Ago**naute
amp	**amp**icillin
BF	**b**right **f**ield
bp	**b**ase**p**air(s)
CMV	**c**yto**m**egalo**v**irus
DNA	**d**eoxyribo**n**ucleic **a**cid
dNTP	**d**eoxyribo**n**ucleotide **tri**phosphate
dsRNA	**d**ouble-**s**tranded **RNA**
EBV	**E**pstein-**B**arr **v**irus
E. coli	***E**scherichia **c**oli*
(e)GFP	**e**nhanced **g**reen **f**luorescent **p**rotein
ER	**e**ndoplasmic **r**eticulum
FF luc	**f**ire**f**ly **luc**iferase
FBS	**f**etal **b**ovine **s**erum
FITC	**f**luorescein **iso**thio**c**yanate
g	**g**rams
g	**g**ravity acceleration
h	**h**our(s)
HCMV	**h**uman **c**yto**m**egalo**v**irus
HSV	**h**erpes **s**implex virus
IE	**i**mmediate **e**arly
IP	**i**mmuno**p**recipitation
kbp	**k**ilo **b**ase **p**airs
KSHV	**k**aposi's **s**arcoma-associated **h**erpes**v**irus

L	**l**iter
LB	**L**uria-**B**ertani (medium)
M	**m**olar
MCMV	**m**urine **c**yto**m**egalo**v**irus
μg, μL	**microg**rams, **microl**iter
mg, mL	**mi**lli**g**rams, **mi**lli**l**iter
min	**min**ute(s)
miRNA	**mi**cro **RNA**
mm	**mi**lli**m**eter
mM	**mi**lli**m**olar
MOI	**m**ultiplicity **o**f **i**nfection
mRNA	**m**essenger **RNA**
mut	**mut**ant
NCS	**n**ewborn **c**alf **s**erum
NEAAs	**n**on-**e**ssential **a**mino **a**cid**s**
nf	**n**uclease-**f**ree
ng	**n**ano **g**rams
Norm	**n**ormalisation
nt	**n**ucleo**t**ide(s)
o/n	**o**ver**n**ight
OD_x	**o**ptical **d**ensity at the wavelength of x nm
ORF	**o**pen **r**eading **f**rame
PAR-iCLIP	**p**hoto**a**ctivated **r**ibonucleoside-enhanced **i**ndividual nucleotide resolution **c**ross**l**inking and **i**mmuno**p**recipitation
PBS	**p**hosphate **b**uffered **s**aline
PCR	**p**olymerase **c**hain **r**eaction
PEI	**p**oly**e**thylen**i**mine
pfu	**p**laque **f**orming **u**nits
POL	**p**oly**m**erase
pre-miRNA	**pre**cursor **miRNA**
pri-miRNA	**pri**mary **miRNA**
RISC	**R**NA **i**nduced **s**ilencing **c**omplex
RNA	**r**ibo**n**ucleic **a**cid
RNAi	**RNA i**nterference

rpm	**r**evolutions **p**er **m**inute
r/t	**r**oom **t**emperature
sec	**sec**ond(s)
siRNA	**s**mall **i**nterfering **RNA**
snRNA	**s**mall **n**uclear **RNA**
TXR	**t**e**x**as **r**ed
U	**u**nit(s)
UTR	**un**translated **r**egion
UV	**u**ltra**v**iolet
wt	**w**ild-**t**ype

Summary

Gene expression in eukaryotic cells is regulated by the combinatorial action of numerous gene-regulatory factors, among which microRNAs (miRNAs) play a fundamental role at the post-transcriptional level. miRNAs are single-stranded, small non-coding RNA molecules that emerge in a cascade-like fashion via the generation of primary and precursor miRNAs. Mature miRNAs become functional when incorporated into the RNA induced silencing complex (RISC). miRNAs guide RISCs to target mRNAs in a sequence-specific fashion. To this end, base-pairs are usually formed between the miRNA seed region, spanning nucleotide positions 2 to 8 (from the 5' end) and the 3'UTR of the target mRNA. Once miRNA-mRNA interaction is established, RISC represses translation and occasionally induces direct or indirect target mRNA degradation.

Interestingly, miRNAs are expressed not only in every multicellular organism but are also encoded by several viruses, predominately by herpesviruses. By controlling both, cellular as well as viral mRNA transcripts, virus-encoded miRNAs confer many beneficial effects on viral growth and persistence. Murine cytomegalovirus (MCMV) is a β-herpesvirus and so far, 29 mature MCMV-encoded miRNAs have been identified during lytic infection.

Computational analysis of previously conducted photoactivated ribonucleotide-enhanced individual nucleotide resolution crosslinking immunoprecipitation (PAR-iCLIP) experiments identified a read cluster within the 3' untranslated region (3'UTR) of the immediate early 3 (IE3) transcript in MCMV. Based on miRNA target predictions, two highly abundant MCMV miRNAs, namely miR-m01-2-3p and miR-M23-2-3p were found to potentially bind to two closely positioned target sites within the IE3 PAR-iCLIP peak.

To confirm this hypothesis, we performed luciferase assays and showed that activity values of a luciferase fused with the 3'UTR of IE3 were downregulated in the presence of miR-m01-2 and miR-M23-2. In a second step, we investigated the effect of pre-expression of miR-m01-2 and miR-M23-2 on the induction of virus replication. After optimizing the transfection procedure by comparing different reagents and conditions, plaque formation

was monitored. We could demonstrate that the replication cycle of the wild-type but not of our MCMV mutant that harbored point mutations in both miRNA binding sites within the IE3-3'UTR, was significantly delayed in the presence of miR-m01-2 and miR-M23-2. This confirmed that miR-m01-2 and miR-M23-2 functionally target the major transcription factor IE3 which acts as an indispensable regulator of viral gene expression during MCMV lytic infection.

Repression of the major immediate early genes by viral miRNAs is a conserved feature of cytomegaloviruses. The functional role of this type of regulation can now be studied in the MCMV mouse model.

Zusammenfassung

In eukaryotischen Zellen wird die Expression von Genen durch das Zusammenspiel vieler verschiedener biologischer Regulatoren, wie microRNAs (miRNAs), kontrolliert. MiRNAs sind einzelsträngige, kurze, nicht-kodierende RNA-Moleküle, die aus sogenannten primären miRNAs und Vorläufer-miRNAs entstehen und die Genexpression auf Ebene der Posttranskription beeinflussen. Um ihre Funktion ausüben zu können, werden reife miRNAs in RNA-induzierte Silencing-Komplexe (RISCs) eingebaut und zu ihren Ziel-mRNAs geführt. Durch Wechselwirkungen zwischen der miRNA "seed-Region“, die die Nukleotide 2 bis 8 vom 5'-Ende überspannt und der 3'UTR (3' untranslatierte Region) der Ziel-mRNA, unterdrückt RISC die Translation der Ziel-mRNA und kann deren Abbau durch direkte sowie indirekte Mechanismen induzieren.

Die Expression von miRNAs wurde nicht nur in multizellulären Organismen, sondern in bereits zahlreichen Viren, insbesondere in der Virusfamilie der Herpesviridae, nachgewiesen. Viruskodierte miRNAs kontrollieren dabei zelluläre wie auch virale mRNA-Transkripte und verleihen dem Virus einen Selektionsvorteil bzgl. Wachstum und Persistenz. Das murine Cytomegalievirus (MCMV) ist ein β-Herpesvirus, das nach aktuellem Wissensstand 29 reife miRNAs kodiert, die allesamt während der lytischen Infektion identifiziert wurden.

Bioinformatische Analysen eines vor dieser Arbeit durchgeführten PAR-iCLIP-Experiments (photoactivated ribonucleotide-enhanced individual nucleotide resolution crosslinking and immunoprecipitation), zeigten einen PAR-iCLIP Peak in der 3'UTR (3' untranslatierte Region) des immediate early 3-Transkripts (IE3) von MCMV. Unter Verwendung von RNAhbybrid, einem miRNA target prediction tool, fanden sich zwei virale miRNAs, nämlich miR-m01-2-3p und miR-M23-2-3p mit potentiellen Bindestellen innerhalb der 3'UTR des MCMV IE3 Transkripts. Unsere konsekutiv durchgeführten Luciferase-Assays bestätigten, dass sowohl miR-m01-2 als auch miR-M23-2 an die 3'UTR von IE3 binden. Beide viralen miRNAs führten zu einer verminderten Luciferaseaktivität unter Verwendung von Reportern, in denen die 3'UTR des IE3-Gens mit dem Luciferase-Transkript fusioniert war.

Das IE3 Protein gilt während des lytischen Zykluses als einer der wichtigsten Transkriptionsfaktoren von MCMV.

Ebenfalls wurde der Einfluss der beiden viralen miRNAs auf die virale Reproduktion von uns untersucht. Hierfür wurden murine Zelllinien vor Infektion mit miR-m01-2 und miR-M23-2 transfiziert. Das Transfektionsverfahren optimierten wir zunächst durch Testung verschiedener Reagenzien und experimenteller Bedingungen. Schließlich zeigten wir mittels Plaqueassays, dass eine vor Infektion durchgeführte Transfektion mit miR-m01-2 und miR-M23-2 die Replikation von MCMV signifikant verzögerte. Unter Verwendung einer MCMV-Mutante, die durch Punktmutationen in beiden miRNA-Bindungsstellen innerhalb der IE3-3'UTR charakterisiert war, ließ sich dieser Effekt aufheben. Unsere Experimente weisen somit stark darauf hin, dass miR-m01-2 und miR-M23-2 die Expression des IE3 Proteins regulieren und damit indirekt Einfluss auf die Genexpression während der lytischen Phase des Replikationszykluses von MCMV nehmen.

Die miRNA-mediierte Repression der immediate early Genexpression stellt ein evolutionär konserviertes Merkmal von Zytomegalieviren dar. Für eine weitere Einordnung der Rolle dieser Genexpressionskontrolle bedarf es zukünftige Untersuchungen im MCMV-Tiermodell.

Chapter 1

Introduction

1.1 Cytomegalovirus

Cytomegaloviruses (CMVs) are a member of the beta-*herpesvirinae* which is one of the three subfamilies in the family of *Herpesviridae* [1]. CMVs are around 200 nm in diameter and contain the largest linear double-stranded DNA genome amongst all herpesviruses. Indeed, CMV particles contain roughly 230 kB of genomic material, from which more than 170 proteins as well as several non-coding RNAs are expressed [2, 3, 4]. The genome is located within a viral nucleocapsid which itself is embedded in an amorphous protein matrix, called tegument (Figure 1.1) that presumably plays a pivotal role during the early phases of infection. The tegument is surrounded by a lipid bilayer, which originates from the host cells. Studded with numerous spikes composed of various viral glycoproteins, the viral envelope is an essential element for attachment to cell surface receptors, virion maturation, and cell-to-cell spreading [4].

The genus CMV embraces 11 species that can be isolated from many mammals, including humans. Unfortunately, *in vivo* studies on the human CMV (HCMV) have been a major challenge, as CMV species are genetically highly adapted to their respective hosts featuring strict species specificity [8]. Lacking an adequate animal model for HCMV *in vivo* studies, murine CMV (MCMV) infection has been a widely used model setting for studying HCMV, in particular, as MCMV and HCMV share many characteristics [9].

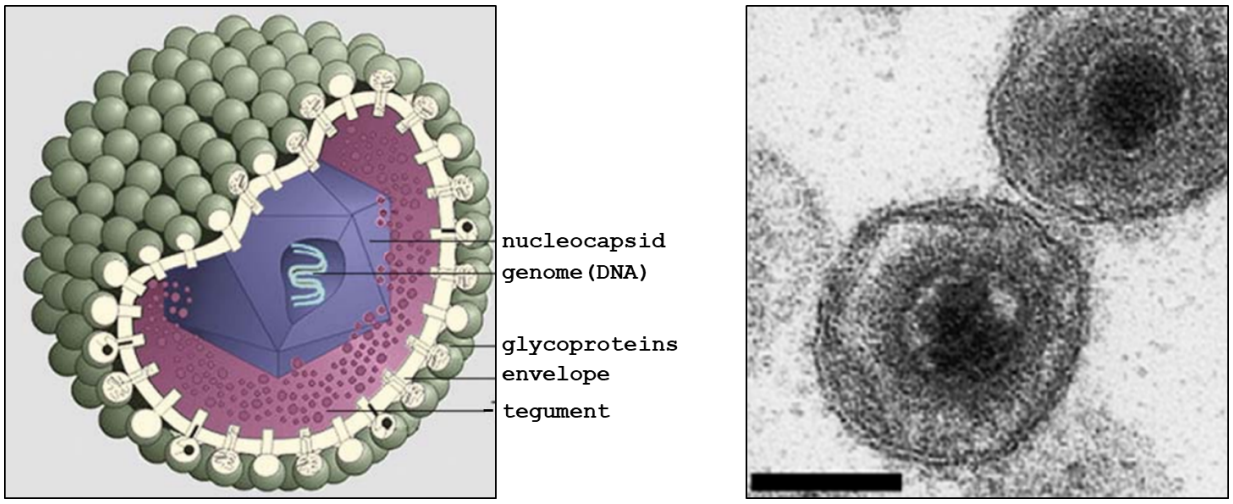

Figure 1.1: Morphology of CMV. A schematic representation (left) and an electron micrograph (right) show structural characteristics of a CMV particle. The icosahedral, DNA-enclosing nucleocapsid is embedded within a proteinaceous matrix, known as tegument, and an envelope which is enriched with numerous different viral glycoproteins forming spikes on the viral membrane. Bar = 100 nm (right). The figure to the left was obtained with courtesy of Dr. Marko Reschke in Berlin (Germany) [5] and modified by [6]. The figure to the right was taken from [7] with granted permission.

1.1.1 Prevalence, clinic, and treatment options of HCMV infection

HCMV is one of the most potent pathogens considering its ubiquitous spread. Its seroprevalence is estimated to range from 40 to 100% depending on the geographically socioeconomic status [10, 11, 12]. Fortunately, HCMV infections are generally benign causing no or only mild symptoms in healthy individuals [2, 13, 14]. Nevertheless, virion particles are produced in the infected but mostly unsuspecting host and shed in body fluids like urine, saliva, milk, tears, and semen for months to years [4].

Following the resolution of acute primary infection, HCMV persists in the host for the entire lifetime by maintaining silenced viral genomes at privileged sites in a state termed latency. Latency is generally defined by the absence of detectable viral particle production due to a drastic downregulation of viral replication. Consequently, entering the state of latency almost abolishes the risk of virus transmission but poses a threat of viral reactivation [15]. Similar to primary infection, reactivation is usually asymptomatic. While CD34+ stem cells appear to constitute a viral reservoir for latency maintenance [16], definable characteristics of the cellular sub-population need yet to be specified [4].

In contrast to the absence of symptoms in healthy patients, clinically apparent and dev-

astating HCMV infections occur in congenitally infected newborns and immunocompromised patients, particularly in those who suffer from human immunodeficiency virus (HIV)-infection or who receive immunosuppressive treatment, e.g. after organ transplantation [1, 17]. Spreading of HCMV within immunocompromised individuals is greatly facilitated by the virus' ability to successfully infect many different cell types, including epithelial cells, smooth muscle cells, fibroblasts, macrophages, dendritic cells, hepatocytes, endothelial cells, amongst others [11, 18, 19, 20]. HCMV infection may result in severe inflammation of the respective tissues (e.g. hepatitis, pneumonitis, retinitis, amongst others) [18] rendering immunocompromised patients at risk of developing life-threatening diseases [2]. Furthermore, the placental transmission of HCMV is a significant cause of congenital infections and subsequent disabilities worldwide [12, 21]. HCMV can lead to a broad spectrum of birth defects, including severe neurological disorders, e.g. sensorineural hearing loss, mental retardation, and microcephaly [2, 12, 22, 23].

Current treatment options for CMV infection in immunocompromised patients or newborns are restricted to antiviral drugs that slow productive replication, but do not eliminate the virus. To date, the drug of choice for active HCMV infection is intravenous ganciclovir, while second-line drugs include foscarnet and cidofovir. All of these drug options use the viral polymerase pUL54 as the target and become collectively ineffective once resistance mutations appear in the target gene [24]. Other drugs are used off-label, e.g. leflunomide, or in investigational clinical trials, e.g. maribavir, which targets a new anti-HCMV compound, namely the viral kinase UL97. A recently approved anti-HCMV antiviral is letermovir, which constitutes a terminase complex inhibitor and exhibits activity only against HCMV [24, 25]. Letermovir treatment is restricted to adult CMV-seropositive, allogeneic hematopoietic stem cell transplant recipients for CMV prophylaxis. Unfortunately, despite great effort, no vaccine has yet been available to protect immunocompromised individuals from HCMV infections and embryos from in-utero transmission.

1.1.2 Life cycle

Mediated by glycoproteins of the envelope, CMV binds to receptors on the cellular host membrane and crosses the latter either by direct fusion or endocytosis (Figure 1.2). Once the nucleocapsid reaches the cytoplasm, tegument proteins interact with microtubules which facilitate the transport to the nucleus [26]. At the nuclear pores, the linear gen-

ome is released and either becomes degraded by the action of nucleases or circularizes (and becomes chromatinized) which augments its stability and allows for intranuclear persistence [8, 11]. The viral genome can further get reversibly silenced by enzymatic multiprotein-complexes containing histone deacetylases resulting in the downregulation of viral transcription and genome replication. As a consequence, lytic replication is inhibited while latency is established during which only a minimal set of viral genes is transcribed [8].

The decision between lytic and latent CMV infection is dictated by the infected cell type [27]. Infection of fully-differentiated cells is usually accompanied by productive replication cycles which invariably culminate in cell disruption and release of virions. By contrast, protracted replication cycles are observed in less differentiated cells, e.g. CD34+ hematopoietic progenitor cells in the bone marrow or CD14+ monocytes [28, 29, 30]. Those infected cells contain only low levels of viral transcripts and are hence believed to play a key role in viral latency and reactivation [2, 31].

The production of CMV proteins is a highly regulated process that takes place in a sequential fashion and involves the action of a broad range of regulatory proteins. Three phases are defined, immediate early (IE), early (E), and late (L), in which distinct sets of genes are expressed [32]. IE gene transcription occurs in the presence of transactivators (which are proteins originating from the viral tegument [13] or the host cell itself) and is independent of de novo viral protein products [33]. Starting from the major immediate early enhancer-containing promoter (MIEP), polymerase II [34] produces a primary transcript comprising five exons. Differential splicing gives rise to multiple isoforms [35] that are sub-grouped into IE1 and IE2 transcripts, or IE1 and IE3 in the case of MCMV. IE1 contains exons 1 to 4, while IE2 or the MCMV homolog IE3 comprises exons 1-3 and 5 [36, 37, 38]. Translation starts at exon 2 and produces several proteins, among which the 72-kDa IE1 and the 86-kDa IE2 (in HCMV) [39, 40], or the 88-kDa IE3 (in MCMV) [38] are the major proteins during the immediate-early phase.

Given that IE proteins are non-structural, they primarily participate in immune evasion processes and act as transcription factors for E gene expression [40]. E gene products are essential for viral genome replication and L gene expression. L genes encode for structural proteins and allow for the packaging, egress, and shedding of viral particles [2, 39]. L genes initiate the assemblage of premature capsid structures that, once generated in the nucleus (reviewed in [41]), encapsidate the viral genome. The latter emerges from concatemeric

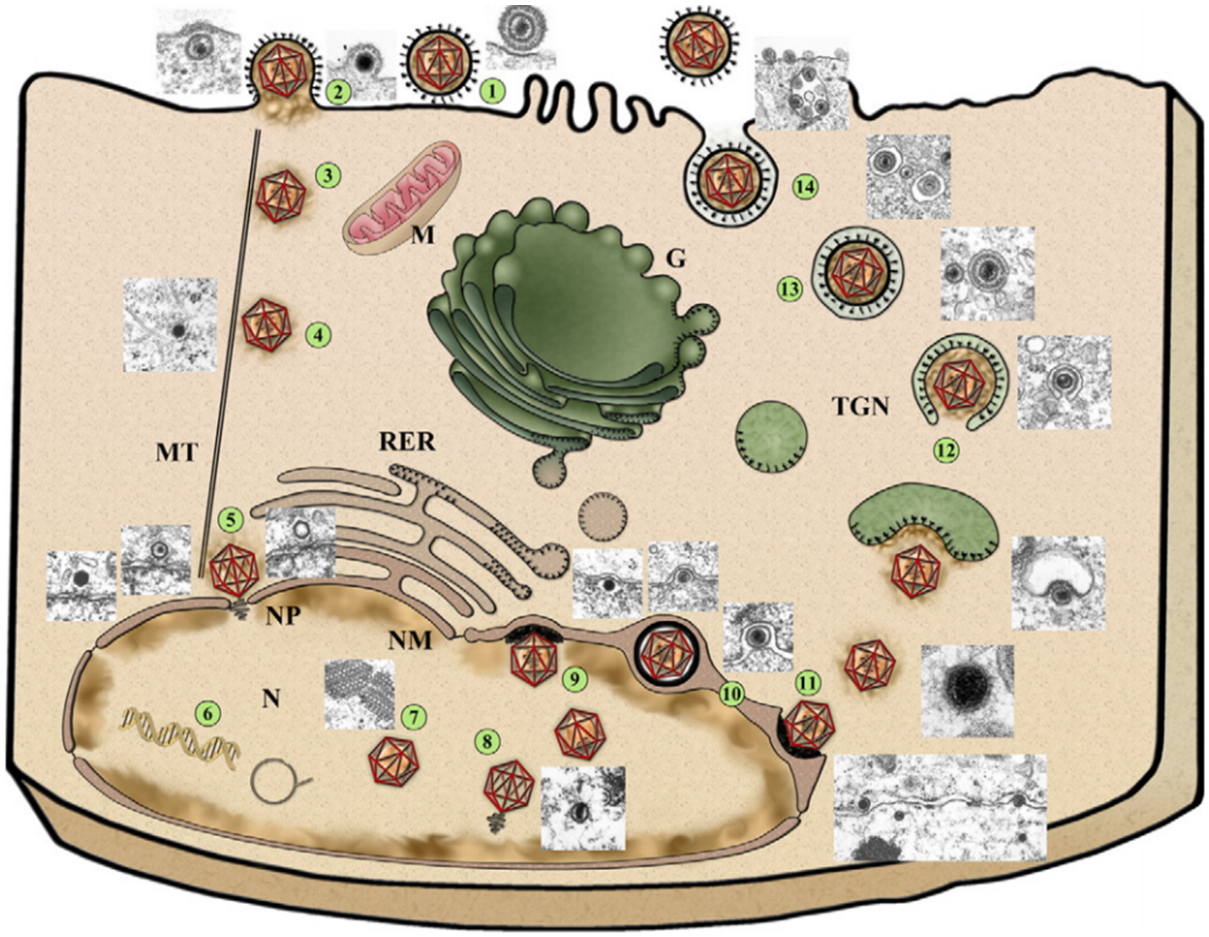

Figure 1.2: Replication cycle of herpesviruses during lytic infection. The cartoon depicts key steps of the lytic replication cycle, which are further visualized by electron micrographs. After docking and attaching to the cell surface (1), virus particles fuse with the cellular membrane (2) to reach the internal of the cell. Once in the cytoplasm, virions bind to microtubules (3) to get transported to the nuclear pores (4) through which the viral DNA genomes pass. In the nucleus, transcription and replication of the viral genomes take place (6). Furthermore, concatemeric DNA is cut into unit-length fragments (8) and become enveloped by preformed, icosahedral nucleocapsids (7) before such DNA-containing capsids leave the nucleus by budding (9) and fusion with the inner and outer nuclear membrane (10,11). Final maturation steps occur in the cytoplasm. Virions fuse with vesicles of the endoplasmic reticulum (containing viral glycoproteins, depicted as black lines), Golgi apparatus, and endosomal machinery to become enveloped (12), transported to the cell surface (13) and released by exocytosis (14). M, mitochondrion, MT; microtubule; NP, nuclear pore; N, nucleus; NM, nuclear membrane; RER, rough endoplasmic reticulum; TGN, trans-Golgi network, G, Golgi apparatus. The figure was taken from [7] with granted permission.

DNA which is cut into unit-length genomic strands. DNA-containing capsids leave the nucleus and travel to the cytoplasmatic viral assembly complex (cVAC) to undergo the final

maturation steps. At the cVAC, which contains parts of the endoplasmic reticulum (ER), Golgi apparatus, and endosomal machinery [42, 43], capsids recruit tegument proteins and becomes enveloped through fusion with vesicles. Finally, infectious virions are transported to the cellular membrane and reach the extracellular plasma, however, the mechanistic details of this process are not fully understood (Figure 1.2).

1.2 MiRNAs

1.2.1 MiRNAs as key regulators of gene expression

Considering that CMV adapts its life cycle to the differentiation state of the infected cell and further expresses its genes in a fixed cascade-like manner, the virus must be capable of regulating transcription in accordance with cellular cues and signals.

In general, gene expression is controlled by the combinatorial action of numerous gene-regulatory factors. These factors build a network of intertwined signal pathways that regulate gene expression not only during transcription but also at the post-transcriptional level. One important class of post-transcriptional gene regulators are microRNAs (miRNAs), which belong to the group of small, noncoding RNAs. MiRNAs are single-stranded, 21 to 23 nucleotides in length, and usually highly conserved. Interestingly, they are encoded by every multicellular organism, ranging from plants and fungi to animals (nematodes, flies, and mammals) [44, 45, 46, 47]. Ever since the first report about miRNAs in metazoans appeared ∼25 years ago [48], miRNAs and their roles in governing cellular levels of transcripts and proteins have become an area of intense study. Today, more than 48,000 mature miRNAs are described in hundreds and thousands of organisms [49].

MiRNAs are regarded as pivotal regulators of many if not all biological processes [46, 50]. Functional studies indicated that cellular miRNAs target mRNAs related to cell proliferation, differentiation, apoptosis, metabolism, and viral host defense, to list a few examples [44, 51, 52, 53]. Therefore, miRNAs are regarded as key elements in maintaining homeostasis [54], while dysregulated miRNA expression is associated with disease, including cancer [55, 56, 57] and neurodegeneration (e.g. Alzheimer's disease [58] or multiple sclerosis [59]).

1.2.2 Gene structure of miRNAs

Early analysis of the genomic localization of miRNAs indicated that most miRNAs form autonomous transcription units in intergenic spacer regions, separated from annotated genes by $>$ 1 kb [47, 60, 61, 62, 63]. By contrast, more recent studies revealed that the majority of mammalian miRNAs are encoded within defined transcription units, primarily within intronic regions of protein-coding as well as non-coding genes [64, 65, 66]. Some other miRNAs are placed in exons of non-coding genes. Roughly half of the miRNAs are found in clusters and encode for polycistronic transcripts [47, 61, 63, 67].

1.2.3 MiRNA maturation

miRNA genes are transcribed as long primary miRNA strands (pri-miRNAs), which are highly variable in size and contain hundreds to thousands of nucleotides [63, 68]. Transcription is predominantly mediated by polymerase II (Pol II) [68, 69], while the involvement of Pol III has been described for only a small number of miRNA genes [70]. Pri-miRNAs become 3' polyadenylated and 5' capped [68, 69]. Unlike any other group of polymerase II transcripts, pri-miRNAs form intrinsic base-pairs and fold into imperfect but characteristic hairpin-stem structures, that are essential for enzymatic processing mediated by two RNase III proteins, i.e. Drosha and Dicer (Figure 1.3).

In the nucleus, Drosha is associated with its cofactor DiGeorge syndrome critical region gene 8 (DGCR8) [71] to form a large, functional protein complex, called Microprocessor. DGCR8 possesses two double-stranded RNA-binding domains (dsRBDs) that recognize and bind to pri-miRNAs at the single-stranded/double-stranded RNA junctions (SD junctions) located at the bases of the stems [72]. Upon this interaction, Drosha positions its two effector domains, which comprise RNase III sites, to conduct the catalytic reaction (see Fang et al. [73] and Nguyen et al. [74] for mechanistic details). Around 11 bp away from the SD junction, both strands of each stem are cleaved and the precursor miRNAs (pre-miRNA) are released. Pre-miRNAs are usually hairpins ~60-80 nt (nucleotides) in length with 5' phosphate and 2 nt overhangs at the 3' ends [60, 75].

Interestingly, some studies indicated that in the case of intronic miRNAs, the binding of Drosha occurs simultaneously (i.e. co-transcriptionally) with the assembly of transcripts into the spliceosomal machinery. When Drosha binds to pri-miRNAs originating from exonic regions, mRNA stability becomes reduced leading to a drop in the rate of mRNA translation (an example of this scenario is given in [76]).

In some rarer instances, an alternative, non-canonical pathway is used to generate pre-miRNAs [77]. Splicing of protein-coding genes releases branched circular introns (lariats). Upon resolving their loop-like shapes, debranched introns can fold into stem-loop structures that might mimic pre-miRNAs [77, 78, 79, 80, 81]. This minor group of miRNA-like RNAs are called "mirtons". They enter the miRNA biogenesis pathway during the transport across the nuclear membrane [78, 79, 80].

Nuclear export of pre-miRNAs, including mirtons, requires Exportin-5 which binds molecules with short 3' overhangs (1-8 nt) [82] and $>$ 14 bp of dsRNA stem. These molecules are shuttled into the cytoplasm in a Ran-GTP dependent fashion [83, 84, 85, 86] .

Subsequently, pre-miRNAs are processed by the cytoplasmatic RNase III enzyme Dicer that binds 3' overhangs of pre-miRNAs, similar to Exportin-5 [87]. Dicer excises the terminal loops from the hairpins to liberate $\sim$22 nt short-lived duplexes [51, 88]. The duplexes are incorporated into Argonaute (AGO) containing multiprotein complexes. Usually, one strand of each duplex is non-functional (known as passenger or miRNA* strand) and becomes actively degraded. The other strand remains within the complex which is called RNA-induced silencing complex (RISC) once a single-stranded miRNA is bound [89, 90]. Mechanistic details of strand selection have been derived from studies of siRNA (small interfering RNA) duplexes indicating that thermodynamic properties of the Watson-Crick base pairing at the 5' end most probably explain the observed strand-bias for selection and degradation [91, 90, 92]. Analysis of the mechanisms of RISC formation in *Drosophila melanogaster* provided evidence that R2D2, a protein containing two dsRBDs, acts as a sensor for thermodynamic differences and binds to the more stable ends of siRNA duplexes and some miRNA duplexes [93, 94]. Following R2D2 interaction, AGO2 (found in *Drosophila* as well as in human and mice [95]) is directed to the duplexes to slice the passenger strand (miRNA* strand) by its endonucleolytic enzymatic cleavage activity accelerating the generation of a single-stranded RNA [96]. Unlike siRNAs duplexes, however, most miRNA duplexes contain central bulges and mismatches that hamper R2D2 interaction and prevent the loading into AGO2 complexes. This restricts the majority of miRNAs duplexes to AGO effectors other than AGO2 (e.g. AGO1, AGO3 or AGO4 in humans) [97, 98]. Unlike AGO2, many of them lack the slicing activity of the passenger strand as well as of the targeted mRNA.

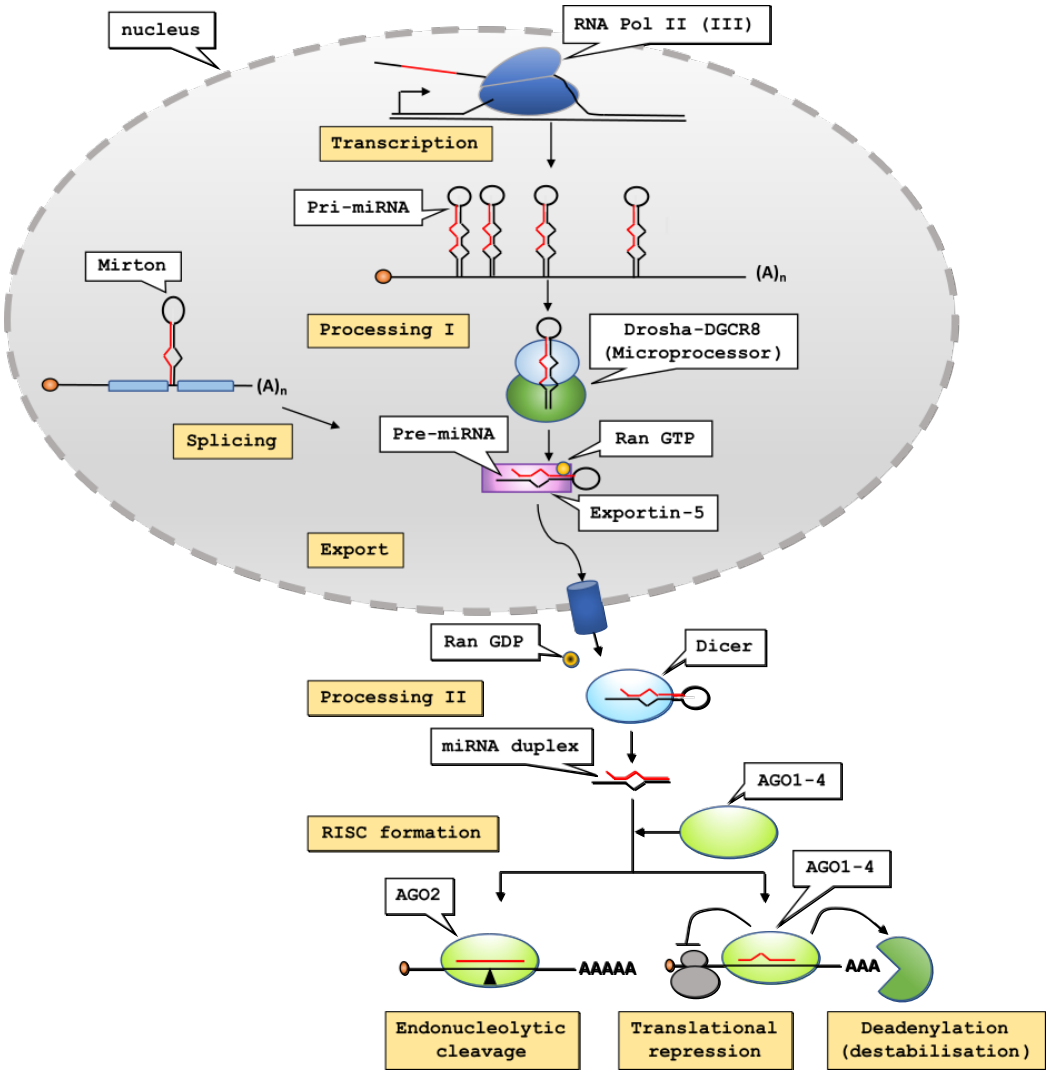

Figure 1.3: Schematic model of miRNA maturation and RISC formation. Pri-miRNAs are primarily transcribed by RNA polymerase II (Pol II) (and only rarely by RNA pol III) and frequently contain a cluster of stem-loop shaped miRNAs. The first processing step is carried out by the nuclear Drosha-DGRC8 Microprocessor complex which crops pri-miRNA into a $\sim$ 70 nt pre-miRNA with 2 nt overhangs at the 3'. The latter feature is recognized by Exportin-5, which shuttles pre-miRNAs in complex with Ran GTP through nuclear pores. The second procession step occurs in the cytoplasm and is mediated by Dicer to produce miRNA duplexes which are loaded onto human AGO1-4 to form RISCs (RNA-induced silencing complexes). Normally, one strand of each duplex is selected (guide strand), while the other one becomes degraded (passenger strand). Of note, mammals encode four Argonaute proteins (AGO1-4) that induce translational repression. Slicing activity, however, is restricted to AGO2, which performs endonucleolytic cleavage in the case of perfect base-pairing between miRNA and target sequence. One out of several non-canonical pathways of miRNA maturation is bypassing Drosha-mediated cropping. Mirtons are pre-miRNAs that are produced upon splicing and debranching. They enter the canonical pathway at the step of Exportin-5-mediated shuttling. The scheme was crafted by modifying figures from [50, 60, 99] with granted permission.

1.3 MiRNA-mRNA interaction

1.3.1 Principles of miRNA targeting

In the scope of functional miRNA analysis, it is important to decipher the mechanisms of how mRNA targets are identified by RISC for subsequent RNA silencing.

In a sequence-specific fashion, miRNAs guide RISCs to target mRNAs. The process of miRNA-mRNA pairing was originally thought to be initiated by a so-called miRNA seed region that spans nucleotide positions 2 to 8 (beginning at the 5' end of the aligned miRNA) [44]. Today, crystal structures of miRNAs in AGO have revealed that only a sub-segment of the miRNA seed, namely nucleotides 2-5, is readily accessible for target pairing, while nucleotides 6-8 are sterically blocked by AGO α-helix 7 [100]. Consequently, miRNA nucleotides 2-5 are considered the lead segment to nucleate and propagate miRNA-mRNA pairing [101]. As interaction extends to miRNA nucleotides 6-8, α-helix 7 undergoes a conformational change to potentially catalyze the seed target complementarity [102].

MiRNA seeds can bind to complementary sequences along the entire mRNA target strands [103, 104, 105]. However, post-transcriptional repression is most efficient when miRNA target sites are positioned within the 3' untranslated region (3'UTR) [106, 107]. Among several theories concerning the primacy of miRNA binding at mRNA 3'UTR, one suggests that interactions of RISCs with the 5' untranslated region (5'UTR) or an open reading frame (ORF) are directly hampered by ribosomes that move from 5' to 3' during active translation [44, 107, 108].

While base-pairing between the miRNA seed and the 3'UTR of mRNAs seems to be a major determinant for interactions, several additional factors have been identified either experimentally or via in silico analysis, that contribute to the architecture of miRNA-mRNA binding and determine target site affinity and efficacy. The canonical miRNA-mRNA association generally requires perfect base pairing of the miRNA seed to the target site. As such, a 6-nt seed match (6mer site) denotes a zone of six contiguous nucleotides with Watson-Crick pairing to the miRNA seed (nucleotides 2-7). A 6mer may be further rimmed by an adenosine opposite of miRNA position 1 (7mer-A1-site) [109] or base pairs to miRNA nucleotide 8 (7mer-m8-site) [109, 110, 111], or both (8mer site) [109]. Downregulation of mRNA translation is most efficient with 8mer sites, followed by 7mer-m8, 7mer-A1, and 6mer [106].

While the central region of the miRNA-mRNA duplex commonly forms bulge structures

due to mismatches [112], supplementary base pairing is frequently found along the miRNA 3' region, in particular at miRNA nucleotides 13-16 [110, 113]. However additional 3'-base complementarity increases site efficacy in less than 5% of canonical sites [107, 114]. Furthermore, effective miRNA-mRNA interactions require accessible seeds and target sites [115]. Weak secondary structures due to a local AU context as well as site positions close to the polyA-tail are favorable in this regard [107, 116].

1.3.2 Modes of miRNA silencing mechanisms

Once mRNAs are captured by RISC-bound miRNAs via base pairing, translation and stability of the transcripts can be affected in multiple ways (Figure 1.3, lower part) (reviewed by Filipowicz et al. [50] and Fabian et al. [117]). First, translation might be blocked at the initiation [118, 119, 120] or elongation step [121, 122]. Second, bound transcripts might be destabilized [51, 123, 124], e.g. by inducing poly-A tail trimming [125, 126, 127] followed by 5' decapping [128, 129]. Third, RNA-cleaving enzymes within RISCs (e.g. AGO2 in humans) might directly slice mRNAs [98, 129, 130, 131].

The balance between suppression of productive translation and destabilization or degradation of mRNAs within RISCs is primarily achieved through the extent of complementarity between miRNA and mRNA. When there is a mismatch in the sequence that results in RNA bulges on miRNA binding, RISCs primarily inhibit translation rather than directly cleaving mRNA [88, 132]. AGO-catalyzed degradation generally requires strong miRNA-mRNA interactions through full-length complementarity, although few exceptions have been described [109]. This mode of translational repression is frequently found in plants [133] as well as in sea anemones [134] and is further used in RNA interference-based therapies [135]. While perfect or near-perfect complementarity is a hallmark of most miRNAs of plants, almost all mammalian miRNAs base pair to mRNAs only with partial complementarity [50, 129, 136]. Consequently, AGO-mediated slicing of the target mRNA is rarely seen in mammals.

The relative distribution of the different mechanisms of repressing mammalian protein synthesis was a long-term matter of debate. While several studies revealed that miRNA binding predominantly induces translational repression without changing mRNA levels (summarized by [50]), some other reports claimed that most mRNAs become destabilized after removing the 3' poly-A tail or the 5' cap upon RISC binding [123, 137]. Today, mRNA decay is commonly believed to play a more crucial role in controlling protein synthesis than

direct translational repression, at least in post-embryonic cells [138].

1.3.3 Bioinformatic approaches for miRNA target site predictions

Within the last decades, many algorithms have been developed to detect putative miRNA targets, among which miRanda [139], PicTar [111], PITA [140], TargetScan [109] and RNAhybrid are most prominent. Although much effort has been made to improve such tools [141, 142], no adequate algorithm has yet been developed that would reliably predict miRNA targets. Bioinformaticians are challenged with the complex nature of miRNA-mRNA interactions. MiRNAs target up to several hundreds of mRNAs and most targeted mRNAs contain multiple binding sites either for the same or different miRNAs [109, 110, 143]. Finally, several types of miRNA-mRNA interaction patterns exist [144], canoncial as well as non-canonical ones, that bioinformaticians must consider. On top of that, miRNAs are rather small, which makes it tricky to identify targets with statistical significance [144].

Currently, a multitude of different prediction algorithms exist. They identify and rank targets based on different rules that potentially govern the miRNA-mRNA network. Most programs incorporate base pairing patterns [109, 110, 111, 144] combined with additional features, including target site accessibility, thermodynamic characteristics [109, 145, 146, 147], and the evolutionary conservation status across related species [114, 144, 146]. These biological elements, which are commonly implemented in computational algorithms, are described in the following.

Base pairing pattern: Predictions algorithms usually start filtering miRNA targets by identifying base pairing patterns [148]. As it is commonly assumed that binding sites are most efficient when located in the 3'UTR (see section 1.3.1), a vast majority of prediction tools limit their search for target sites to datasets containing merely the 3'UTR segments of mRNAs. Only a few prediction tools check the 5'UTR and ORFs for target sites (e.g. RNA22 [149] and miRTar [18]). Most, if not all prediction tools test for complementarity between the miRNA seed regions and the 3'UTR of mRNAs. This step is often implemented as the key feature for predictions. Of note, base pairing is not necessarily restricted to the seed but might also occur in the miRNA 3' region, which is considered e.g. by miRanda.

Thermodynamic aspects: Putative miRNA-mRNA interactions can be assessed by taking into account the thermodynamic binding properties. In general, reactions with a negative change in the free energy ($\triangle$G) result in more stable products. Consequently, calculating $\triangle$G of the duplex formation allows for estimating the strength of the miRNA-mRNA

binding. However, thresholds of free energy for stable vs. non-stable interactions haven't been yet determined, which renders the choice for appropriate cut-off values fairly arbitrary [146]. Knowledge of the minimum free energy can further be exploited for evaluating secondary structures of mRNAs that potentially hamper miRNA binding. In that way, $\triangle$G further helps to assess target site accessibility [140, 150]. Commonly, algorithms that conduct thermodynamic analysis, implement the Vienna RNA package [151] for calculating energy values and estimating secondary structures.

Conservation: Many tools conduct comparative sequence analysis of putative binding sites (i.e. of orthologous 3'UTR sequences) to maximize specificity [152]. In accordance to evolutionary gene selection, the degree of target site conservation across closely related species can be correlated with the reliability of predictions [114].

Unfortunately, in silico predictions generally suffer from high numbers of false positive and false negative results [153]. Furthermore, comparing high-ranked targets between different tools usually yields only poor overlaps. As such, the performance of each prediction algorithm requires critical evaluation, and more than one tool might be used to filter high-confidence predictions that are made by several algorithms [141, 153]. A clearer understanding of the regulatory network that dictates miRNA-mRNA pairing is critical for building more accurate target prediction models.

1.3.4 Experimental methodologies for validating miRNA target predictions

After an algorithm search has been performed for determining miRNA binding sites, the functionality of predicted targets needs to be experimentally validated [154]. Unfortunately, virtually every tool produces long lists of miRNA-mRNA interactions, among which biologists have to identify those that are worthy to experimentally verify. Assays that identify functional miRNA-mRNA interactions are usually labor-intensive, time-consuming, and expensive. In general, they are classified into low- and high-throughput techniques depending on the amount of data output they deliver [155].

Low-throughput techniques: Luciferase Assay and indirect methodologies

Low-throughput techniques are usually applied to conduct gene-specific analyses, among which reporter assays are most convenient for identifying and validating the exact loca-

tions of miRNA binding sites. One of the commonly used reporter methodologies employs plasmids that contain a reporter gene fused with a segment of the target gene in which the predicted target site is embedded. Most frequently, it is the entire 3'UTR that is cloned behind a reporter gene [154, 156]. The latter generally encodes for a luciferase that produces luminescence signals when adding luciferin reagents after inducing cell lysis. Often, a so-called dual-luciferase system is used, which implies that a second luciferase gene is encoded on either a different plasmid or the same reporter plasmid but driven by a separate promotor. The additional luciferase gene lacks any downstream miRNA binding site and hence features a constitutive luciferase expression that serves as an internal normalization reference to account for variances in translation, transfection efficiency, and cell viability [156, 157]. To investigate miRNA binding sites by luciferase reporter assays, co-transfections with miRNAs and luciferase reporter vectors are usually conducted, ideally in cells with high transfection efficiency [156]. When using cells that already express the miRNA(s) of interest, e.g. after stable transfection, only the luciferase reporter constructs need to be transfected. At 16-24 hours post-transfection, luciferase measurements are generally conducted that allow for indirect measurement of miRNA-mediated repression of translation by measuring the reporter activities after adding the respective enzymatic substrates.

Apart from reporter assays, other methodologies exist, including western blot, ELISA, or qRT-PCR that measure the downstream effects of miRNAs on protein and mRNA levels. However, these approaches do not differentiate between the primary and secondary effects of miRNAs [53].

High-throughput methods: Immunoprecipitation of RISC

Recent progress in next-generation sequencing (NGS) methodologies has greatly affected the experimental approach for characterizing mRNA targets in large numbers [155]. The vast majority of miRNAs were detected by deep (i.e high-throughput) sequencing of small RNAs [49].

mRNA targets can be isolated by immunoprecipitating RISC protein components, such as AGO [158, 159, 160] which is usually followed by analyzing the co-purified RNA strands by high-throughput methods, including microarray assays and NGS [53]. However, one considerable drawback of co-immunoprecipitation experiments is the inability of excluding artificial ribonucleoprotein complexes that are formed due to the breakdown of cellular compartments after cell lysis [161]. Additionally, reliable results from immunoprecipita-

tion approaches require strong bondage between miRNA-mRNA target pairs and AGO within RISC to withstand the purification steps [53]. A more recent methodology, which is referred to as Crosslinking immunoprecipitation (CLIP)-seq, employs ultraviolet light (245 nm) to crosslink RNA with RNA-binding proteins for enhanced RNA recovery after immunoprecipitation. Unfortunately, the efficiency of introducing covalent bonds between RNA and associated proteins by UV irradiation is limited. To address this major problem, a superior technique has been introduced that uses modified, photoactivatable nucleotides, e.g. 4-thiouridine, which are added to the culture medium for incorporation into newly transcribed RNA. This technique, known as photoactivated ribonucleotide-enhanced individual nucleotide resolution crosslinking and immunoprecipitation (PAR-iCLIP) achieves greatly improved immunoprecipitation results due to a substantial increase in the number of UV crosslinking events at 365 nm as compared to CLIP-seq [162]. Additionally, PAR-iCLIP experiments allow to precisely identify sites of interaction by thymidine (T) to cytidine (C) conversions introduced during complementary DNA (cDNA) preparation due to erroneous transcription of incorporated 4-thiouridine at cross-linked sites. After deep sequencing and mapping of the reads, T to C mismatches are not only enriched at cross-linked sites but more specifically, predominate within the corresponding seed segments. Hence T to C transitions offer the possibility to pinpoint the locations of miRNA target sites [162]. PAR-iCLIP is one of the most potent high-throughput techniques among currently available miRNA target identification methodologies [163].

1.4 Viral miRNAs

In 2004, the existence of virally encoded miRNA was first described in EBV-infected B-cells [164]. Since then, several hundreds of viral miRNAs have been discovered, among which a vast majority were assigned to herpesviruses [49, 88, 165]. Human herpesviruses that were shown to express miRNAs include HSV 1 and 2 [166], HCMV [167], EBV [168] and KSHV [169]. Recently, also VZV was confirmed for miRNA expression [170].

Since miRNA expression in CMV was first reported by Pfeffer et al. in 2005 [171], 29 mature MCMV and 22 mature HCMV miRNAs have been identified during lytic infection [49, 172, 173]. MiRNAs of CMVs are located along the entire viral genome [171, 174]. By contrast, α herpesviruses, including HSV 1/2 and VZV, encode miRNAs within genomic clusters [2, 175] and express them in particular during latency [176].

A plethora of studies have been published, demonstrating the role of CMV-encoded miRNAs in regulating viral replication [177, 178, 179, 180, 181, 182, 183] and manipulating cellular immune responses [184, 185, 186]. In general, the expression of miRNAs by viruses is associated with several potential benefits to the viral life cycle. First, a single viral miRNA can bind and manipulate a great number of viral and cellular targets, which enables the virus to modulate various signal pathways. Second, miRNAs are non-immunogenic (i.e. they are invisible to the immune system). Third, they are small and encoded within only short regions of the viral genome [187]. Notably, miRNAs mostly account for subtle decreases in transcript levels (roughly 2 fold [136]), which nonetheless may enable them to exert functional effects [188]. Considering these aspects, viral miRNAs are powerful elements in reshaping the cellular environment, supporting virus proliferation, and increasing infection rates [88]. It is thus not surprising that most herpesviruses have independently evolved to encode miRNAs.

1.4.1 Herpesvirus miRNAs repress immediate early gene expression

Herpesviruses' miRNAs influence both cellular and viral transcripts. Despite a lack of sequence conservation, the function of several herpesviruses' miRNAs appears to be similar (summarized by Skalsky et al. [189]). Their cellular mRNA targets commonly encode proteins involved in cell proliferation, apoptosis, and host defense [190]. Viral mRNA targets are associated with immune evasion and guidance of lytic infection and latency [190, 191, 192]. Accordingly, studies have reported on disparate miRNA expression profiles in lytically and latently infected cells [193]. Several herpesvirus-encoded miRNAs were identified that counter viral replication and viral protein synthesis, possibly to drive the virus from productive infection into latency or to maintain the latter [178, 194]. MiRNAs encoded by KSHV were shown to suppress the lytic switch protein, RTA, hence supporting the viral life cycle during latent infection [195, 196]. Three HCMV miRNAs, miR-US25-1, miR-US25-2, and miR-UL112-1, were detected to effectively block viral growth, e.g. by targeting the 3'UTR of the immediate early gene IE72 amongst others, which culminates in a significant decrease in virus DNA levels and viral titers, thereby supporting latency [2, 178, 183]. Two miRNAs in HSV-1 were reported to reduce ICP0 and ICP4 protein levels in latently infected neurons, leading to an inhibition of immediate early and early gene expression [197]. Collectively, these examples suggest that several herpesviruses encode

for viral miRNAs that support the establishment and maintenance of latency or suppress reactivation, in particular by regulating key immediate early gene expression.

1.4.2 Identification of MCMV miRNAs targeting IE3 transcripts

MCMV encodes for a 88-kDA IE3 protein [38] that is deemed crucial in triggering the lytic replication cycle during primary infection and upon viral reactivation [33]. IE3 is produced with immediate early kinetics from the major immediate-early gene region which is regulated by a strong promotor on the viral chromosome. IE3 protein plays an indispensable role in early and late viral gene expression [33] and is hence a major viral transcription factor if not the master regulator of MCMV gene expression.

Consistent with the notion presented above that repression of immediate early gene expression is a conserved feature of various herpesviruses, IE3 was recently predicted to contain two closely positioned miRNA target sites [198]. Computational analysis of a PAR-iCLIP dataset identified a read cluster within the 3'UTR of the IE3 transcript (Figure 1.4). MiRNA target predictions (using RNAhybrid) indicated two viral miRNAs, i.e. miR-m01-2-3p and miR-M23-2-3p to bind within the IE3 PAR-iCLIP cluster (Figure 1.5). We hence hypothesized that both miR-m01-2-3p (8-mer seed match) and miR-M23-2-3p (6-mer seed match) regulate the IE3 transcript in MCMV.

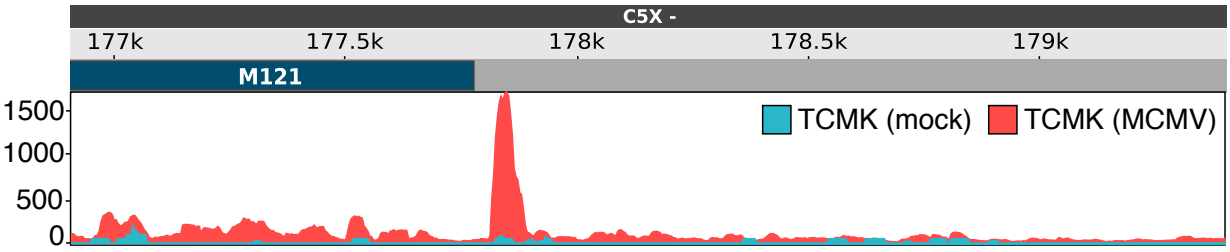

Figure 1.4: Computational analysis of a PAR-iCLIP dataset revealed a putative miRNA binding site within the IE3-3'UTR in MCMV. A murine cell line (i.e. TCMK) was infected with either MCMV or mock (negative control) to perform an AGO2 pull-down 72 h post-infection. A PAR-iCLIP read cluster was found within the IE3-3'UTR.

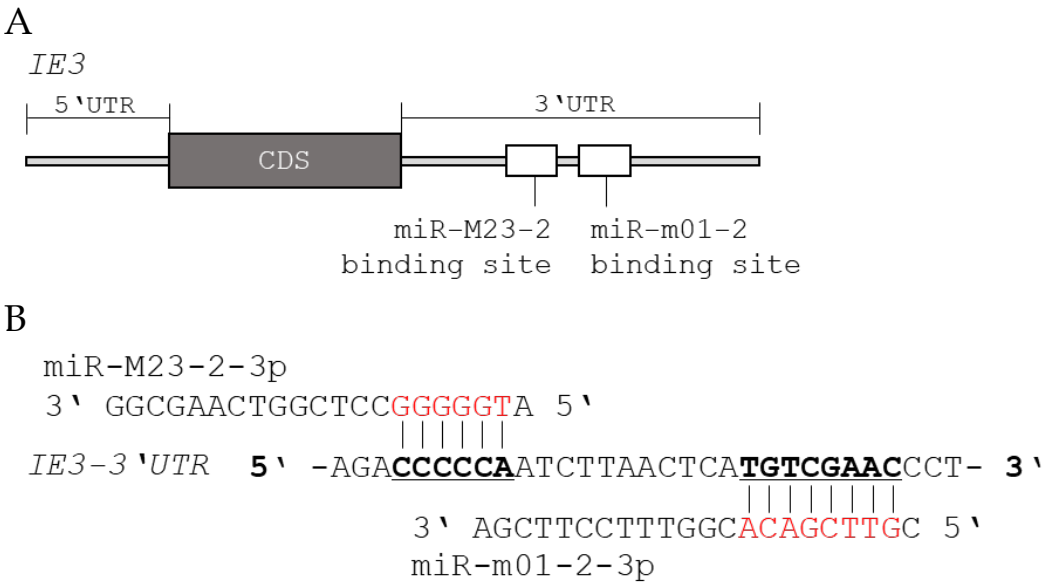

Figure 1.5: The IE3 transcript expressed by MCMV harbors two putative miRNA target sites in its 3'UTR. **A** IE3 is assumed to be directly regulated by two MCMV miRNAs, i.e. miR-m01-2-3p and miR-M23-2-3p. Their putative target sites are both located within the 3'UTR. **B** Sequences of the mature miRNAs and the IE3-3'UTR. 5' seeds of miR-m01-2 as well as of miR-M23-2 base pair to their putative target sites in the 3'UTR. MiRNA seed regions are highlighted in red and target sites are underlined. Note the differences in length of the respective seed regions. While seed and target site interact via 8 nt in the case of miR-m01-2-3p (8-mer seed match), only 6 nt are involved in the case of miR-M23-2-3p (6-mer seed match). CDS = coding sequence.

1.5 MCMV infection: An animal model system for the pathogenesis of HCMV

CMV species virtually exist in all mammalians and are characterized by a strict host-species specificity [199]. Thus, HCMV infection and replication are completely restricted to cells of human origin. *In vivo* studies of HCMV use closely related CMVs in appropriate animal settings. CMVs adopted to non-human primates are phylogenetic more related to HCMV than any CMV species [199, 200]. In this way, investigating Rhesus CMV (RhCMV) infection has been suitable for studying HCMV proteins and can further be used to interrogate the relevance of CMV miRNAs in a closely related *in vivo* system [2, 201]. However, considering ethics, costs, and scalability, infecting mice with MCMV has resulted in a more widespread and well-established model for HCMV infection [202]. Despite genetic and phenotypical differences, the pathogenesis of MCMV and HCMV displays remarkable similarities [2, 203]. Of note, MCMV investigations in mouse models have contributed towards

elaborating the role of CMV-encoded miRNAs in the pathogenesis of lytic infection, viral latency, and reactivation *in vivo* [172, 177]. To this end, we performed our *in vitro* studies on MCMV (instead of HCMV) to allow feature research to use an animal model.

1.6 Goal of this study

The first goal of this study was to validate functional miRNA targeting of IE3, a major immediate early gene product of MCMV. On the basis of an in silico analysis of previously conducted PAR-iCLIP experiments, we performed luciferase assays and confirmed that the IE3-3'UTR is subjected to translational repression by two viral miRNAs, miR-m01-2 and miR-M23-2. Both miRNAs are highly abundant in the viral life cycle during lytic infection [172, 177]. Denoted as a multifunctional protein, IE3 regulates viral gene expression and might further be involved in evading host defenses. Most importantly, IE3 is essentially required for effective viral replication [9, 33].

Considering the indispensable role of IE3 during acute infection, we set our second goal in investigating the effect of the pre-expression of both miRNAs prior to MCMV infection. To this end, we scheduled to engineer NIH-3T3 cells with stable expression of the two viral miRNAs, miR-m01-2 and miR-M23-2. However, owing to a failed approach, we instead transfected mimics of the two viral miRNAs to achieve transient expressions. Ultimately, we performed plaque assays and analyzed the infectivity of mutant (harboring point mutations in the two miRNA seed target sites of IE3) and revertant MCMVs in transiently transfected NIH-3T3 cells.

Chapter 2

Materials and Methods

2.1 Materials

2.1.1 Reagents

Name	Manufacturer	Catalog #
1-Methylimidazole	Sigma-Aldrich	M50834
Agarose	Carl Roth	2267.3
APS	ThermoFisher	17874
BioScience Grade Water	Carl Roth	T143
Blasticidin	bioWORLD	40210012-4
BLOCK-iT^{TM} Fluorescent Oligo	ThermoFisher	13750062
Collagen coating solution	Cell Applications	125-50
CutSmart® Buffer	NEB	B7204S
DEPC	Sigma-Aldrich	D5758
Dimethyl sulfoxide (DMSO)	Sigma-Aldrich	D4540
DMEM (1x)	Gibco	41966029
dNTP mix	NEB	N0447S
DPBS	Sigma-Aldrich	D8537
Ethanol	Carl Roth	5054.5
Ethidium bromide	Carl Roth	2218.3
Fetal bovine serum (FBS)	In house	-
Gel Loading Dye, Purple (6x)	NEB	B7024S
Isopropanol	Carl Roth	6752.5
LB-Medium (Lennox)	Carl Roth	X964.3
N-(3-Dimethylaminopropyl)-N'-ethylcarbodiimide hydrochloride	Sigma-Aldrich	E7750

List of table continued:

Name	Manufacturer	Catalog #
NEBuffer 3.1 (10x)	NEB	B9200S
Newborn calf serum (NCS)	In house	-
OptiMEM® I (1x)	Gibco	31985062
Penicilline/Streptomycin	Sigma-Aldrich	P4333
Polythylenimine (PEI)	Polysciences, Inc.	23966
Q5® Reaction Buffer	NEB	B9027S
Q5® Reaction Enhancer	NEB	B9028A
Quick Load 1 kb DNA Ladder	NEB	N3232S
Quick Load 100bp DNA Ladder	NEB	N3231S
RNA loading dye (2x)	NEB	B0363A
Rotiphorese® Gel 40 (Acrylamide solution)	Carl Roth	A515.1
RPMI Medium 1640 (1x)	Gibco	21875034
SDS (10%, ultra pure)	Invitrogen	24730020
SSC buffer (20x, ultra pure)	Invitrogen	15557044
SYBR® Green I Nucleic Acid Gel Stain (10,000x)	Invitrogen	S7563
T4 DNA Ligase Reaction Buffer	NEB	B0202S
T4 polynucleotide kinase buffer	NEB	B0201S
TBE buffer (10x, ultra pure)	Invitrogen	15581044
TEMED (Sure Cast^{TM})	Invitrogen	HC2006
TransIT-X2® Transfection Reagent	Mirus	MIR 6004
Tri Reagent	Sigma-Aldrich	T9424
Urea	Carl Roth	3941.1

2.1.2 Commercially available kits

Name	Manufacturer
Dual-Glo® Luciferase Assay System	Promega
GenElute^{TM} Plasmid Miniprep Kit	Sigma-Aldrich
In-Fusion® HD Cloning Kit	Takara Clontech
Lipofectamine® 3000 Transfection Kit	Invitrogen
MycoAltert^{TM} Mycoplasma Detection Kit	Biozym
NucleoSpin® Gel and PCR Clean-up	Macherey-Nagel
PureYield^{TM} Plasmid Midiprep System	Promega
QIAquick Gel Extraction Kit	Qiagen
Qubit^{TM} RNA BR Assay Kit	Thermo Fisher
Quick^{TM}-DNA Microprep Kit	Zymo Research

2.1.3 Software

Name	Manufacturer
Excel 2001	Microsoft
Geneious 9.2.1	Biomatters
Inkscape 0.92.4	Inkscape Community
LAS X software 1.1	Leica
Prism 8.3.0	GraphPad Software

2.1.4 Plasmids

Table 2.1: Plasmids available in the lab

Name	Comments
F6gw	3^{rd} generation lentiviral plasmid expressing eGFP
pBAD-mTag-BFP	exclusively expressed in bacteria; employed as carrier DNA for transfection of small RNA into NIH-3T3 cells using TransIT-X2
pCMV-VSV-G	[204]; encodes for VSV-G glycoprotein
pLenti-Blast-eGFPintron	[205]; encodes for the human EF1a promotor that regulates the expression of an intron containing eGFP gene
psPax2	packaging plasmid which encodes for Gag, Pol, rev, and tat; provided by Axel Rethwilm
pW-MR8Ch	encodes for mCherry
p/empty	Dual-luciferase reporter which lacks any additional sequence in the firefly UTR
p/PM-m01-2	Dual-luciferase reporter which encodes for a recombinant firefly transcript fused with a 22 bp long sequence perfectly matching miR-m01-2-3p
p/PM-M23-2△N1	Dual-luciferase reporter which encodes for a recombinant firefly transcript fused with a 21 bp long sequence perfectly matching miR-M23-2-3p. This reporter lacks the N1 sequence upstream of the firefly ORF.
p/IE3-3'UTR (WT)	Dual-luciferase reporter which encodes for a recombinant firefly transcript fused with MCMV IE3-3'UTR
p/IE3-3'UTR/mut-m01-2	Dual-luciferase reporter which encodes for a recombinant firefly transcript fused with MCMV IE3-3'UTR. The latter features a 3-nt change within the seed target site of miR-m01-2-3p.

Table 2.1 continued

p/IE3-3'UTR/ mut-m01-2	Dual-luciferase reporter which encodes for a recombinant firefly transcript fused with MCMV IE3-3'UTR. The latter features a 3-nt change within the seed target site of miR-m01-2-3p.
p/IE3-3'UTR/ mut-M23-2	Dual-luciferase reporter which encodes for a recombinant firefly transcript fused with MCMV IE3-3'UTR. The latter features a 3-nt change within the seed target site of miR-M23-2-3p.
p/IE3-3'UTR/ mut-m01-2/M23-2	Dual-luciferase reporter which encodes for a recombinant firefly transcript fused with MCMV IE3-3'UTR. The latter features two 3-nt changes within the seed target sites of miR-m01-2-3p and miR-M23-2-3p.

Table 2.2: Plasmids generated during this study

Name (resistance)	Backbone and enzymatic digestion	Insert[1]	Cloning method	Constitutive expression of
pSH1-m01-2.NheI (amp, blast)	pLenti-Blast-eGFPintron treated with NheI	oligo pair 1/2	infusion	pre-miR-m01-2
pSH2-m01-2.NsiI (amp, blast)	pLenti-Blast-eGFPintron treated with NsiI	oligo pair 3/4	infusion	pre-miR-m01-2
pSH3-M23-2.NheI (amp, blast)	pLenti-Blast-eGFPintron treated with NheI	oligo pair 5/6	infusion	pre-miR-M23-2
pSH4-M23-2.NsiI (amp, blast)	pLenti-Blast-eGFPintron treated with NsiI	oligo pair 7/8	infusion	pre-miR-M23-2
pSH5-m01-2.NheI-M23-2.NsiI (amp, blast)	pSH1-m01-2(NheI) treated with NsiI	oligo pair 7/8	infusion	pre-miR-m01-2 + pre-miR-M23-2

[1]Sequences of oligonucleotide pairs encoding for the forward and reverse strands of either pre-miR-m01-2 or pre-miR-M23-2 are listed in Table 5.2.

Table 2.2 continued

pSH6-M23-2.NheI-m01-2.NsiI (amp, blast)	pSH2-m01-2(NsiI) treated with NheI	oligo pair 5/6	infusion	pre-miR-m01-2 + pre-miR-M23-2
p/PM-M23-2 (amp)	p/IE3-3'UTR(WT) treated with XbaI	XbaI-treated amplicon generated by PCR on p/PM-M23-2△N1 (Table 2.4)	ligation	luciferases (Renilla and recombinant firefly)

[1]Sequences of oligonucleotide pairs, encoding the forward and reverse strands of either pre-miR-m01-2 or pre-miR-M23-2, are listed in Table 5.2 (section 5).

Dual-luciferase reporters (psiCHECK2 vectors)

To prove the validity of miRNA-mRNA interactions between the 3'UTR of MCMV IE3 and miR-m01-2-3p as well as miR-M23-2-3p (henceforth referred to as miR-m01-2 and miR-M23-2, respectively), psiCHECK2 vectors (Promega) were employed that expressed two luciferases, i.e. firefly and Renilla that served as the reporter and control luciferases, respectively (Figure 2.1). Within this dual-luciferase system, the 5' end of the firefly-encoding sequence was fused to the 3' UTR of IE3, which contained the wild-type or mutated miRNA target sites of interest (Figure 2.2, Table 2.1).

Firefly expression was driven by the HSV TK promotor and further enhanced by a m169 5'UTR sequence (N1 sequence). Renilla luciferase expression was dependent on a SV40 early promotor and functioned as a normalization reference to correct for reporter delivery (i.e. transfection efficiency), cell number, and cell viability as well as for other unknown factors that affect translation [156]. Further, two positive psiCHECK2 control vectors were used that lacked the 3'UTR, but instead contained either a 22 or 21 nt long sequence that perfectly matched with miR-m01-2 and miR-M23-2, respectively (Figure 2.3, Table 2.1). Utilized as a negative control vector, one psiCHECK2 vector was deprived of any miRNA binding site downstream of the firefly luciferase (Table 2.1).

psiCHECK2 vectors were constructed previously [198], except for the one containing the perfect match sequence for miR-M23-2. This plasmid was manipulated during my studies

by introducing the missing N1 sequence upstream of the firefly luciferase gene (Table 2.2 and section 3.1.1).

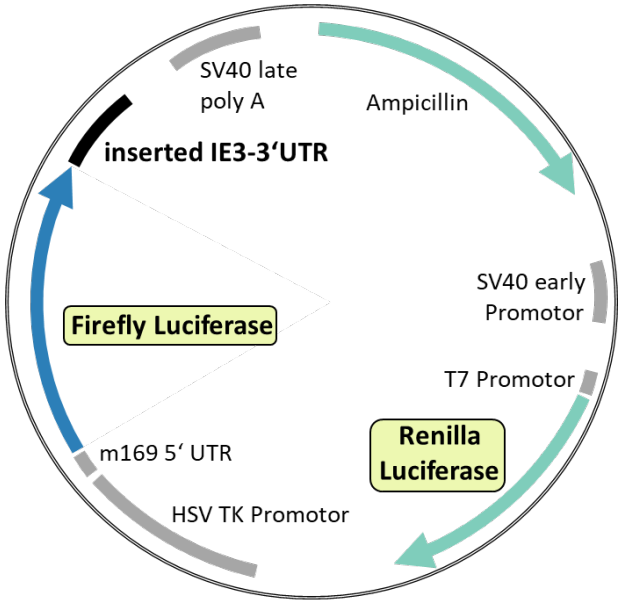

Figure 2.1: Scheme of a psiCHECK2 vector in which the full-length IE3-3'UTR of MCMV was cloned behind the firefly luciferase gene. The 5'UTR of the firefly luciferase was replaced by the MCMV m169 5'UTR (referred to N1 sequence) to enable enhanced expression at comparable levels as the control Renilla luciferase. The inserted IE3-3'UTR contained either wild-type or mutated miRNA binding sites.

MiRNA-expressing vectors

The lentiviral expression plasmid pLenti-Blast-eGFPintron (kindly provided by Robert Jan Lebbink Department of Medical Microbiology, University Medical Center Utrecht) was chosen for stable expression of MCMV miR-01-2 and miR-M23-2, as previous experiments showed high expression levels of miRNAs and GFP fluorescence from this vector [205]. Pre-miRNA sequences of mcmv-miR-m01-2 and mcmv-miR-M23-2 along with the flanking segments of 10 nt at either side of the precursors were cloned into the eGFP intron after NheI or NsiI treatment of the plasmid (Table 2.2).

2.1.5 Oligonucleotides

Sequences of miRNA mimics and the siRNA utilized in this study are listed in Table 2.3. Sequences of single-stranded oligonucleotides, encoding pre-miRNAs (i.e. MCMV

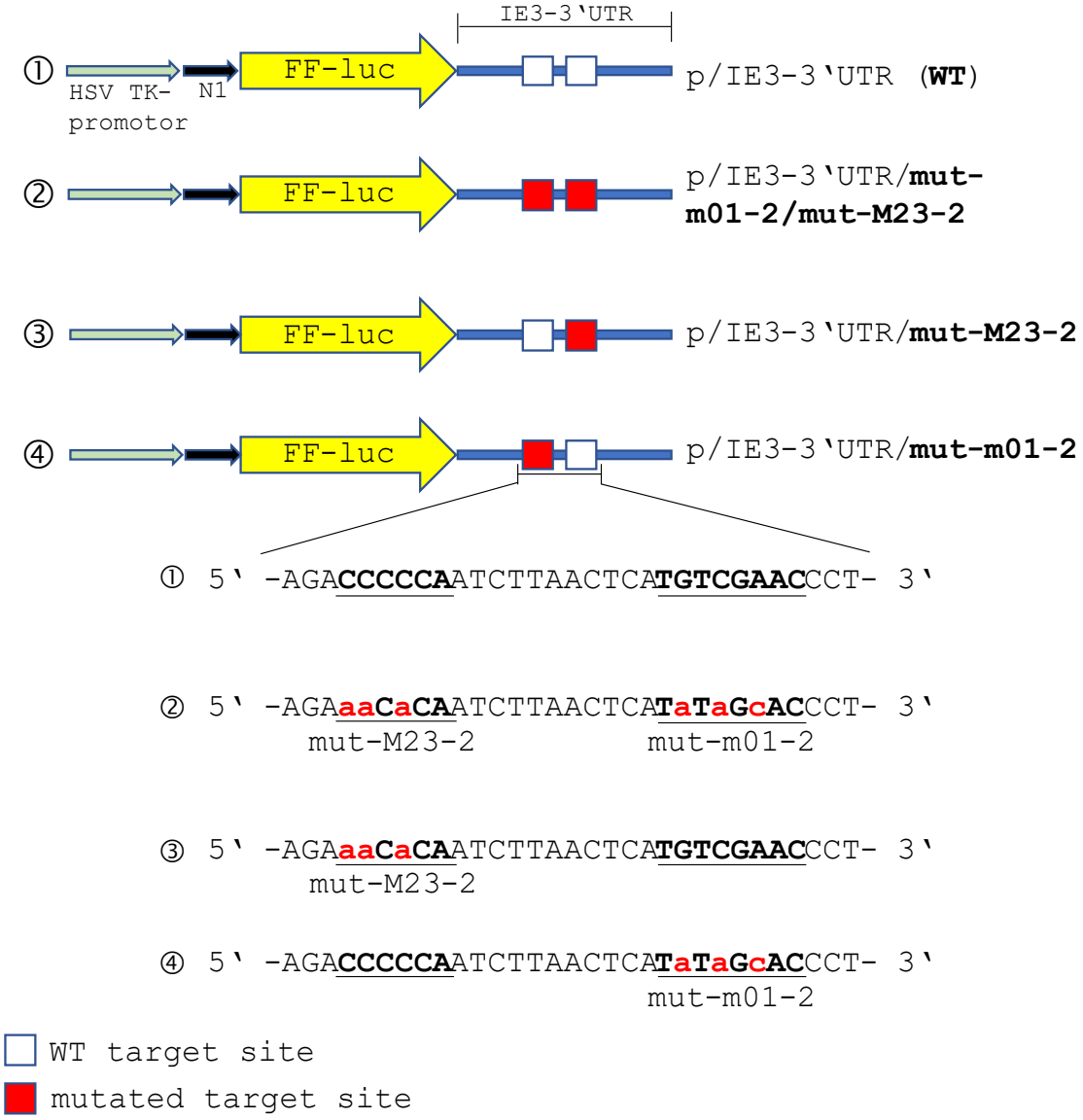

Figure 2.2: Illustrations of the IE3-3'UTR reporter constructs which were used to validate candidate miRNA target sites by luciferase assays. Four different reporter plasmids were used to test miR-m01-2, miR-M23-2, and a non-targeting control (scramble) miRNA on wild-type as well as on mutated targets in the IE3-3'UTR which was cloned behind the ORF of the firefly luciferase (FF-luc). MiRNA seed regions are underlined while introduced point mutations are highlighted in red. Expression of the recombinant reporter gene is driven by the HSV TK promotor, and further enhanced by an N1 segment which comprises a shortened 5'UTR compared to the canonical psiCHECK vector thereby removing unknown inhibitory elements.

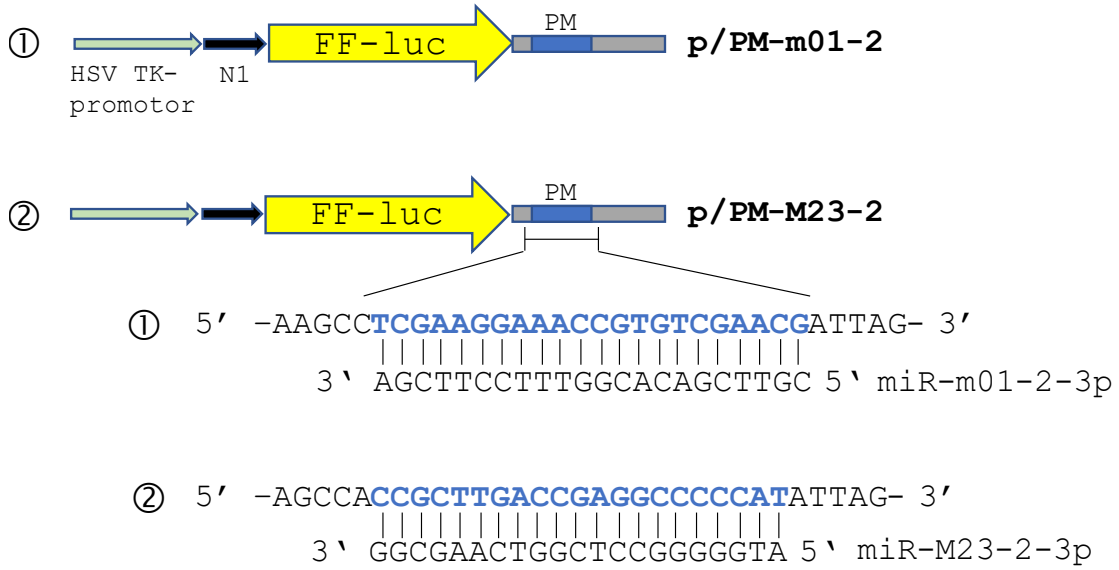

Figure 2.3: Illustrations and sequences of the perfect match reporter constructs. In luciferase reporter assays, positive control reporter vectors were used in which a sequence of perfect complementarity to either miR-m01-2-3p (22 bp in length) or miR-M23-2-3p (21 bp in length) was fused behind the ORF of firefly luciferase (FF-luc). The resulting plasmids were named p/PM-m01-2 and p/PM-M23-2, respectively. Base pairing between the perfect match constructs and respective miRNAs is illustrated. Expression of the recombinant reporter gene is driven by the HSV TK promotor, and further enhanced by the N1 segment which comprises a shortened 5'UTR compared to the canonical psiCHECK vector thereby removing unknown inhibitory elements. PM = perfect match.

pre-miR-m01-2-3p and pre-miR-M23-2-3p), are listed in Table 5.2 (see section 5). In a first step, each oligo was diluted in nf (nuclease-free) water to yield 100 μM stock solutions that were incubated at 98 °C for 3 min to disrupt any strand-internal secondary structure. After mixing equimolar amounts of each oligonucleotide, annealing was performed in a thermocycler which was pre-heated to 98 °C and cooled down to 25 °C within 74 min (-1 °C/min).

2.1.6 Viruses

Mutant (C5X-mCherry/GFP-IE3-3'UTR-mut) and revertant (C5X-mCh/GFP-IE3-mut Rev) MCMVs that were used during this study had been made previously [198]. While mutant MCMVs featured point mutations in both miRNA binding sites within the 3'UTR of the IE3 gene, the wild-type sequences were restored in the case of the revertant viruses (Figure 2.4). Both MCMV constructs were confirmed by sequencing (see section 2.8.3).

Table 2.3: Sequences of small RNA oligos including miRNAs and siRNA

Name of small dsRNA	Sequence (5'-3')	Thermo Fisher Catalog #
MCMV miR-m01-2-3p	GGATGAAGAGAATCGGGTTGGAACGGTGTTTC TTAAGTACGAGCTACCGTTCGACACGGTTTCC TTCGACT	4464066
MCMV miR-M23-2-3p	CCCCGGCTTGAACGTGTCCCCTATCGGTGGTA GTTTACTGCGTGTGCACGATGGGGGCCTCGGT CAAGCGGGG	4464066
scramble miRNA	publicly not available, requires a confidential disclosure agreement with Thermo Fisher	4464058
siRNA-IE3	GTTCGACATGAGTTAAGATTGG	4399665

Furthermore, each virus contained an IRES-mCherry cassette for mCherry protein expression with late kinetics.

2.2 Preparation of lentiviral plasmids

2.2.1 DNA restriction enzyme digest

In the scope preparative digestion, the pLenti-Blast-eGFPintron vector (Table 2.1), selected for subsequent cloning experiments, was linearized by the action of the restriction enzymes NheI or NsiI. Two 50 μL reactions were prepared with 5 μg of plasmid DNA, 5 μL of 10x reaction buffer (CutSmart buffer), 20 U (1 μL) of the respective restriction enzyme, and nf water. Reactions were incubated for 3 h at 37 °C. The linearized vector was purified by gel electrophoresis (see section 2.4.6).

2.2.2 In-Fusion cloning

To engineer plasmids expressing miRNAs of interest (Table 5.2), annealed oligonucleotide pairs encoding for respective pre-miRNAs were cloned into linearized pLenti-Blast-eGFP-intron vectors, using the In-Fusion HD Cloning Kit (Takara Bio USA) and following the manufacturer's instruction (Section B: In-Fusion Cloning Procedure for Spin-Column Puri-

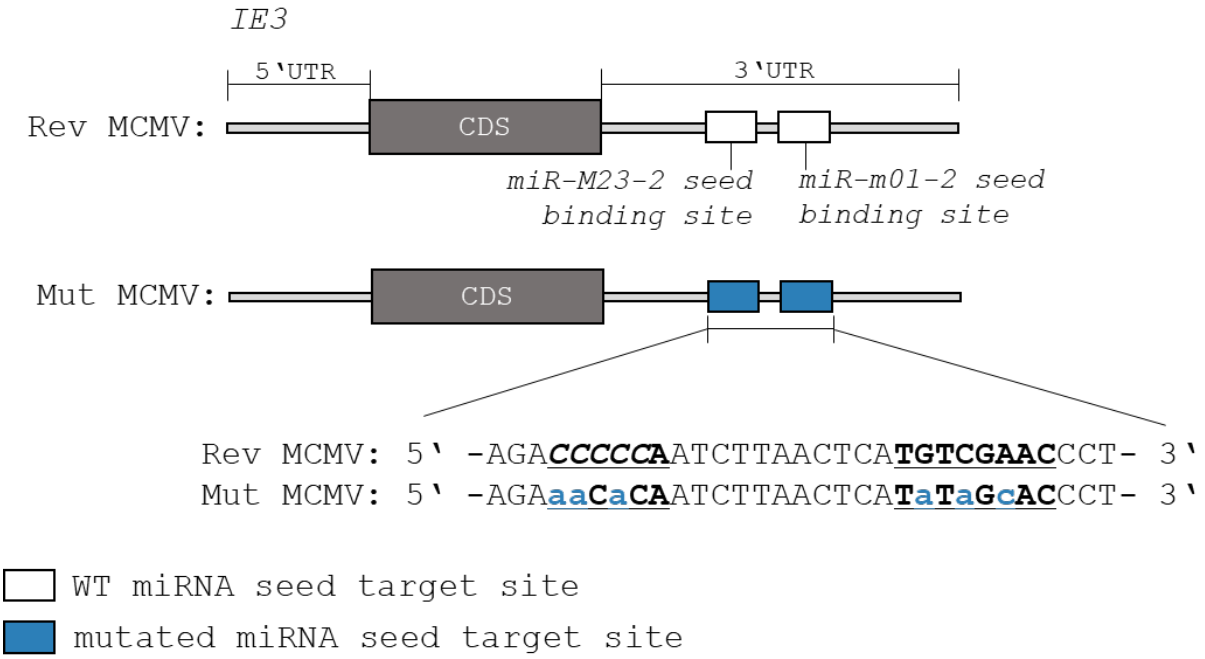

Figure 2.4: Sequences of revertant and mutant MCMVs. Mutant (mut) MCMVs harbored mutations in the seed sites of miR-M23-2 and miR-m01-2 located in the 3'UTR of IE3. By contrast, the wild-type sequence was restored in revertant (rev) MCMVs. MiRNA seed regions are underlined while introduced point mutations are highlighted in blue. CDS = coding sequence.

fied PCR Fragments). To test for different vector-to-insert ratios, 50 ng of linearized vector (around 10 kb in length) was mixed with either 0.5 ng, 1.5 ng, or 5 ng of insert (around 100 nt in length) in a total volume of 5 μL. 2 μL of In-Fusion HD Enzyme Premix (5x) was added to the DNA mix and nf water was used to adjust the reaction volume to 10 μL. Replacing the insert with water in one reaction served as a negative control. Cloning reactions were mixed and incubated for 15 min at 50 °C. After a short cooling on ice (1-2 min), reactions were used to transform Stellar Competent Cells according to section 2.4.1.

2.3 Preparation of luciferase reporter plasmid p/PM-M23-2

2.3.1 PCR and restriction enzyme digest of the insert

To amplify the insert for subsequent cloning experiments, a PCR reaction mix was prepared on ice, which contained 3 ng of template DNA (i.e. p/PM-M23-2$\triangle$N1), 0.5 μM of forward

and reverse primers, 200 μM of dNTPs, 0.02 U/μL of Q5 High-Fidelity DNA polymerase and 1/5 volume of each 5x GC buffer and 5x Q5 reaction buffer. The reaction was filled up with nf water to a total volume of 50 μL and was gently mixed. The thermocycling conditions are presented in Table 2.4.

PCR products were gel purified using the QIAquick Gel Extraction Kit (Qiagen), eluted in 45 μL of elution buffer (10 mM Tris-HCl, 1 mM EDTA, pH 8.0), and mixed with 5 μL of 10x CutSmart buffer and 1 μL of XbaI. The reaction was incubated at 37 °C for 3 h and again gel purified using NucleoSpin® Gel and PCR Clean-up (Macherey-Nagel). DNA concentration was measured using a NanoDrop Spectrophotometer according to section 2.4.4.

Table 2.4: PCR primers and cycle steps for amplifying the miRNA binding site downstream of FF of the p/PM-M23-2△N1 plasmid.

Sense primer: prW745 (5'-3')	ACATTTCCCCGAAAAGTGC			
Antisense primer: prW253 (5'-3')	CCGAGCTGGAGTCTATCCTG			
PCR settings				
	enzyme activation	98 °C	3 min	
	denaturation	98 °C	20 sec	35 cycles
	annealing (TM)	64 °C	20 sec	
	extension	72 °C	1 min	
	final extension	72 °C	3 min	
	cooling	8 °C	∞	

2.3.2 Linearization and dephosphorylation of the backbone

A preparative digest of the backbone plasmid, i.e. p/IE3-3'UTR, was performed by setting up a 40 μL reaction with 5 ng of DNA, 20 U (1 μL) of the selected restriction enzyme (Table 2.2), and nf water. The reaction was incubated at 37 °C for 3 h, before removing the phosphorylated ends to prevent the re-circularisation of the linearized vector. 2.5 U of CIP (Alkaline Phosphatase, Calf Intestinal) was used to dephosphorylate 5 ng of the linearized DNA in a total volume of 40 μL containing the recommended 10x reaction buffer. Following an incubation time of 45 min at 37 °C, DNA was purified using the NucleoSpin® Gel and PCR Clean-up (Macherey-Nagel) according to the manufacturer's instructions. DNA was eluted in 15 μL of elution buffer and DNA concentration was determined according to

section 2.4.4.

2.3.3 Ligation reaction

PCR product and CIP digested backbone were mixed at a ratio of 4:1 and suspended in a total volume of 20 μL containing the recommended 10x reaction buffer and 200 U of T4 ligase. After incubation at 16 °C for 1 h, 5 μL of the ligation mix was used to transform Stellar Competent Cells according to section 2.4.1.

2.4 Cloning procedure

2.4.1 Bacterial transformation

Stellar Competent Cells were used for all transformation procedures. After thawing the bacteria on ice, 5 μL of DNA (i.e. In-fusion cloning reaction) was tap mixed into 50 μL of cells. Transformation reactions were incubated on ice for 30 min and heat shocked at 42 °C for 40-45 sec before cooling them on ice for 2 min. Tubes were topped up to a total volume of 1 mL with LB-medium and incubated on a shaker for 1 h at 37 °C and 800 rpm. 1/100 and 1/10 of bacterial culture were then plated on LB agar plates containing ampicillin for selection (a resistance gene against this antibiotic was transferred by the backbone). The remainder of each reaction was plated after resuspending the pellets from a 5-minute spin-down. Plates were incubated at 37 °C o/n (overnight).

2.4.2 Small-scale isolation and purification of plasmid DNA (Miniprep)

Transformed bacteria cultures were grown on LB agar plates for 16-18 h. Depending on the number of colonies counted on the negative control plates, 3-10 isolated colonies were picked for each transformation to inoculate a volume of 10 mL LB-medium in 50 mL falcons (for small-scale plasmid yield). LB-medium was supplemented with ampicillin (50 μg/mL). Cultures were incubated at 37 °C and 225 rpm o/n. After 14-16 h, ~1 mL of bacteria solution was stored at 4 °C for glycerol stock preparation. The remaining solution was taken for isolating plasmid DNA using the GenElute^{TM} Plasmid Miniprep Kit (Sigma-Aldrich) and following the manufacturer's instructions. Plasmids were eluted

in elution buffer or nf water and stored at 4 °C. Plasmid concentrations were determined by spectrophotometric analysis using NanoDrop. 3-4 μg of plasmid DNA was taken for diagnostic digestion.

2.4.3 Large-scale isolation and purification of plasmid DNA (Midiprep)

A high quantity of plasmid DNA was obtained from 100-200 ml bacteria cultures prepared in Erlenmeyer flasks, containing LB-medium, ampicillin (50 μg/ml), and the scratch of a glycerol stock (see section 2.4.8). Cultures were incubated on a shaker at 37 °C and 225 rpm o/n. Plasmid DNA was purified using the PureYield^{TM} Plasmid Midiprep System (Promega) and following the manufacturer's instructions.

2.4.4 DNA quantitation

DNA quantity and purity in solutions were derived from optical density (OD) measurements using NanoDrop 2000 Spectrophotometer. OD_{260} and OD_{280} were determined by exposing the samples to ultraviolet light at 260 nm and 280 nm, respectively. Resultant concentration values were calculated from OD_{260} by applying the conversion factor for dsDNA: 1 U = 50 μg/mL. The ratio OD_{260}/OD_{280} was used to evaluate sample purity to exclude contamination with organic compounds. An OD_{260}/OD_{280} ratio of $\sim$1.8 and $\sim$2.0 is considered ideal for DNA and RNA samples, respectively.

2.4.5 DNA diagnostic restriction enzyme digest

To verify the engineered plasmids, diagnostic digestion of purified plasmid solutions was conducted. 3-4 μg of DNA was mixed with 10 U (0.5 μL) of respective restriction enzymes and 10x reaction buffer. Reactions were filled up with nf water to a total volume of 40 μL and incubated for 2 h at 37 °C. Parental plasmids (undigested), which served as negative controls, as well as digested fragments, were separated by gel electrophoresis and examined under UV light.

2.4.6 Agarose gel electrophoresis

DNA fragments produced by restriction enzyme digests were separated by horizontal, non-denaturing gel electrophoresis. To this end, a 0.7-3% TAE agarose gel was prepared containing either Ethidium bromide (1 μg /mL) or SYBR Safe (10,000x) for staining DNA. Purple loading dye (6x) and DNA were combined and thoroughly mixed before loading the samples into the wells of a solidified gel. All gels run in 1x TAE buffer (40 mM Tris-HCl, 20 mM acetic acid, 1 mM EDTA, pH 8.0) at 90 – 100 V. DNA bands stained with Ethidium bromide or SYBR Safe, were examined during UV light exposure (at 312 nm) or under blue light (470 nm). In the case of preparative electrophoresis, bands were excised from the gel with clean scalpels and DNA was subsequently purified using the NucleoSpin® Gel and PCR Clean-up (Macherey-Nagel) according to the manufacturer's instructions.

2.4.7 DNA sequencing

Generated plasmids that were digested into correctly sized fragments were further verified for accuracy by Sanger sequencing using the service of Mycrosynth (Switzerland). 450 – 1500 ng of DNA was diluted in nf water (40-100 ng/μL) and sent for sequencing. Sequence data were analyzed using the software Geneious.

2.4.8 Glycerol stocks

After sequencing confirmed the correctness of the constructs, glycerol stocks were prepared for long-term storage of the plasmid DNA within bacteria. A 25% glycerol solution was prepared by adding 500 μL of 50% glycerol (100% glycerol diluted in LB-medium) to 500 μL of liquid bacteria culture. Glycerol stocks were stored in thermostable cryo-tubes at -80 °C. To recover bacteria from freeze downs, scratches of glycerol stocks were plated on LB agar applying the streak-plate method. Petri dishes were incubated at 37 °C o/n to finally prepare 100-200 mL of suspension cultures to form single clones.

2.5 Cell culture

All cells were stored in incubators at 37 °C, in 5% CO_2 and 95% humidity. Cells were split in accordance with Table 2.5. In general, PBS, trypsin, and media were pre-warmed to r/t (room temperature) before usage. Adherent cells were split by removing the old media,

washing with 1-4 mL of PBS, and adding a small volume of trypsin to the cells (up to 2 mL depending on the size of the surface area). Flasks and dishes were incubated at 37 °C for 1-2 min, gently tapped, and checked under the microscope to ensure cell detachment. Trypsinization times were kept to a minimum to prevent cell damage. Since FBS and NCS inactivate the trypsin, the latter was neutralized by resuspending the cells in the respective complete media, which was at least twice the volume of trypsin. The medium was dispersed over the surface layer to detach the remaining cells and pipetted up and down to reduce cell clumping. Aliquots were prepared and seeded into cell culture flasks. HEK/293T cells were transferred to new flasks to allow appropriate adhesion. For all other cells, flasks were reused up to five times.

Table 2.5: Conditions of cell cultures

Cell name	Description	Growth media	Ratio and intervals of splitting
HEK/293T	human kidney carcinoma cells expressing the SV40 large T antigen	DMEM, 10% NCS, P/S[1]	1:10, 3-4 days
M2-10B4	bone marrow stroma cells isolated from a mouse	RPMI, 10% FBS, P/S[1]	1:6, 2-3 days
NIH-3T3	fibroblasts isolated from a mouse embryo	DMEM, 10% NCS, P/S[1]	1:10, 2-3 days

[1]P/S = 0.6% (w/v) penicillin, 1.3% (w/v) streptomycin

2.5.1 Counting of cells

For seeding a specific amount of cells, cell concentration needed to be determined. To this end, 10 μL of the cell suspension was transferred to a counting chamber and cells within at least two diagonally opposite squares of a hemocytometer grid were counted using a microscope. Following equation was used to determine the amount of cells per mL:

$$cells/mL = \frac{\text{number of cells counted}}{\text{number of squares counted}} \times 10^4$$

2.5.2 Freezing and thawing of cell lines

For long-term preservation of mammalian cells with low-passage numbers, cell stocks were generated and stored in liquid nitrogen. In the first step, a freezing medium was prepared, containing 10% DMSO and 90% FBS, and cooled down on the ice before usage. Cells were trypsinized (according to section 2.5), transferred to falcons, and spun down for 5 min at 300 × g. After aspirating the supernatant, cells were resuspended in 4 mL of ice-cold freezing medium. Aliquots of 1 mL were prepared, transferred to cryo-tubes, and placed into isopropanol-based cryo-containers to gently cool down the cells from 4 °C to -80 °C by -1 °C/min. For long-term storage, cryo-tubes were finally transferred into liquid nitrogen tanks.

For thawing, cells were removed from the liquid nitrogen tank and placed in an insulated container filled with dry ice for ∼30 min to reduce the pressure within the tubes by nitrogen evaporation. Cells were then thawed in a 37 °C water bath for 1-2 min (just until the ice crystals became invisible) and transferred to 9 mL of the appropriate complete medium (Table 2.5). Cell were then pelleted at 300 × g for 5 min. After aspirating the supernatant, cell pellets were resuspended in 13 mL of complete medium and seeded into collagen-coated T25 flasks.

Collagen coating of flasks aided adherent cells to attach to the dishes' surfaces. To prepare a pre-coated surface, collagen solution was mixed in an equivalent volume of PBS and added to the culture flasks to cover the entire surface layer. Flasks were incubated at r/t o/n, then carefully washed with PBS and either immediately used for cell culture or stored at 4 °C.

2.6 Dual-Glo Luciferase reporter assay

The Dual-Glo reporter assay was conducted to test for functionally relevant binding of miRNA mimics to predicted target sites within psiCHECK2 constructs.

2.6.1 Preparation of serial dilutions

To determine the concentration of miRNAs needed to yield the highest reduction of relative luciferase activity compared to a negative control, a dose response experiment was carried out. 2.2 μL of two-fold serial dilutions of a miRNA mimic (50 μM stock) was prepared

in six tubes, among which tube 1 was filled with 4.84 μL of miRNA mimic (400 nM final concentration), while tubes 2-6 contained 2.42 μL of the diluent, i.e. nf water (Figure 2.5). Serial dilutions were performed by removing 2.42 μL of undiluted miRNA mimic from tube 1 and adding it to tube 2. The diluted solution was thoroughly mixed before transferring 2.42 μL of it from tube 2 to tube 3. This process was repeated until 5 tubes were made of 200 nM, 100 nM, 50 nM, 25 nM, and 12.5 nM, respectively.

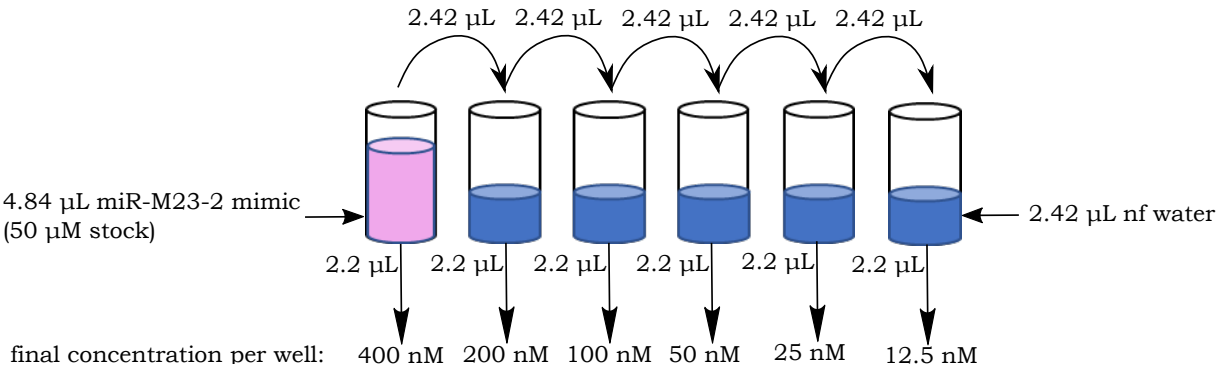

Figure 2.5: Illustration of two-fold serial dilution of miR-M23-2 mimic. To determine the potency of miR-M23-2 mimic, different concentration of miR-M23-2 mimic were prepared for transfection with the p/IE3-3'UTR and the p/IE3-3'UTR/mut-M23-2 vector.

2.6.2 Assay procedure

TransIT-X2 Dynamic Delivery System® (Mirus Bio) was used to perform co-transfection of plasmid DNA and miRNA mimic into HEK/293T cells. For each transfection, 0.11 μL of a 50 μM stock of (double-stranded) miRNA mimic or scramble miRNA for 50 nM final (or serial dilutions according to section 2.6.1), 5 ng of psiCHECK2 plasmid as well as 95 ng of mCherry encoding DNA were mixed with 9 μL of serum free Opti-MEM in a total volume of 9.7 μL. After adding 0.3 μL of TransIT-X2, nucleic acid-transfection reagent complexes were incubated for 15-30 min at r/t and subsequently transferred to a 96-well clear flat-bottom plate in triplicates before seeding HEK/293T cells (4×10^4 cells in 100 μL of media per well) to allow for reverse transfection.

Following 16–24 h of incubation at 37 °C, transfected cells were tested by fluorescence microscopy (Leica DFC300G, FLUO-Filtercube TXR). 40 μL of supernatant was removed from each well to bring the culture medium volume to around 50 μL per well before performing the Dual-Glo® Luciferase Assay (Promega) accordingly to the manufacturer's protocol. Dual-Glo Reagent was thawed in a polystyrene box and mixed, before adding 50

μL of the reagent to each well. After incubating the plate for at least 10 min at r/t, firefly luciferase signals were detected on the Centro XS LB 960 Luminometer (Berthold Technologies). For measuring Renilla luminescence, Dual Glo Stop & Glo reagent was diluted 1/100 in Stop Glo Buffer. 50 μL of this solution was transferred to each well, followed by an incubation and measuring procedure as before.

2.6.3 Normalization steps

Experimental data was analyzed by determining relative changes in the activity of the firefly luciferase reporter. A three-step normalization procedure was performed using Excel. An overview is provided by Table 2.6.

In the first step, firefly luciferase activity values were normalized against their corresponding Renilla luciferase signals, before triplicates of p/empty and p/IE3-3'UTR/mut-m01-2/mut-M23-2 were averaged. Calculated means were used to second normalize respective firefly-to-Renilla-luciferase (FF/Ren) ratios allocated to the same miRNAs, in a way that values of perfect match constructs were normalized to p/empty and 3'UTR containing constructs were normalized to p/IE3-3'UTR/mut-m01-2/mut-M23-2.

Lastly, averages were taken from each triplicate treated with the negative control (scramble) miRNA to conduct a third normalization of respective double normalized values that were allocated to the same psiCHECK2 vectors.

Triple normalization was performed to overcome potential errors that would lead to misinterpretation of the data. As such, the second step of normalization was performed to account for any factors that affect the translation of the firefly luciferase transcripts at regions other than the putative miRNA binding sites. The third normalization step controlled for any cellular factors that act on the luciferase construct, either on the firefly encoding sequence or on the fused 3' segment [206].

2.6.4 Statistical analysis

MiRNA-mediated post-transcriptional regulation was investigated after performing the triple normalization procedure. Statistics were generated using the software package Prism 8.3. (GraphPad Software, San Diego, DA). Relative activity values were compared with values of the respective negative control constructs (either p/empty or p/IE3-3'UTR/mut-

Table 2.6: Overview of the three-step normalization procedure applied for luciferase assays using psiCHECK2 vectors

psiCHECK2 construct	1^{st} norm	2^{nd} norm	3^{rd} norm
p/PM-m01-2	FF/Ren	to primary normalized mean of p/PM-empty	to secondary normalized scramble values transfected with the same psiCHECK2 vector
p/PM-M23-2			
p/PM-empty			
p/IE3-3'UTR (WT)		to primary normalized mean of p/IE3-3'UTR/mut-m01-2/m23-2	
p/IE3-3'UTR/mut-m01-2			
p/IE3-3'UTR/mut-M23-2			
p/IE3-3'UTR/mut-m01-2/ mut-M23-2			

m01-2/mut-M23-2) and tested for significance ($p< 0.05$) using an unpaired t-test.

2.7 Generating stable cell lines

2.7.1 Lentivirus production

Lentiviral vectors that we generated during this study (Table 2.2 and section 2.2) were taken to transfect 40-50% confluent HEK/293T cells in 6 cm dish plates using the Lipofectamine 3000 Reagent protocol (Thermo Fisher Scientific). A DNA mixture was prepared containing 4 μg of transfer plasmid (pLenti-Blast-eGFPintron, pSH1-m01-2.NheI, pSH2-m01-2.NsiI, pSH3-M23-2.NheI, pSH4-M23-2.NsiI, pSH5-m01-2.NheI-M23-2.NsiI and pSH6-M23-2.NheI-m01-2.NsiI, Table 2.2), 3 of μg packaging plasmid (psPax2) and 1 μg of envelope plasmid (pCMV-VSV-G). After diluting the DNA mix in serum-free Opti-MEM, 16 μL of P3000 reagent (DNA:P3000 reagent = 1:2) was added in a final volume of 300 μL. In a separate tube, 24 μL of Lipofectamine 3000 Reagent (DNA:Lipofectamine 3000 = 1:3) was combined with 276 μL of serum-free Opti-MEM. After vortexing both reactions, the DNA mixture was added into diluted Lipofectamine 3000 Reagent, tap mixed, and incubated for 15 min at r/t. The transfection mixture was added dropwise to HEK/293T cells. The fluorescent lentivirus F6gw was exploited as a control for lentiviral production by transfecting HEK/293T cells, following the same protocol. At 16 h posttransfection, the media of transfected cells were carefully renewed. Cells were checked by fluorescence

microscopy (Leica DFC300G) using FLUO-Filtercube FITC.

2.7.2 Transduction of NIH-3T3 cells

48 h post-transfection of HEK/293T cells, lentivirus was harvested by collecting and filtering the viral supernatant using 0.4 μL filter cartridges, which was subsequently added drop-wise on 50% confluent NIH-3T3 cells seeded in 6-well plates (0.3×10^6 cells/well one day prior to transfection). To conduct a spin-transduction, infected plates were pelleted at 800 x ġ for 30 min and subsequently placed in the incubator. Three days post-transduction, cells were checked by fluorescence microscopy (Leica DFC300G, FLUO-Filtercube FITC) and selection was started (see section 2.7.4).

2.7.3 Antibiotic dose-response experiment

For determining the minimal dose of a selected antibiotic needed to kill all non-resistant cells within ∼7 days, cells were treated with increasing antibiotic concentrations ranging from 0.156 to 20 μg/mL. NIH-3T3 cells were seeded in a 12-well plate and grown to ∼20% confluence. Old media was aspirated and 1.5 mL of new media was added to each well, except for the first well. The latter was filled with 20 μg/mL Blasticidin diluted in 3 mL of medium (Table 2.5). Two-fold serial dilutions were made by step-wise transferring 1.5 mL of the thoroughly mixed dilute solution to the next well, starting with well 1. A negative control well without any antibiotics was included. The medium was replaced every 2-3 days. Cell death was daily checked by microscopy.

2.7.4 Antibiotic selection

Stably transduced cell lines were selected by antibiotic treatment at a concentration determined by an antibiotic dose-response experiment (see section 2.7.3). The antibiotic was refreshed every 2-3 days. Upon 100% cell death in the control cell culture which contained untransduced cells that naturally lack Blasticidin resistance, concentration of the antibiotic was reduced to 2.5 μg/mL. Parts of the cells were frozen down according to section 2.5.2.

2.7.5 Cell sorting

Transduced cells were sorted for high fluorescence signals. In the first step, transduced cell lines were trypsinized (see section 2.5), counted (see section 2.5.1), and pelleted at 300 × g for 5 min. Cell pellets were resuspended in the appropriate volume of culture medium to obtain a concentration of 10^7 cells/mL. Cell suspensions were subsequently transferred to sterile FACS tubes.

Non-transduced cells without fluorescence expression served as a negative control for calibrating the FACS machine. 50,000 cells with fluorescence intensities of the top 10% percentile were gated into 15 mL falcons which were subsequently seeded into T25 flasks. Moreover, 10 single clones per cell line with fluorescence intensities of the top 1% percentile were transferred into wells of a 96-well plate.

2.7.6 Mycoplasma screening

Since cells were subjected to non-sterile conditions during the sorting process, a mycoplasma detection assay was performed after 3 days of incubation, using the MycoAlert^{TM} Mycoplasma Detection Kit (Biozym). ∼600 μL of medium from each flask was transferred to a separate tube and centrifuged at 200 × g for 5 min. 40 μL of the clarified sample was added to a white 96-well plate and topped with 40 μL of MycoAlert Reagent. The plate was incubated for 5 min at r/t and luminescence signals were measured using the Centro XS LB 960 Luminometer (Berthold Technologies). In a second step, 40 μL of Myco Alert Substrate was added to each well and mixed. After 10 min of incubation at r/t, luminescence signals were determined once again. Data was exported to Excel. Values of the second reading were divided by the respective results of the first reading. Ratios below 0.9 excluded mycoplasma contamination.

2.7.7 Luciferase Assay

Transduced and selected cell lines were tested for functionally relevant levels of desired miRNAs by dual luciferase assay. The experiment was performed in accordance with the protocol described in section 2.6.2, except for two aspects. First, 0.11 μL of miRNA mimics (50 μM stock) was only used for positive control experiments, while any other transfection sample contained nf-water instead. Second, reverse transfection was performed using 2 x 10^4 transduced cells per well.

Luciferase readout values were triple normalized in accordance to section 2.6.3, except for the last normalization step. Averages of double normalized values of NIH-3T3.GFP (no miRNA expression) were used to conduct the third normalization.

2.7.8 RNA extraction

The expression of desired miRNAs was further investigated by Northern blot. In a first step, transduced cells were seeded in T75 flasks and grown to ∼ 90% confluence. After trypsinizing and pelleting the cells (300 × g, 5 min), the supernatant was aspirated and 1 ml of TRIzol reagent was added to the pellets before storing the tubes at -80 °C until further use.

For RNA extraction, TRIzol-containing samples were thawed at r/t for 5-10 min and mixed with 200 μL of chloroform. After vortexing for 30 sec and incubating for 5 min, samples were centrifuged at 12,000 × g for 15 min at 4 °C. Subsequently, the upper, aqueous phase was transferred to new tubes and combined with 500 μL of isopropanol. Samples were again vortexed for 30 sec, incubated for 10 min, and centrifuged at 12,000 × g for 10 min at 4 °C to allow for RNA precipitation. The supernatant was discarded and the pellet was washed in 1 mL of 80% ethanol before starting the last centrifugation step at 12,000 × g for 10 min at 4 °C. The supernatant was thoroughly removed and dried RNA pellets were resuspended in 20 μL of nf water. To ensure precise measurements, RNA concentrations were determined by a Qubit 3.0 Fluorometer (Thermo Fisher) after preparing the RNA samples using the Quibt^{TM} RNA BR Assay Kit (Thermo Fisher) and following the manufacturer's instructions. Samples were stored at -80 °C before starting the northern blot procedure.

2.7.9 Northern Blot analysis

Denaturing gel electrophoresis

For separating RNA samples (see section 2.7.8) according to size, a 15% denaturing polyacrylamide (PAA) gel was prepared by mixing 37.5 ml of 40% acrylamide, 10 mL of TBE (5x, final concentration = 0.5x) and 48 g of UREA powder. Complete solving of UREA was ensured by heating the solution in the microwave for ∼20 sec and mixing it by magnetic stirring. The gel solution was finally suspended with diethylpyrocarbonate (DEPC) water in a total volume of 100 mL and stored at 4 °C until further usage. DEPC water was

prepared by mixing 1 L of MilliQ water with 1 mL of DEPC. Adding the latter ensured inactivation of most if not all RNase contamination in the solution. DEPC-treated water (0.1% final concentration) was incubated at 37 °C o/n and finally autoclaved to hydrolyze DEPC as well as to inhibit any remaining RNase activity.

On the day of running the RNA samples, the gel cassette, as well as the electrophoresis, apparatus were set up according to Figure 2.6 A and B.

For gel preparation, 40 mL of hand-warm PAA solution was transferred to a 50 mL falcon and placed on ice before adding 400 μL of APS and 10 μL of TEMED (storage on ice decelerates the process of polymerization that starts when adding APS). After thorough mixing, the PAA-gel was immediately pipetted between the two glass plates of the gel cassette until the solution reached the top of the short plate. The well-comb was then put in place before letting the gel solidify for 1 h at r/t. Once the gel polymerized, tapes, bottom spacer, book-binder clamps and the comb were removed. Subsequently, the gel sandwich was clamped into electrophoresis apparatus and submerged ~2 cm in TBE buffer (1x), that was contained in the bottom reservoir. TBE buffer (1x) was further poured into the top reservoir to cover the wells. Using a syringe, wells were rinsed with TBE buffer to remove any remaining UREA. The gel was pre-run by the setting power supply to 200 V (constant voltage) for 30 min. In the meantime, RNA samples were thawed and prepared on ice. 30 ng of RNA was mixed with equal volumes of RNA loading dye (2x). To remove and prevent the re-formation of secondary structures, samples were heat denatured at 95 °C for 3 min and immediately placed on ice for 1 min before performing a quick spin down. Samples were stored on ice until the pre-run of the gel was finished. Wells were once again rinsed and subsequently loaded. After assembling the lid, the gel was run by setting the power supply to 200 V (constant voltage) during the first 15 min, and 300 V (constant voltage) thereafter. When the dye front reached 2-3 cm above the end of the gel (after 2-3 h), the gel sandwich was removed from the electrophoresis apparatus and opened. Unused gel areas were cut off before rinsing the gel in a baking dish filled with TBE buffer (1x) to leach any remaining UREA.

RNA transfer via electroblotting

In the next step, RNA was transferred from the gel onto Hybond N+ positive charged nylon membrane through electroblotting. By using nylon membranes, we benefited from mechanical strength, resistance to heat and, high affinity to nucleic acids as compared to nitrocellulose membranes. For the transfer, a blotting cassette was assembled according

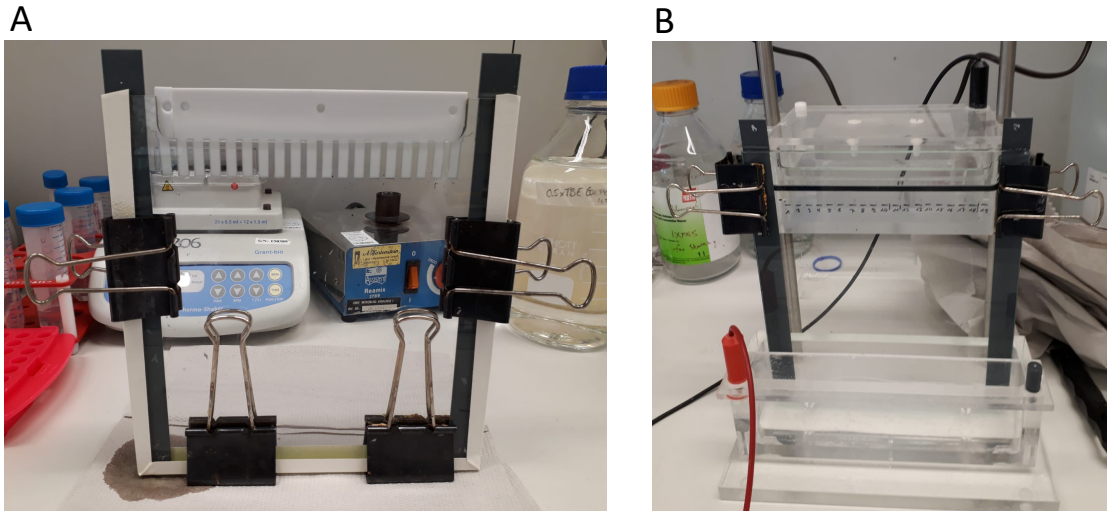

Figure 2.6: Construction of gel cassette (A) and vertical electrophoresis apparatus (B) for RNA separation. Once the PAA gel was solidified in the gel cassette, the glass plates were transferred into the electrophoresis apparatus, in which the lower and upper reservoir was filled with running buffer (TBE buffer, 1x).

to Figure 2.7. All layers were pre-wet in TBE buffer (1x). Air bubbles between the layers were carefully removed by a roller. A blotting chamber was placed at 4 °C and filled with TBE buffer (1x). A stirring magnet ensured constant circulation of the fluid, preventing localized heating. The blotting cassette was inserted into the chamber and the power supply was set to 400 mA at a constant current for 2 h.

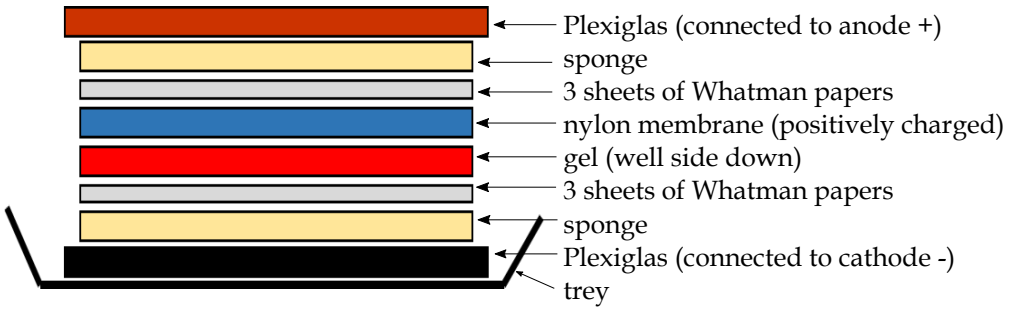

Figure 2.7: Schematic representation of a blotting cassette. The transfer of denatured RNA from a PAA gel to a positively charged nylon membrane was achieved by electroblotting.

UV and chemical cross-linking

Once the transfer was finished, RNA strands became crosslinked to the nylon membrane, first by a short UV exposure at 120,000 $\mu J/cm^2$ in a Stratalinker UV crosslinker (Stratagene), which, however, only immobilized ∼30% of RNA strands. To increase the rate of covalently linked RNA, a chemical cross-linking procedure followed. To this end, a Whatman membrane was soaked in crosslinking solution (4.5 mL DEPC water, 122.5 μL 1-Methylimidazole, 150 μL 1 M HCl, 0.3765 g of EDC (N-(3-Dimethylaminopropyl)-N'-ethylcarbodiimide hydrochloride, filled up to 12 mL with DEPC) onto which the nylon membrane was overlayed with the RNA-side facing up. Wrapped in plastic foil, the membranes were incubated at 65 °C for 1 h.

Furthermore, the PAA gel was placed in water supplemented with Ethidium bromide to test for any remaining bands of RNA under UV light after 15 min of incubation on a tilting shaker.

Pre-hybridization (blocking)

After 1 h of chemical cross-linking, the nylon membrane became pre-hybridized (blocked) to minimize background hybridization signal resulting from non-specific interactions between the membrane and the probes, which were added in the next step. The nylon membrane was transferred into a glass tube, washed with DEPC water (to minimize air bubbles), and incubated with pre-warmed hybridization solution (9 mL SSC buffer (20x), 21 mL 10% SDS) on a rolling shaker at 60 °C for 30 min. SDS functioned as a blocking agent of nylon.

Radiolabeled probe hybridization

In a next step, probes complementary to the miRNAs of interest (i.e. miR-m01-2 and miR-M23-2) were radiolabeled (see Table 5.1 for sequences). 1 μL of each 1:10 diluted probe (100 μM stock) was suspended in 5 μL of nf water and further mixed with 1 μL of T4 polynucleotide kinase buffer (10x), 1 μL of T4 polynucleotide kinase and 2 μL of γ ^{32}P ATP. During 1 h of incubating on a shaker at 300 rpm, T4 polynucleotide kinase was allowed to catalyze the 5' labeling of RNA strands using the radioactive ATP as a phosphate donor. Furthermore, we also radioactively labeled snRNA U6 oligo (see Table 5.1 for sequence), to include an RNA-loading control for northern blot analysis.

Subsequently, 5 μL of the radioactive mix was combined with 20 μL of nf water, mixed with 30 mL of pre-warmed hybridization solution, and added to the membrane within the tubes to allow for radiolabeled probe hybridization at 42 °C o/n.

Washing and phosphor imaging

The next day, the radioactive mix was decanted, prior to exposing the membrane to a pre-warmed wash solution (DEPC water supplemented with 7% of 20x SSC buffer and 10% SDS) on a rolling shaker at 42 °C for 20 min. The washing step was repeated four times in total to rinse off any unhybridized probe. The membrane was subsequently dried and placed in a cassette containing a phosphor screen. During a fairly variable time of incubation (ranging from hours to days) at -80 °C, an image was produced on the screen, which was finally monitored by a phosphor imager.

Hybridization of a new probe

Before exposing the membrane to a new probe, the old one was removed by incubating the membrane in 30 mL of hybridization solution at 60 °C for 1 h. Following this stringent washing step, the hybridization of a new radiolabeled probe was performed as described above.

2.8 Virological methodologies

2.8.1 Generation of MCMV stocks

For virus passage, a confluent 15 cm cell culture dish of M2-10B4 cells was trypsinized (according to section 2.5), resuspended in 12 mL of media, and inoculated with 1 mL of either revertant or mutant MCMV (virus reconstitution from BAC DNA was not required since virus inocula were available). Following incubation at 37 °C for 30 min, the virus-cell suspension was adjusted to a total volume of 20 mL with media and replated on a new 15 cm cell culture dish. Upon complete cell lysis, which was usually observed on day four to six post-infection, cells were scraped from the dish surfaces and collected together with the supernatant. Virus inoculum was centrifuged at 5,000 × g for 5 min. The supernatant was stored on ice until further usage. After resuspending the pellet in 1 mL of virus suspension, cell lysis was induced via three cycles of freezing down in liquid nitrogen for 1 min and complete thawing at 37 °C. The virus was purified from cellular debris by centrifuging the virus-cell suspension at 3,000 × g for 10 min at 4 °C. The supernatant was collected and combined with the previous supernatant stored on ice. Aliquots of 200-300 μL were prepared and immediately snap frozen in liquid nitrogen for 2-5 min before transferring

the aliquots to -80 °C. Virus concentration was quantified by plaque assay.

2.8.2 Virus quantification by plaque assay

To determine viral infectivity of virus inoculum, a plaque assay was performed by inoculating serially diluted virus onto NIH-3T3 cells. Cells were seeded one day prior to infection at 6×10^4 cells/well in a 48-well plate. 10-fold dilutions of the virus material were prepared by setting up 6 tubes which were filled with 450 μL of DMEM media (supplemented with 10% NCS and P/S), except for the first tube which contained 5 μL of thawed virus inoculum in 495 μL of the same media. After thorough mixing, 50 μL of the starting dilution, i.e. 10^{-2}, was transferred into the second tube to get the second dilution, i.e. 10^{-3}. This step was repeated until the 6th dilution, i.e. 10^{-7}.

Media of the 48-well plate of NIH-3T3 cells was then removed and 200 μL of each virus dilution was transferred twice to one well of the plate. After incubating the plate for 1 h at 37 °C, the inoculum was aspirated and the infected NIH-3T3 cells were covered with 500 μL of 37 °C pre-warmed medium containing carboxymethyl cellulose (MEM (10x) supplemented with 7.5 g/L carboxymethyl cellulose, 5% FBS, 1% glutamine, 0.5% of non-essential amino acids (NEAAs), 0.6% (w/v) penicillin, 1.3% (w/v) streptomycin, 4.9% $NaHCO_3$ and 2.5% NCS and 77.6% water). Employing carboxymethyl cellulose overlay media instead of standard liquid culture medium prevented viral cell-to-cell spread and allowed for localized plaque formation during 3 days of incubation at 37 °C.

After 3 days, wells were checked by fluorescence microscopy (Leica DFC300G, FLUO-Filtercube TXR) and clusters of mCherry protein expressing viruses were counted. In the second step, plaques were counted by light microscopy. To this end, a crystal-violet staining was conducted. The medium was aspirated and 1 mL of crystal violet solution (10x) (1% crystal violet in PBS (1x) containing 10% paraformaldehyde) was added to each well in the fume hood. After incubating the plate on a shaker for 15 min at r/t, crystal violet solution was rinsed off the wells with DI water, and plaques were counted under the light microscope. The following equation was used to determine the virus titer:

$$\text{virus titer}[pfu/mL] = \frac{\text{average of counted plaques}}{\text{volume of infectious dilution} \times \text{dilution}}$$

2.8.3 Sequencing of viral DNA fragments

To confirm the accuracy of previously generated MCMV strains, DNA was isolated from virus inocula using the Quick^{TM} DNA Microprep Kit (Zymo Research). The manufacturer's instructions were followed. 1 μL of purified DNA of virus inoculum was subsequently used for amplifying the fragment of interest. PCR reaction mixes were prepared according to section 2.3.1. To ensure low levels of non-specific PCR products resulting from off-target priming effects, a PCR touch-down program was chosen (Table 2.7) [207].
DNA concentrations were measured using a NanoDrop Spectrophotometer according to section 2.4.4. $\sim$1 μg of DNA diluted in 20 μL nf water was finally sent for sequencing.

Table 2.7: Touch-down PCR for amplifying the 3'UTR of IE3 in mutant and revertant MCMV

Sense primer: prW1413 (5'-3')	GCTCTGGGAAGGGAGAGACT		
Antisense primer: prW1414 (5'-3')	AGCACACCAAGCCCATTAAC		
PCR settings			
	initial denaturation	98 °C	3 min
Touch-down:	denaturation	98 °C	20 sec
20 cycles	annealing	68-58 °C	20 sec
(-1 °C per cycle)	extension	72 °C	1 min
	denaturation	98 °C	30 sec
20 cycles	annealing	55 °C	15 sec
	extension	72 °C	1 min
	final extension	72 °C	5 min
	cooling	16 °C	∞

2.8.4 Optimization of miRNA transfection

TransIT-X2, Lipofectamine 3000, and polyethylenimine (PEI) were checked for delivering short oligonucleotides into NIH-3T3 cells. Fluorescence image-based assays were performed by transfecting a fluorescent RNA-duplex that resembled the structure of siRNAs (i.e. BLOCK-iT^{TM} Fluorescent Oligo). Transfection mixes were prepared according to Table 2.8 and transferred to the wells of a 48-well plate just prior to seeding NIH-3T3 cells at a density of 6 x 10^4 cells/well. Transfection efficiency was assessed by fluorescence microscopy (Leica DFC300G) using FLUO-Filtercube FITC. Cell density and viability were monitored by light microscopy.

Table 2.8: Transfection mixes used for optimizing efficiency of transfecting small RNA into NIH-3T3 cells

	Mix	Comments
TransIT-X2	26 μL Opti-MEM Fluorescent Oligo (20 μM stock) 50 nM final 0.78 μL TransIT-X2	TransIT-X2 was warmed to r/t and vortexed before usage; incubated for 30 min at r/t
TransIT-X2	26 μL Opti-MEM Fluorescent Oligo (20 μM stock) 50 nM final 260 ng pBAD-mTag-BFP (pW150) 0.78 μL TransIT-X2	pBAD-mTag-BFP functioned as carrier DNA; TransIT-X2 was warmed to r/t and vortexed before usage; incubated for 30 min at r/t
Lipofectamine	*DNA-mix:* 15 μL Opti-MEM Fluorescent Oligo (20 μM stock) 50 nM final *Lipofectamine dilution:* 15 μL Opti-MEM 0.1 μL Lipofectamine 3000	DNA-mix was added to diluted Lipofectamine which was priorly vortexed; incubated for 10 min at r/t
PEI	15 μL Opti-MEM Fluorescent Oligo (20 μM stock) 50 nM final 0.1 μL or 0.25 μL PEI	incubated for 10 min at r/t

2.8.5 Transfection of miRNAs

NIH-3T3 cells were transfected with 50 nM of a small RNA (miRNA mimics or siRNA) or the BLOCK-iT^{TM} Fluorescent Oligo. Mastermixes for 4 replicates per sample were prepared according to Table 2.9. Transfection mixes were pipetted into a 48-well plate just prior to adding 4.5 x 10^4 cells in 273 μL of complete medium per well. After ~24 h of incubation at 37 °C, cells were monitored using the fluorescence microscope (Leica DFC300G), FLUO-Filtercube FITC and LAS X software to take images.

2.8.6 Infection of transfected cells with MCMV

Transfected cells were infected to perform plaque assays in accordance with section 2.8.2. Aiming at ∼100 plaques per well, 1.1 μL of mutant MCMV (2.5×10^5 pfu/mL) and 4 μL of revertant MCMV (9.6×10^5 pfu/mL) were each diluted in 250 μL of DMEM media, supplemented with 10% NCS. Transfection mixes were aspirated and 200 μL of diluted virus inoculum was added per well to prepare two technical replicates per transfection sample and virus. Following 1 h of incubation at 37 °C, the viral supernatant was replaced by 500 μL of medium containing carboxymethyl cellulose (see section 2.8.2). After three days, mCherry protein expression was exploited as an infection marker to manually count the number of small and large virus plaques under the fluorescence microscope (Leica DFC300G, FLUO-Filtercube TXR, 5x objective). We defined small plaques by infected areas containing up to three red-appearing cells and distinguished them from large plaques comprising any higher amount of infected cells. Additionally, plaques were imaged using LAS X software.

Table 2.9: Transfection mastermixes used for transient expression of miR-m01-2 and miR-M23-2

Mastermixes for 4 wells of a 48-well plate	**Comments**
104 μL Opti-MEM 1.28 μL miR-m01-2 (50 μM stock, ∼50 nM final) 1.28 μL miR-M23-2 (50 μM stock, ∼50 nM final) 3.12 μL TransIT-X2	Opti-MEM and TransIT-X2 were warmed to r/t, the latter was further vortexed before usage. After finally adding TransIT-X2, samples were thoroughly mixed with 20 and 200 μL pipette tips and incubated for 25 min at r/t before transferring 4 times 27.2 μL of each mastermix into one well of a 48-well dish.
Positive control: 104 μL Opti-MEM 1.28 μL siRNA-IE3 (50 μM stock, ∼50 nM final) 3.12 μL TransIT-X2	
Tranfection control: 104 μL Opti-MEM 3.14 μL Fluorescent Oligo (20 μM stock, ∼50 nM final) 3.12 μL TransIT-X2	

Chapter 3

Results

3.1 Two MCMV miRNAs regulate the major viral immediate early protein IE3

3.1.1 Generation of the reporter p/PM-M23-2 encodes for the N1 sequence

Unlike all other psiCHECK2 vectors available for this study, the psiCHECK2 vector p/PM-M23-2△N1 did not contain the N1 sequence upstream of the firefly ORF, which enhances the expression of the latter (see section 2.1.4). Consequently, a new psiCHECK2 vector was generated featuring the N1 sequence at the 5' and the miR-M23-2 perfect match sequence at the 3' of the firefly ORF. To this end, a DNA segment containing the perfect match sequence of miR-M23-2 was amplified by PCR. The PCR amplified insert as well as the backbone p/IE3-3'UTR were digested by XbaI, gel purified, and cloned within bacteria. To confirm correct insertion, plasmids were sequenced after analyzing them by diagnostic restriction enzyme digest and gel electrophoresis (Figure 3.1). HincII cut p/IE3-3'UTR as well as the newly generated p/PM-M23-2, indicating that both plasmids contained the N1 sequence. In the presence of the perfect match sequence of miR-M23-2, the restriction enzyme pattern of EcoRV and EcoRI resulted in a specific 0.1kb band, which was visible in the case of p/PM-M23-2. As such, inserting N1 into p/PM-M23-2△N1 was successful.

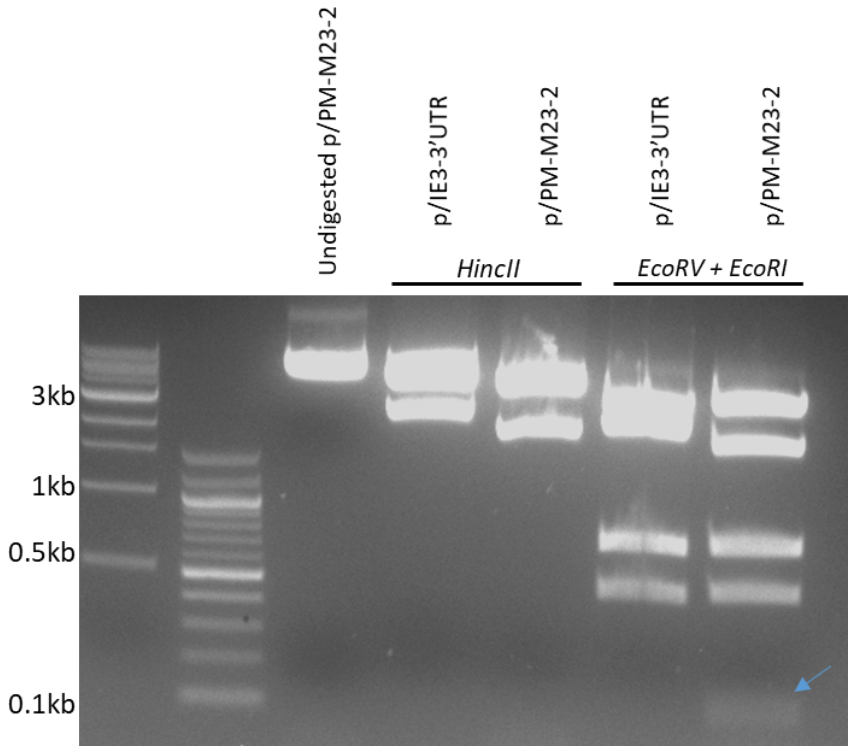

Figure 3.1: Restriction pattern analysis of the generated luciferase plasmid p/PM-M23-2. Restriction digests confirm the presence of N1 and the perfect match sequence for miR-M23-2 miRNA in p/PM-M23-2. The perfect match sequence of miR-M23-2 was PCR amplified using 3 ng of p/PM-M23-2△N1. The PCR product as well as the selected backbone, i.e. p/IE3-3'UTR, were digested by XbaI, ligated, and cloned in Stellar Competent cells. To confirm accuracy of the insertion reaction, diagnostic digests were performed using the restriction enzymes HincII as well as EcoRI and EcoRV. HincII cuts within the N1 sequence, while the cutting pattern of EcoRI and EcoRV proves the presence of the PM-M23-2 sequence.

3.1.2 MiRNA mimics downregulate luciferase activity of perfect match reporter constructs

Once the reporter p/PM-M23-2 was generated, we confirmed the functionality of our miR-m01-2 and miR-M23-2 mimics by testing their potency in downregulating firefly luciferase activity of target sensors containing perfect match bindings sites for miR-m01-2 and miR-M32-2 downstream of the firefly ORF. To this end, HEK/293T cells were co-transfected with reporters and miRNAs as listed in Table 3.1.

Results of dual luciferase assays showed that both the miR-m01-2 mimic (Figure 3.2 upper part) and the miR-M23-2 mimic (Figure 3.2 lower part) significantly repressed relative luciferase activity of their respective perfect match target sensors, but not of the other

Table 3.1: Co-transfected reporters and miRNAs used for validating the functionality of miR-m01-2 and miR-M23-2 mimics by luciferase assay

	miR-m01-2	miR-M23-2	scramble miRNA
p/PM-m01-2	x	x	x
p/PM-M23-2	x	x	x
p/empty	x	x	x

targeting vectors. Downregulation was ∼75% relative to the negative control experiments that were set to 100%.

3.1.3 Optimizing miRNA concentrations for transfection experiments

To analyze whether miR-M23-2 regulates IE3 via its 3'UTR, we performed a dose-response experiment in which two-fold serial dilutions of miR-M23-2 mimic (50 μM stock) were transfected with either p/IE3-3'UTR or the negative control p/IE3-3'UTR/mut-M23-2. We observed a significant decrease of relative luciferase activity using a miRNA mimic concentration of 50 nM (Figure 3.3). Interestingly, miRNA mimic concentrations higher than 50 nM did not lead to any increase in target downregulation, not even at 200 nM of miR-M23-2 mimic. On the basis of these results, the final concentration of transfected miRNA mimics and scramble miRNAs was always chosen to be 50 nM.

3.1.4 Validation of miRNA binding sites

In a second step, the regulatory activity of miR-m01-2 and miR-M23-2 mimics directed against the 3'UTR of IE3 was investigated by site-directed mutagenesis of the respective seed matches. We transfected the same set of miRNAs used in the positive control experiment (i.e. miR-m01-2, miR-M23-2 and scramble miRNA, see section 3.1.2) with reporter plasmids containing either the wild-type or mutated versions of the two miRNA binding sites within the IE3-3'UTR. Co-transfection mixes of respective reporters and miRNAs are listed in Table 3.2.

Our dual-luciferase assays confirmed that miR-m01-2 mimic (Figure 3.4 upper part), as well as miR-M23-2 mimic (Figure 3.4 lower part), significantly decreased firefly luciferase

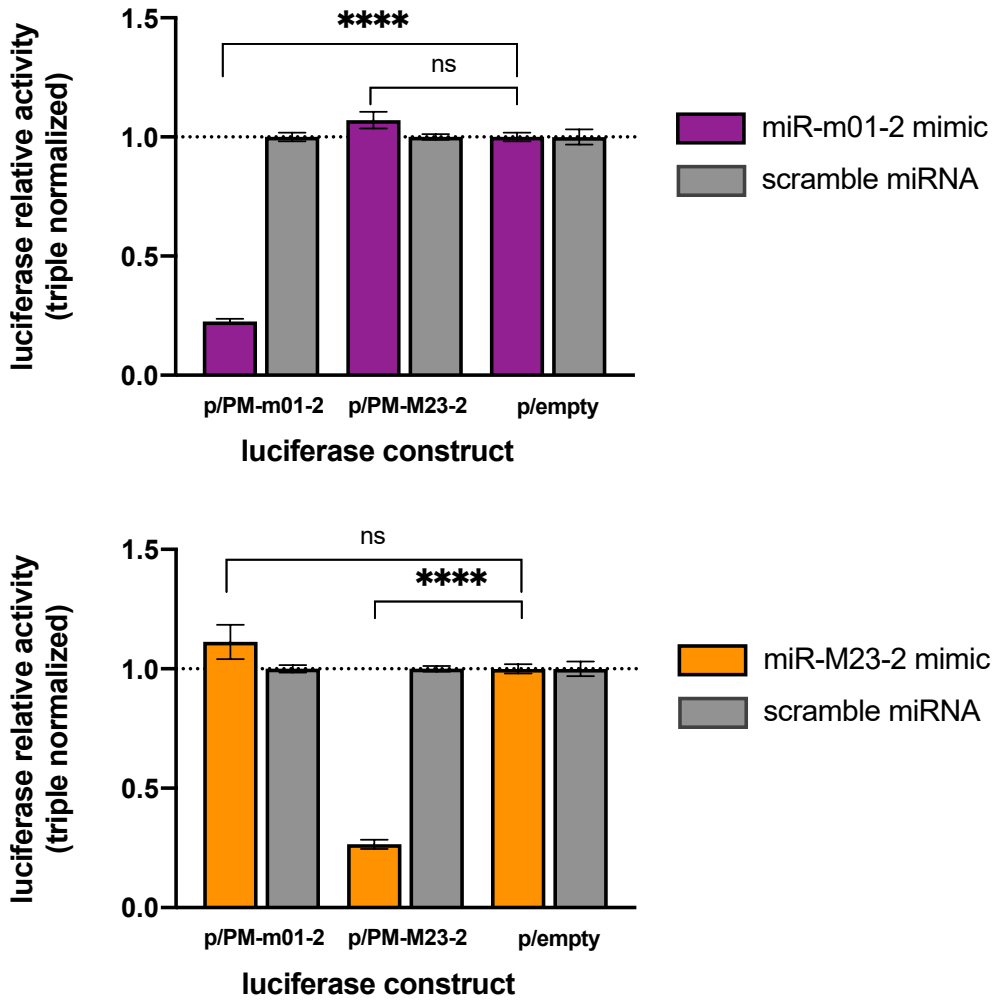

Figure 3.2: MiR-m01-2 mimic and miR-M23-2 mimic harbor silencing activity on target reporters in dual-luciferase assays. HEK/293T cells were co-transfected with miR-m01-2, miR-M23-2 or a negative control miRNA mimic and psiCHECK2 constructs. The latter contained either a perfect match binding site (for miR-m01-2 or miR-M23-2) or lacked any cloned sequences downstream of the firefly ORF (negative control). Triple normalized luciferase activity values were obtained by calculating firefly-to-Renilla ratios before setting averages of relative values of negative control samples to 1. All experiments were performed in triplicates, with n = 5 and n = 6 for miR-m01-2 and mir-M23-2 transfection, respectively. Data are represented as mean±SEM, ns $p > 0.05$; $^{****}p < 0.0001$.

activity of the IE3-3'UTR containing wild-type reporter similarly by ∼40% relative to activity values of the double mutated reporter.

The effects of miR-m01-2 and miR-M23-2 were further tested with single mutated reporter constructs (i.e. p/IE3-3'UTR/mut-m01-2 and p/IE3-3'UTR/mut-M23-2) in which the two miRNA target sites harbored point mutations individually. MiR-m01-2 decreased

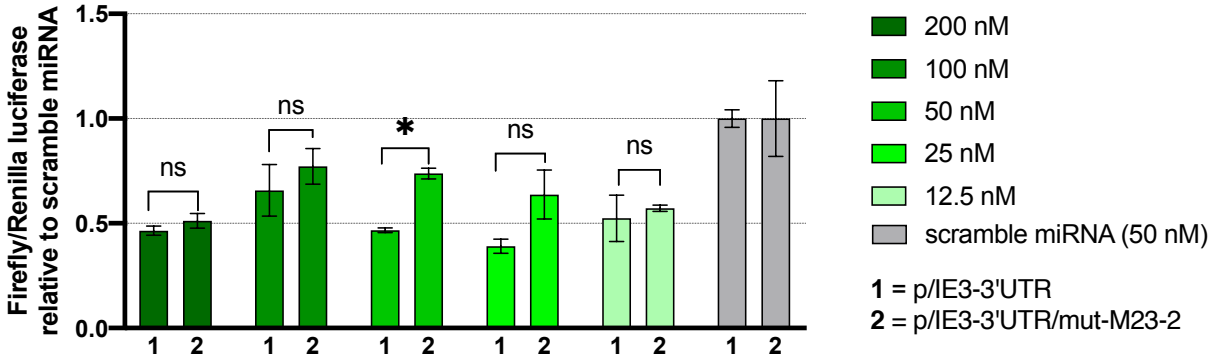

Figure 3.3: MiR-M23-2 regulates IE3 via its 3'UTR in a dose-dependent manner. A dual-luciferase assay was performed by co-transfecting HEK/293T cell with either p/IE3-3'UTR or p/IE3-3'UTR/mut-M23-2 and miR-M23-2 at the concentrations indicated. Double normalized activity values ± SEM from one transfection experiment are depicted (ns $p > 0.05$; $^*p < 0.05$).

Table 3.2: Co-transfected reporters and miRNAs used for validating target sites within the IE3-3'UTR by luciferase assay

	miR-m01-2	miR-M23-2	scramble miRNA
p/IE3-3'UTR (WT)	x	x	x
p/IE3-3'UTR/mut-m01-2	x	x	x
p/IE3-3'UTR/mut-M23-2	x	x	x
p/IE3-3'UTR/mut-m01-2/mut-M23-2	x	x	x

the relative luciferase activity of the reporter with a mutated miR-M23-2 binding site by ∼50% (Figure 3.4 upper part). Importantly, this effect was abrogated when using the reporter, containing mutations in the miR-m01-2 binding site. Analogous results were obtained for miR-M23-2 (Figure 3.4 lower part). Co-transfection of miR-M23-2 with the reporter containing a mutated seed match for miR-m01-2 (i.e. p/IE3-3'UTR/mut-m01-2) significantly lowered relative luciferase level (by ∼45%). By contrast, no significant reduction in luciferase level was observable when transfecting miR-M23-2 with the reporter holding a mutated seed sequence for miR-M23-2 (i.e. p/IE3-3'UTR/mut-M23-2). These observations confirm that the 3'UTR of IE3 is regulated by miR-m01-2 and miR-M23-2 which was previously indicated by an in silico analysis of a PAR-iCLIP dataset and miRNA target predictions.

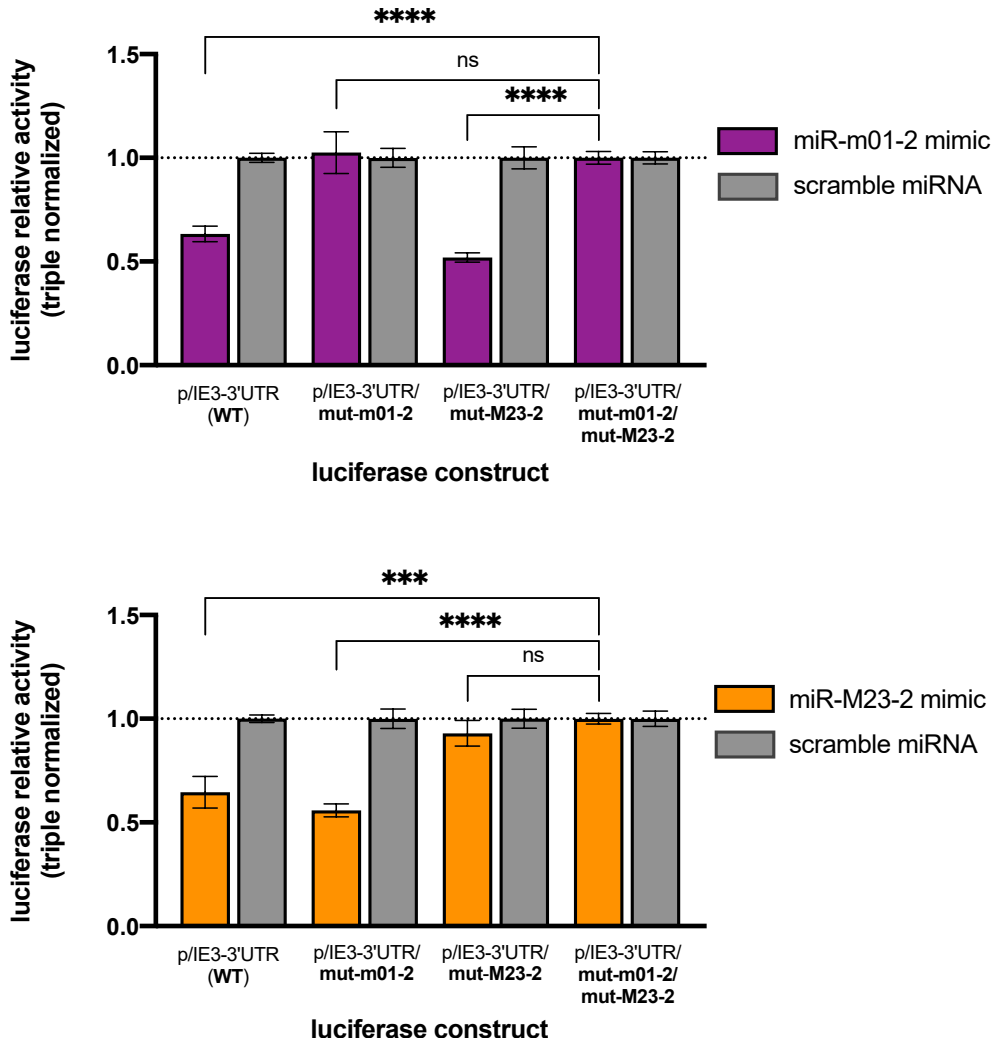

Figure 3.4: Both miR-m01-2 mimic and miR-M23-2 mimic target the IE3-3'UTR via single binding sites. HEK/293T cells were co-transfected with miR-m01-2 mimic, miR-M23-2 mimic, or scramble miRNA (a negative control miRNA), and a dual luciferase reporter system in which a recombinant firefly luciferase was fused with the wild-type or a mutant IE3-3'UTR sequence. Triple normalized luciferase activity values were obtained by calculating firefly-to-Renilla ratios before setting averages of relative values of negative control samples to 1. All experiments were performed in triplicates, with n = 4. Data are represented as mean±SEM, ns $p > 0.05$; $^{***}p < 0.001$; $^{****}p < 0.0001$.

3.2 Construction of NIH-3T3 cells expressing viral miRNAs

After demonstrating that both, miR-m01-2 and miR-M23-2 significantly decreased expression of a luciferase ORF fused to the 3'UTR of IE3 from psiCHECK2 plasmids, we wanted

to assess whether pre-expression of these miRNAs affects MCMV replication *in vitro*. We hypothesized that in the presence of miR-m01-2 and miR-M23-2, IE3 downregulation would hamper the lytic life cycle of MCMV as IE3 is an essential viral protein for lytic virus replication [9, 33]. We thus aimed to establish a murine cell line with constitutive expression of both viral miRNAs for subsequent viral infection experiments.

3.2.1 Generating and transducing pre-miRNA expressing lentiviral particles

Two oligonucleotides encoding for pre-miR-m01-2-3p and pre-miR-M23-2-3p with 10 nt of flanking region at each end, were inserted into an intron-containing eGFP gene expressed by the pLenti-Blast-eGFPintron vector. The vector was linearized by either NheI or NsiI treatment and gel purified. To work out optimal conditions for high plasmid output, ligation reactions were conducted using different vector-to-insert ratios. In detail, 50 ng of linearized pLenti-Blast-eGFPintron vector (around 10 kb in length) was mixed with either 0.5 ng, 1.5 ng or 5 ng of insert. Best transformation results were yielded when using 5 ng of insert (data not shown). Cloned and purified plasmids were subsequently analyzed by diagnostic digestion (Figure 3.5) and verified by DNA sequencing.

Once lentiviral particles were manufactured upon transfecting HEK/293T cells, NIH-3T3 cell lines were stably transduced for constitutive expression of miR-m01-2 and miR-M23-2. Three days post-transduction, NIH-3T3 cells were selected by Blasticidin treatment. The antibiotic concentration was chosen after performing a Blasticidin dose-response experiment, in which non-resistant NIH-3T3 cell line were treated with two-fold serial dilutions of Blasticidin, starting from 20 μg/mL. After 7 days of incubation, 10 μg/mL of Blasticidin was the minimal dose at which all cells were observed to be dead. Derived from this dose response experiment, transduced NIH-3T3 cells were cultured in 10 μg/mL of Blasticidin containing medium. Antibiotic concentration was reduced to 2.5 μg/mL once 100% cell death was observed in the control wells.

Upon Blasticidin selection, NIH-3T3 cells were sorted for high GFP signal. GFP expression was assumed to be positively correlated with high viral miRNA expression since miR-m01-2 and miR-M23-2 were inserted into the intron of an eGFP gene. An overview of generated NIH-3T3 cell lines is provided in Table 3.3.

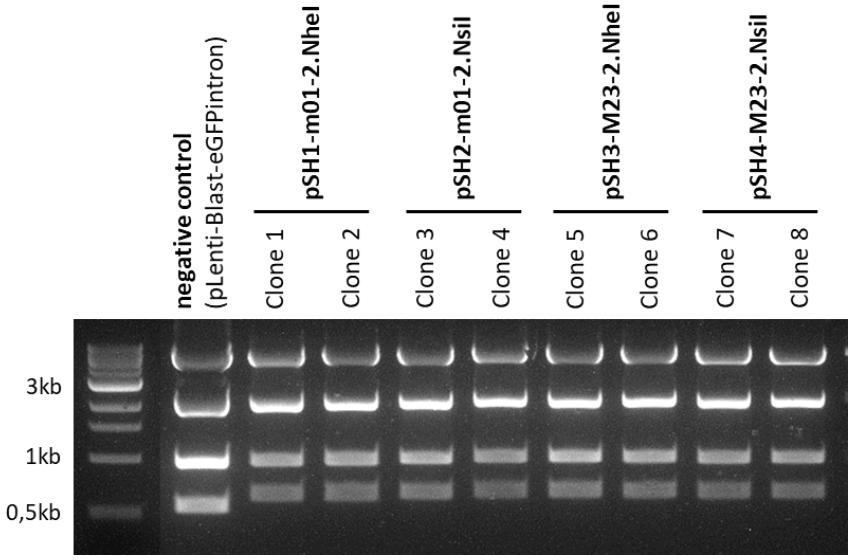

Figure 3.5: Restriction digests confirm the presence of pre-miRNAs cloned into the pLEnti-Blast-eGFPintron vector. pLEnti-Blast-eGFPintron vector was treated with NheI or NsiI prior to cloning either pre-miR-m01-2-3p and pre-miR-M23-2-3p into the linearized vector. In the scope of diagnostic digestion, samples were co-treated with KpnI and BamHI. Clones harboring the insert were identified by the smallest band at 0.7 kb. By contrast, the smallest fragment appeared at 0.6 kb in the case of the negative control.

3.2.2 Transduced NIH-3T3 cells lack expression of viral miRNAs

To check for functionally relevant miRNA expression, we investigated whether luciferase levels of psiCHECK2 reporters with perfect match binding sites for either miR-m01-2 or miR-M23-2 become downregulated by our generated stable cell lines. To this end, perfect match psiCHECK2 constructs, i.e. p/PM-M23-2 and p/PM-m01-2 (Table 2.1) were transfected into our stable cell lines. To include positive controls, transduced NIH-3T3 cell lines with the putative expression of miR-m01-2 miRNA (listed in Table 3.3) were co-transfected with miR-m01-2 mimic and the p/PM-m01-2 construct. Accordingly, transduced NIH-3T3 cell lines with expected expression of miR-M23-2 miRNA (listed in Table 3.3) were co-transfected with the miR-M23-2 mimic and the p/PM-M23-2 construct. Negative controls were transfected with the p/empty reporter lacking the IE3-3'UTR behind the firefly gene. Unfortunately, repression of relative firefly luciferase values was not observable in any of our tested cell lines (Figure 3.6) indicating that neither miR-m01-2 nor miR-M23-2 was expressed at functionally relevant levels in any of our transduced NIH-3T3 cells. A significant downregulation of the firefly luciferase was only seen in our positive controls where

Table 3.3: Transduced NIH-3T3 cell lines

Name	NIH-3T3 transduced with (see Table 2.2)	Potentially expressing (restriction site)
NIH-3T3.GFP. m01-2(NheI)	pSH1-m01-2.NheI	pre-miR-m01-2 (NheI)
NIH-3T3.GFP. m01-2(NsiI)	pSH2-m01-2.NsiI	pre-miR-m01-2 (NsiI)
NIH-3T3.GFP. M23-2(NheI)	pSH3-M23-2.NheI	pre-miR-M23-2 (NheI)
NIH-3T3.GFP. M23-2(NsiI)	pSH4-M23-2.NsiI	pre-miR-M23-2 (NsiI)
NIH-3T3.GFP. m01-2(NheI). M23-2(NsiI)	pSH5-m01-2.NheI-M23-2.NsiI	pre-miR-m01-2 (NheI) + pre-miR-M23-2 (NsiI)
NIH-3T3.GFP. M23-2(NheI). m01-2(NsiI)	pSH6-M23-2.NheI-m01-2.NsiI	pre-miR-M23-2 (NheI) + pre-miR-m01-2 (NsiI)
NIH-3T3.GFP	empty pLenti-Blast-eGFPintron	xxxxxxx

target sensors were co-transfected with respective miRNA mimics.

After luciferase assays had revealed the incapability of our transduced NIH-3T3 cells to effectively downregulate luciferase activity values from the perfect match vectors, we investigated cellular expression levels of precursor and mature forms of miR-m01-2 and miR-M23-2 miRNAs. To this end, total RNAs were extracted from five transduced NIH-3T3 cell lines and subjected to northern blots, using two radioactive, 5' ^{32}P-labeled probes with a sequence complementary to miR-m01-2 and miR-M23-2. MCMV-infected NIH-3T3 cells served as positive controls. Hybridization signals corresponding to miR-m01-2 and miR-M23-2 miRNAs and their respective precursor forms were detectable in the positive control (MCMV-infected cells) but were absent in each sample of the transduced NIH-3T3 cells (Figure 3.7). In conclusion, northern blot analysis demonstrated that miR-m01-2 and miR-M23-2 were not expressed from the eGFP-intron splicing system transduced into NIH-3T3 cells.

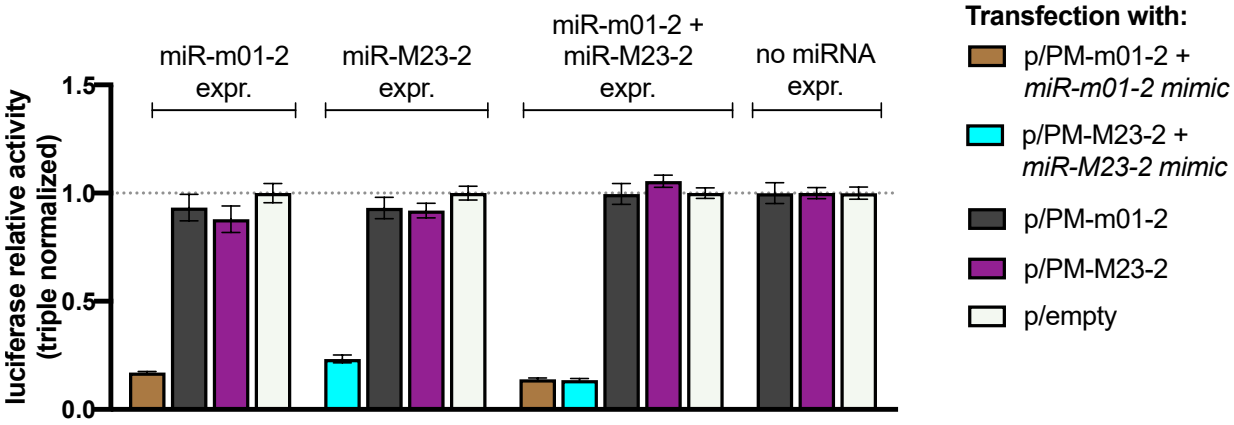

Figure 3.6: Transduced NIH-3T3 cells lack functionally relevant miR-m01-2 and miR-M23-2 expression. NIH-3T3 cells were lentivirally transduced to constitutively express miR-m01-2 and/or miR-M23-2 from an intron-containing eGFP gene. To test whether miR-m01-2 and miR-M23-2 are produced at functionally relevant levels, transduced cells were transfected with psiCHECK2 plasmids, containing a perfect match for miR-m01-2 or miR-M23-2 downstream of the firefly luciferase. Co-transfection with miR-m01-2 or miR-M23-2 mimics served as positive controls. In negative control experiments, transfection was performed using the p/empty psiCHECK2 construct (deprived of any miRNA binding site in the 3'UTR of the firefly gene). Negative control cell lines, transduced with an eGFP sequence element lacking any miRNA coding sequence, were further included in the experiments. Triple normalized luciferase activity values were obtained by calculating firefly-to-Renilla ratios before setting averages of relative values of negative control samples to 1. All experiments were performed in triplicates, with n = 2 (n = 1 in case of the positive controls). Data are represented as mean±SEM.

3.3 Functional analysis of miR-m01-2 and miR-M23-2 *in vitro*

As our transduced NIH-3T3 cells did neither express miR-m01-2 nor miR-M23-2 at any detectable levels (see section 3.2.2), we decided to transiently transfect miRNAs into NIH-3T3 cells prior to MCMV infection to check whether pre-expression of miR-m01-2 and miR-M23-2 affects the lytic life cycle of MCMV.

3.3.1 Comparative analysis of different transfection reagents and conditions

Before investigating the effect of miR-m01-2 and miR-M2-2 pre-expression prior to infection, we first aimed at optimizing the pivotal step of transfecting small RNA molecules (miRNAs and siRNAs) into NIH-3T3 cells. To this end, we tested three different transfec-

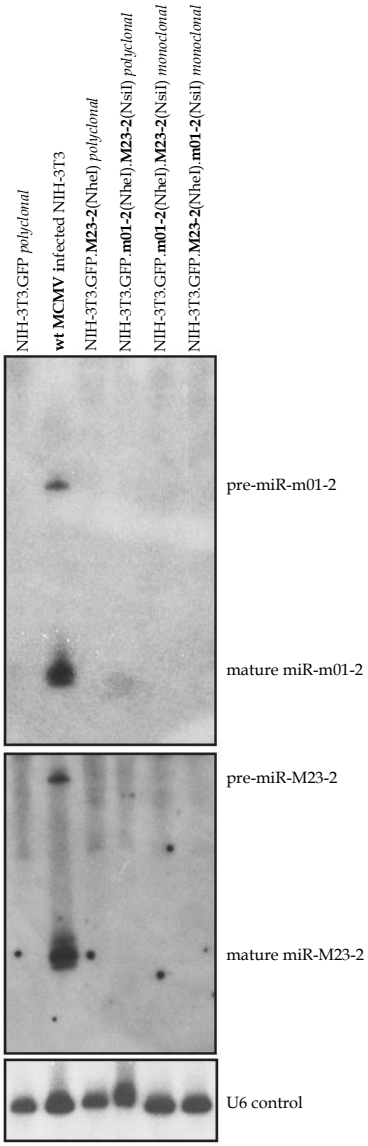

Figure 3.7: Northern blot analysis confirms that transduced NIH-3T3 cells are deficient in miR-m01-2 and miR-M23-2 expression. Total RNAs (30 ng), extracted from transduced and MCMV-infected NIH-3T3 cells using TRIzol, were separated on a 15% denaturing polyacrylamide gel and transferred to a nylon membrane. The latter was hybridized with a ^{32}P probe for miR-m01-2 and monitored after three days of incubation. Once the probe was removed from the membrane, the hybridization step was repeated with a ^{32}P probe for miR-M23-2. The small nuclear RNA U6 was finally probed to include a gel loading control.

tion reagents, including TransIT-X2, Lipofectamine 3000, and PEI for their applicability in delivering a fluorescent control into NIH-3T3 cells. Cells were imaged 24 h post-transfection to assess each reagent by its respective transfection efficiency and cytotoxicity.

Out of the three transfection reagents, TransIT-X2 clearly demonstrated the best results with regards to the transfection rates observed in NIH-3T3 cells (almost 100%, Figure 3.8 A). By contrast, fluorescence uptake was low and even not detectable in the case of Lipofectamine 3000 and PEI, respectively (Figure 3.8 B and C). We further observed by light microscopy that PEI was very toxic to the cells causing detrimental changes in the cell morphology, including cell rounding and shrinkage (Figure 3.8 C). As expected, lower concentrations of PEI rescued the cells, nevertheless, not a single cell was observed to turn green (data not shown). TransIT-X2 and Lipofectamine 3000 both showed only mild cytotoxicity (Figure 3.8 A and B).

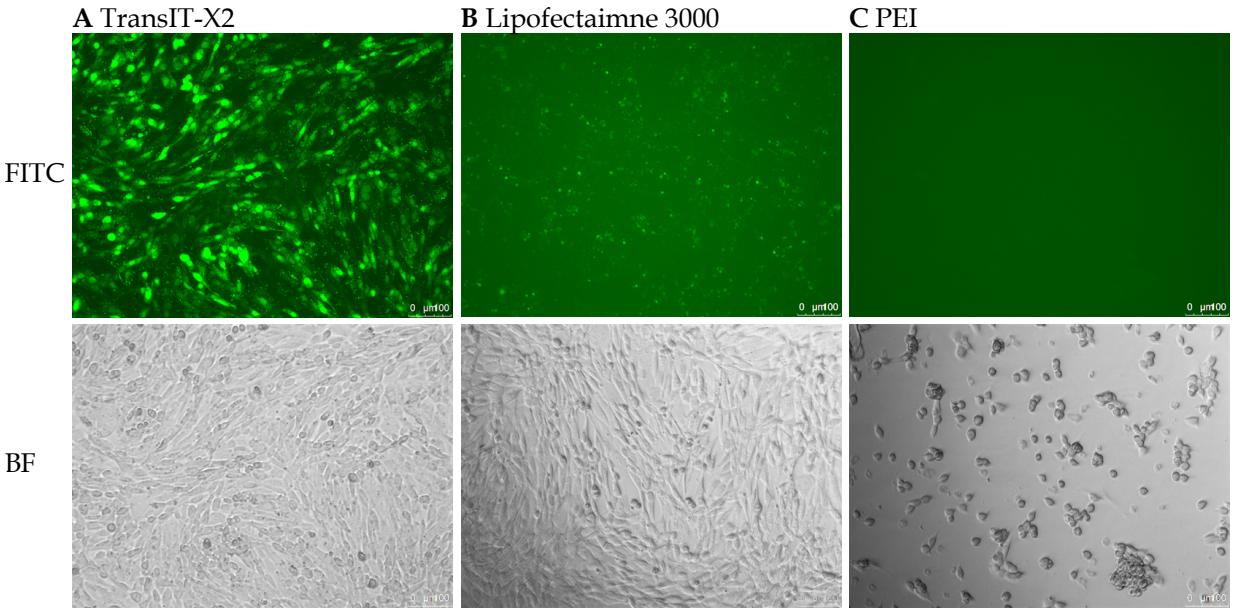

Figure 3.8: Transfection efficacy and cytotoxicity of three different transfections reagents. Freshly trypsinized NIH-3T3 cells were reverse transfected with either 0.78 μL of TransIT-X2 (**A**), 0.1 μL of Lipofectamine 3000 (**B**), or 0.25 μL of PEI (**C**), together with a fluorescent dsRNA (BLOCK-iT^{TM} Fluorescent Oligo, 50 nM final) in a 48-well plate. 24 h post-transfection, cells were monitored by light and fluorescence microscopy. PEI = polyethylenimine, FITC = fluorescein isothiocyanate, BF = bright field.

Interestingly, while the manufacturer Thermo Fisher claims that the fluorescence uptake can be assessed as early as 6 h post-transfection [208], we experienced that even after 12 h, the transfection efficacy of TransIT-X2 is prone to be highly underestimated. 12 h post-transfection, transfected fluorescent oligos were predominantly found within small aggregates (Figure 3.9 A). By contrast, 24 h post-transfection, these clump-like structures became almost fully resolved rendering transfected cells entirely green. Consequently, we used the latter time point henceforth for monitoring the cells and evaluating the trans-

fection rate. Besides, we could not show that the addition of a non-coding carrier DNA improves throughput transfection efficiency using TransIT-X2 (Figure 3.9 B) as it was reported for PEI by Pradhan et. al [209]. We further investigated the effect of passage number on the transfectability of NIH-3T3 cells by comparing cell cultures of low and high passage numbers. In contrast to early-passage cells, which showed a homogeneous uptake of fluorescence, transfectability of late-passage cultures was found to be highly variable between cells (Figure 3.9 C). Interestingly, while some high-passage cells shone brightly green, several others within the same culture did not take up any of the fluorescence signals at all. We thus used low-passage cells for all future experiments. Additionally, we employed a repetitive transfection protocol to compare transfection efficiencies between cell cultures that were transfected either only once or a second time 12 h after the first transfection step. Of note, we did not find any significant difference in the number of transfectants between the samples (data not shown).

Overall, we optimized the transfection procedure of small RNA molecules into NIH-3T3, by first employing TransIT-X2 as transfection reagent, second using low-passage cultures in good conditions, third dropping the ideas of repetitive transfection and co-transfection with non-coding carrier DNA and last but not least, assessing transfection rates, not at any time point earlier than 20 h post-transfection.

3.3.2 Pre-expression of miR-m01-2 and miR-M23-2 affects the lytic replication cycle of MCMV

In previous studies, an IE3 dual miRNA binding site mutant and its revertant MCMV were generated [198]. While the mutant virus harbored point mutations at both respective seed sites of miR-m01-2 and miR-M23-2 within the IE3-3'UTR, the wild-type sequence was reconstructed in the case of the revertant virus. We passaged mutant and revertant MCMVs several times to establish MCMV stocks of adequate viral titer for subsequent infection experiments. Viral infectivity of generated virus inocula was determined by counting plaques using fluorescence and light microscopy 3 days after infecting NIH-3T3 cells. Once mutant and revertant MCMV stocks of adequate virus titer had been produced, viral DNA was purified to amplify a fragment of ∼1200 nt covering the 3'UTR of IE3, which was sent for sequencing. The accuracy of the constructs was hence confirmed.

To determine whether pre-expression of miR-m01-2 and miR-M23-2 affects the initiation of the lytic cycle *in vitro* by downregulating IE3 promptly after infection, NIH-3T3 cells

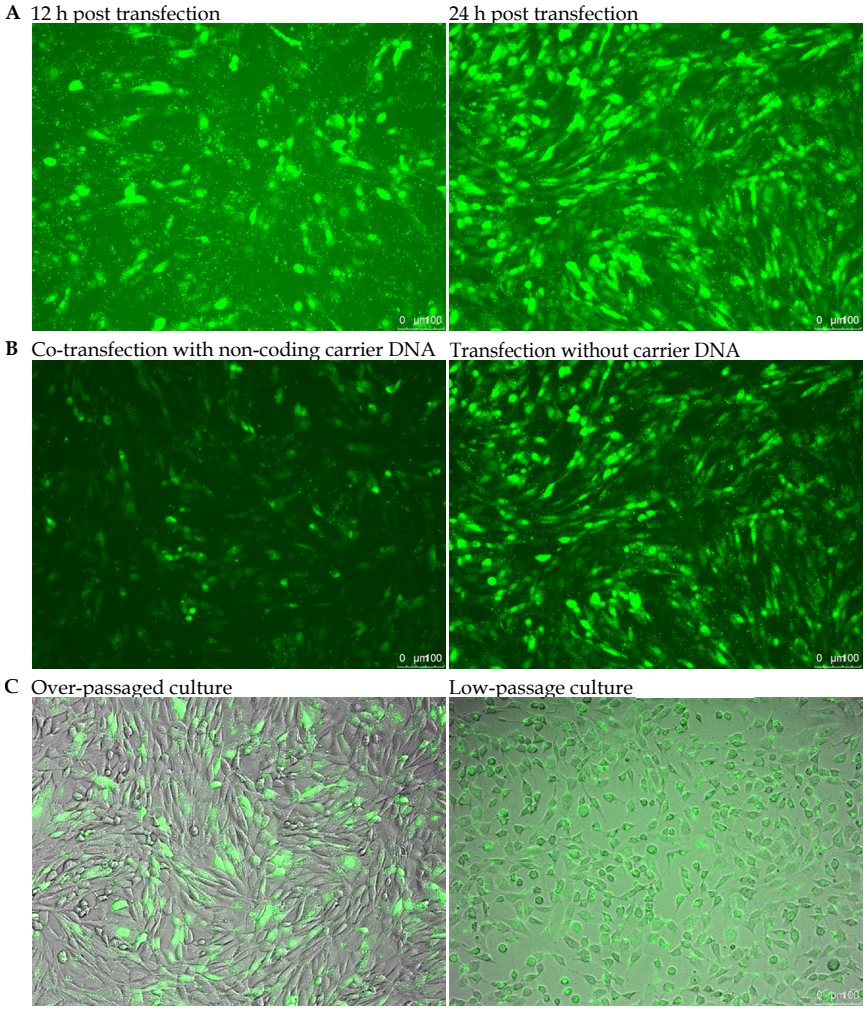

Figure 3.9: Optimization of transfection conditions in NIH-3T3 cells using TransIT-X2. Trypsinized NIH-3T3 cells were reverse transfected with BLOCK-iT^{TM} Fluorescent Oligo (50 nM final concentration) in wells of a 48-well plate using 0.78 μL of TransIT-X2. **A** Fluorescence uptake after 12 h and 24 h post-transfection. **B** Carrier DNA impairs transfection efficiency. 260 ng of pBAD-mTag-BFP plasmid was co-transfected with the fluorescent dsRNA oligo (left). By contrast, transfection of the fluorescent oligo alone is seen on the right side. Imaging was performed 24 h later. **C** Bright field overlay showing passage-related differences. NIH-3T3 at very high (left) and fairly low passage levels (right) were transfected to analyze the impact of cell culture-related factors on transfection efficiency 24 h later.

were transfected with either 50 nM of miR-m01-2 and miR-M23-2 or one out of two control dsRNAs (i.e. siRNA-IE3 or fluorescent oligo). Transfection of siRNA-IE3, which is a small interfering RNA targeting the IE3-3'UTR in between the two miRNA binding sites (not affected by point mutations), was taken as a positive control for IE3 knockdown. Using a fluorescent oligo of arbitrary sequence served as a control to assess transfection efficiency

24 post-transfection. In case of confirmed high transfection rates (> 70%), the infection experiment was continued by incubating the cells in mutant or revertant MCMV-containing media for 3 days. Plaque formation was finally monitored by counting the number of plaques. We defined areas comprising up to three infected cells as 'small plaques' and distinguished them from 'large plaques' containing four or more infected cells.

Pre-expression of miR-m01-2 and miR-M23-2 had no observable effect on the number of plaques arising from the mutant MCMV as compared to the counted number of plaques resulting from transfecting a fluorescent control oligo and using the mutant virus for infection (Figure 3.10, left side of A). By contrast, inoculating miRNA pre-expressing cells with the revertant MCMVs resulted in a significantly lower number of plaques as compared to the respective control (Figure 3.10, right side of A). Transfection of siRNA-IE3 (which targets the IE3-3'UTR in between the miRNA binding sites) significantly repressed the number of plaques from both, the MCMV mutant and revertant virus (Figure 3.10 A) as compared to the controls. Of note, miRNA pre-expression was most evident in reducing the number of large plaques (Figure 3.10 B), while the number of small plaques remained unaffected (Figure 3.10 C).

Taken together, we demonstrated that mutant MCMV, which harbored mutations in the seeds of both viral target sites within the IE3-3'UTR, was resistant to pre-expression of miR-m01-2 and miR-M23-2 *in vitro*. By contrast, miR-m01-2 and miR-M23-2 interfered with the replication cycle of the revertant virus, reducing both plaque number and size. Of note, the number of small plaques in wells transfected with both miRNA mimics or fluorescently labeled oligo were similar in the case of the mutant and revertant virus, indicating that pre-expression of both miRNA mimics did not completely block infection but rather delayed it.

3.3.3 Luciferase assays confirm the effect of siRNA-IE3 on wt and mutated IE3 transcripts

In contrast to both miRNA mimics of miR-m01-2 and miR-M23-2, siRNA-IE3 was capable of effectively impeding lytic infection not only of the revertant MCMVs but also of the mutant viruses (Figure 3.10). By dual luciferase assays, we further validated the observed siRNA-IE3-mediated downregulation of mutated IE3 transcripts (Figure 3.11). We co-transfected HEK/293T cells with 50 nM (final concentration) of either siRNA-IE3, miR-m01-2 mimic (which shares its seed region with siRNA-IE3) or scramble miRNA with the

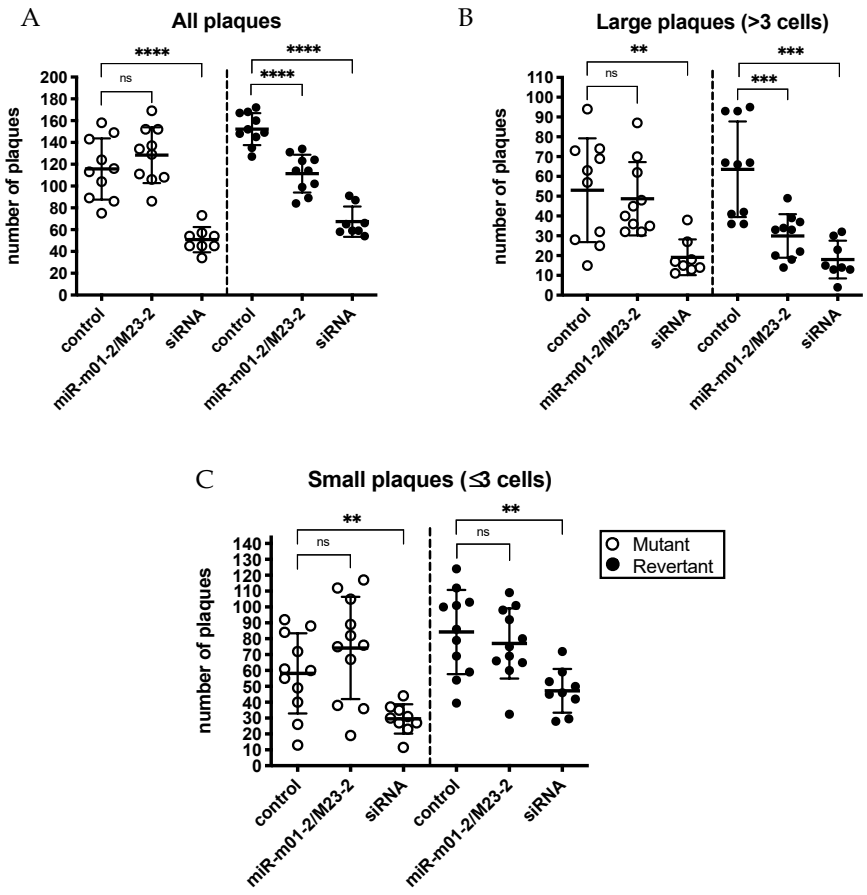

Figure 3.10: Fluorescence plaque count phenotypically characterizes mutant MCMVs by plaque assay. Scatter plots depict relative numbers of manually counted plaques three days post-infection by fluorescence microscopy. 24 h prior to infecting NIH-3T3 cells with either mutant or revertant MCMVs, cells were transfected with 50 nM of miR-m01-2 and miR-M23-2 mimics using TransIT-X2. In case of the negative and positive controls, cells were transfected with 50 nM of BLOCK-iT^{TM} Fluorescent Oligo and 50 nM of siRNA targeting IE3, respectively. Plaques comprising more than three infected cells (i.e. large plaques, see **B**) were discerned from small plaques containing less than three infected cells (see **C**). All experiments were performed in duplicates, with n = 10 (n = 8 for siRNA transfected samples). Horizontal bars represent the mean number of plaques ±SD, $^{**}p < 0.01$; $^{***}p < 0.001$; $^{****}p < 0.0001$.

plasmids listed in Table 3.4.

Transfection of siRNA-IE3 led to a significant decrease in firefly expression from either psiCHECK2 vector with the wt or double mutated IE3-3'UTR fused to the reporter gene. By comparison, the miR-m01-2 mimic, featuring an overlapping target region with siRNA-IE3, was not able to downregulate firefly transcripts fused to the double mutated version. Thus, by targeting a 22 nt segment within the IE3-3'UTR, flanked by miR-m01-2 and miR-M23-2 binding sites at its 5' and 3' ends, the RNA interference process was still successful

Table 3.4: Transfection mixes used for validating the regulatory effect of siRNA-IE3 on wild-type and mutated IE3 transcripts

	siRNA-IE3	miR-m01-2	scramble miRNA
p/PM-m01-2	x	x	x
p/empty	x	x	x
p/IE3-3'UTR (wt)	x	x	x
p/IE3-3'UTR/mut-m01-2/mut-M23-2	x	x	x

even when siRNA-IE3 was not fully complementary to the target strand in case of the mutant MCMVs. This was not unexpected, as the siRNA seed region, lying in between the two miRNA binding sites, remained unaffected by the inserted point mutations. We hence confirmed that in contrast to miR-m01-2 mimic, siRNA-IE3 effectively silences both wt as well as mutated IE3 transcripts, which is in accordance with our observations in the plaque assays (see section 3.3.2).

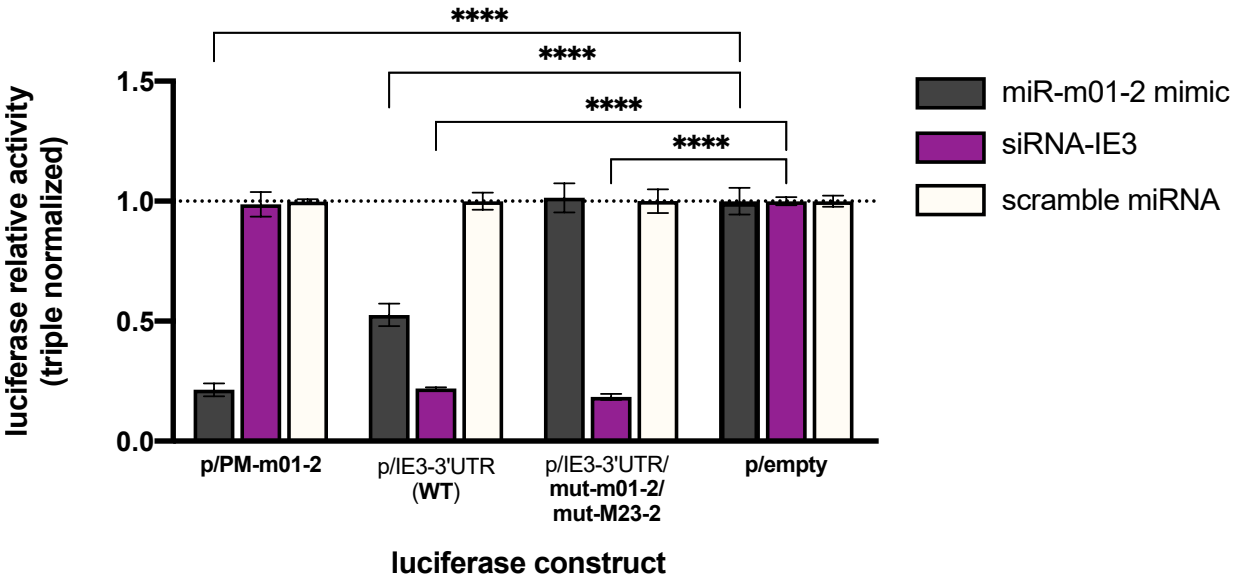

Figure 3.11: SiRNA-IE3 effectively blocks expression of both, wt and mutated IE3 transcripts. HEK/293T cells were reversely transfected using TransIT-X2. 50 nM of either siRNA-IE3, miR-m01-2 mimic or scramble miRNA was co-transfected with 1 μg of psiCHECK2 plasmid containing either no, wt, or double mutated IE3-3'UTR or miR-m01-2 perfect match (PM) sequence behind the firefly ORF. Luciferase readouts were measured 16 h post-transfection and triple normalized to respective values of Renilla activity, p/empty, and scramble miRNA. All experiments were performed in triplicates, with n = 2. Data are represented as mean±SEM, $^{****}p < 0.0001$.

Chapter 4

Discussion

In this study, we demonstrated that two virus-encoded miRNAs, i.e. mcmv-miR-m01-2-3p and mcmv-miR-M23-2-3p (abbreviated as miR-m01-2 and miR-M23-2) are able to specifically repress expression of IE3, an immediate early gene that constitutes the major viral transcription factor of MCMV. We validated that IE3 is subjected to translational repression via two miRNA binding sites located in the 3' UTR of the IE3 mRNA. Finally, we observed a significant reduction of plaque formation and a delay in successful viral replication in infected cells that pre-expressed miR-m01-2 and miR-M23-2 mimics. Owing to the paucity of any applicable antibody against IE3, we did not perform a western blot to directly test for the effect of miR-m01-2 and miR-M23-2 transfection on IE3 protein production. However, considering that IE3 takes an indispensable role in coordinating viral gene expression and inducing efficient replication [9, 33], we conclude that reduced viral infectivity correlates with inadequate levels of IE3 protein during lytic infection. MCMV thus employs viral miRNAs to regulate one of its major immediate early genes similar to HCMV that expresses miR-UL112-1 inhibiting IE72. Our results allow for further research using an animal mouse model to determine the regulatory role of viral miRNAs targeting immediate early genes which is a conserved feature in herpesviruses.

4.1 Validation of miRNA targets by dual luciferase reporter assays

We performed luciferase assays to validate two putative miRNA binding sites that were previously identified by PAR-iCLIP experiments and predicted to be targeted by miR-

m01-2 and miR-M23-2 using RNAhybrid for miRNA target prediction [198]. Luciferase assays are highly appreciated screening tools for miRNA-mRNA target site interactions by analyzing the capability of miRNAs to reduce translation of a recombinant reporter gene. Nevertheless, luciferase assays do not replace experiments, such as PAR-iCLIP that identify the physiological interaction between the miRNA and corresponding mRNA target. A critical caveat of reporter assays is the usage of miRNAs at supra-physiological levels that may artificially facilitate binding to a complementary sequence and hence induce a non-physiological downregulation of the latter culminating in misleading results [53, 154]. Furthermore, testing miRNA binding for functionality in different cells may result in divergent data due to the influence of varying environmental factors [154]. This issue can be bypassed by including control experiments that allow for appropriate normalization (discussed below). Additionally, reporter systems are highly sensitive to imprecise pipetting, complicating the achievement of reproducible results. However, owing to the paucity of better alternatives, we employed luciferase assays and accepted the need for repeating the reporter experiments multiple times.

In general, correct interpretations of luciferase data require a set of controls, including transfections of modified luciferase vectors and non-targeting scramble miRNAs [206]. Control reporter plasmids allow for analyzing the degree to which luciferase reporter transcripts are controlled specifically by their downstream miRNA binding sites. They usually carry either no or a mutated miRNA target site. Additionally, all reporter plasmids should be co-transfected with scramble miRNAs to normalize for any cellular factors that exert control on the translation of the reporter transcripts. Accordingly, we employed four control luciferase plasmids in total, two with point mutations in a single binding site within the IE3-3'UTR, one with mutations in both binding sites, and one which lacked the entire 3'UTR. Moreover, we made use of a scramble miRNA. Thereby, we could convincingly show that two abundant MCMV miRNAs target the IE3 transcript via two closely positioned miRNA binding sites. These results validated the identified PAR-iCLIP clusters.

4.2 Multiple targeting: Cooperative vs. independent target repression by miRNAs

In 2003, Doench et. al gave the first evidence that different miRNAs can have synergistic effects on mutual targets [143]. Accordingly, several groups reported their observation

that pairs of miRNAs can cooperate in silencing genes that feature more than one miRNA binding site [111, 210, 211]. It has hence become clear that target site efficacy not only depends on base pair complementarity between miRNA and mRNA but is further dictated by the contextual surroundings [212]. Moreover, in the absence of a cooperative miRNA (or its binding site, e.g. in a reporter), an effective target site may become weaker or even nonfunctional. Interestingly, cooperative interactions help fine-tune the regulatory role of miRNAs to precisely adapt gene expression to different conditions via patterns of miRNA expression [143].

Seastrom et al. suggested that the phenomenon of cooperative regulation is likely to occur when the distance of two binding sites ranges between 13 and 35 nt [211]. The seed target sites of miR-m01-2 and miR-M23-2 in the 3'UTR of IE3 are separated by only 11 nt. Considering Seastrom's study [211], miR-m01-2 and miR-M23-2 might hence supplement each other rather than work in concert to suppress translation of IE3. This hypothesis is consistent with the results of our luciferase assays demonstrating that miR-m01-2 and miR-M23-2 mimics downregulate expression of IE3 independently of one another without enhanced effectiveness when transfected together (data not shown). However, an enigmatic question arises regarding the motivation for having two miRNAs with equal regulatory effect on IE3 translation that obviously lack cooperativity and are similarly expressed with early kinetics [177]. A simple explanation might be provided by the principle of functional redundancy, which has already been reported for cellular and plant miRNAs [213, 214].

4.3 Caveats of miRNA overexpression: Transient transfection vs. stable transduction

4.3.1 Transient viral miRNA overexpression

Transfection of viral miRNA mimics is a simple and convenient methodology that allows for transient expression of non-endogenous miRNAs. This approach can be valuable in the scope of functional miRNA analysis during virus infection. However, achieving overexpression of viral miRNAs via transfection of chemically modified, double-stranded miRNA mimics is associated with some limitations that need to be taken into consideration.

First, concentrations of transfected miRNA mimics quickly decrease, not only due to cell division, but also as a result of intracellular, enzymatic degradation processes leading to

a fairly limited half-life of transfected miRNAs [215]. Consequently, transient transfection of miRNA mimics might be inapplicable, particularly, in case of long-lasting experiments which require rather constant delivery of miRNAs [216]. We transfected miRNAs 24 h prior to infection and scheduled analysis of the plaque assays as early as three days post-infection to avoid any dramatic drop in transfected miRNA concentrations that would have unleashed the effects of miRNA interference. Interestingly, in some cells that had been transfected with miR-m01-2 and miR-M23-2, we did not observe a complete block but rather a delay of virus infection, which is possibly attributed to a continuous decrease in miRNA concentrations until viral replication was finally successful.

Second, transfection-mediated cellular toxicity is another common challenge that requires the appropriate choice of transfection reagent for successful completion [217]. In this regard, highly efficient miRNA delivery must be balanced against the maintenance of cellular integrity to not torpedo subsequent experiments, such as viral infections and plaque assays that we performed 24 h post-transfection. In fluorescence image-based assays, we tested for transfection efficacy of three synthetic transfection reagents, including TransIT-X2, Lipofectamine 3000, and PEI in NIH-3T3 cells and determined their respective cellular toxicity by light microscopy. Our results identified TransIT-X2 as most suitable for transfecting dsRNA oligomers into NIH-3T3 cells, by achieving transfection rates of ∼100% together with only mild cytotoxicity. By contrast, Lipofectamine 3000 and PEI showed much lower transfection efficacies (∼30% and 0%, respectively) and very high cytotoxicity in the case of PEI. Inconsistent with our findings, Wang et. al reported a positive correlation between the transfection efficacy of different reagents with their respective cellular toxicity [217]. However, TransIT-X2 was not included in their studies and according to the manufacturer (Mirus Bio), this company explicitly optimizes their product formulation for low cytotoxicity [218].

Moreover, transfection efficacy is also determined by several cell-related aspects, including cell type, passage number, seeding density, and health of cells [219, 220]. Accordingly, we showed that transfection of extensively passaged NIH-3T3 cells leads to a high degree of intercellular variability in the uptake of fluorescent dsRNA. By contrast, a uniform distribution of the latter was observed when transfecting NIH-3T3 cells of low passage number.

Taken together, overexpression of miRNAs via transient transfection is limited by various factors, such as the cell culture as well as the selected transfection reagent which altogether determines transfection efficacy, cytotoxicity, as well as degradation and dilution effects of

the transfected mimics. Consequently, optimizing the transfection procedure cell lab dependently, prior to the main experimental project was a prerequisite for conducting our experiments successfully. The downsides accompanied by transfection assays can be alternatively bypassed via stable transduction of cell lines yielding an ectopic but constitutive overexpression of miRNAs. However, we failed to achieve efficient viral miRNA expression with the vector system we employed (see below).

4.3.2 Constitutive miRNA overexpression

Aiming at engineering NIH-3T3 cell lines with stable expression of miR-m01-2 and miR-M23-2, we exploited an eGFP-intron splicing system that intronically encoded for miR-m01-2 and miR-M23-2 within the eGFP ORF. As such, eGFP was expressed from two segments, separated by a synthetic, miRNA encoding intron. A crucial aspect of this approach is the ability to correlate the reporter signal with the event of successful mRNA splicing which releases the intronically-encoded miRNA [221]. Consequently, linking eGFP signals to miRNA expression levels confers the opportunity to maximize the effect of RNA interference via sorting for cells featuring the highest eGFP levels [222]. Furthermore, by placing miRNA encoding sequences inside an intron instead of directly fusing them to the marker gene, we decreased the risk of hampering eGFP translation by Drosha mediated 5' decapping and 3' poly-A-tail trimming during pri-miRNA procession [223].

In luciferase assays, we tested transduced NIH-3T3 cells for successful production of mature miR-m01-2 and miR-M23-2. However, suppression of the firefly reporter signal was not observable when using psiCHECK2 constructs containing perfect match sequences fused to the firefly ORF. We further conducted northern blots to detect any expression levels of precursor and mature miR-m01-2 and miR-M23-2. Each of our samples was negative except for the positive controls, indicating that our eGFP-intron splicing system was not functional, although it was reported to work [205].

The flanking sequences of pri-miRNAs are paramount to ensure precise excision and subsequent efficient procession into pre-miRNAs by Drosha [72, 224]. Consequently, the sequence motif of the miRNA stem-loops should be cloned together with the flanking sequences of their natural pri-miRNAs. Although different lengths of the flanking stretches, ranging from 15 nt [225] to 118 nt [166] in the case of miR-30 proved beneficial for processing, it can be assumed that 40 nt of 5' and 3' flanking sequences are generally sufficient for successful maturation of cloned miRNAs [226, 227]. By contrast, we used pre-miRNA

sequences of miR-m01-2 and miR-M23-2 with flanking segments that were as short as 10 nt. We assume that 10 nt of flanking sequence was not sufficient to facilitate folding into appropriate secondary structures, thereby preventing Drosha from properly recognizing and accessing the natural cleaving sites. We believe that including longer flanking sequences would have been more promising in achieving ectopic miRNA overexpression.

Furthermore, by using a lentiviral-based eGFP-intron splicing system, one must be aware that the genome of lentiviruses is single-stranded RNA. In this regard, insertion of the miRNA containing intron in the sense orientation of a double-stranded, lentiviral vector will most likely lead to a loss of the intron. Degradation of the intron prior to genomic integration results from splicing events after polymerase II transcription. Placing the intron inside the antisense strand rescues the intron and bypasses this problem [228, 229]. Accordingly, our lentiviral vectors encoded for the intron-containing eGFP genes in negative-sense orientation.

4.4 MiRNA-mediated fine-tuning of IE3 expression

Given their pivotal role in particular during the initial phase of lytic infection, the expression of IE genes is supposedly strictly regulated to adjust IE protein levels to the mode and time point of the viral life cycle. For HCMV, IE72 was shown and confirmed to be targeted in its 3'UTR by the virus-encoded miR-UL112-1 [178, 194]. Correspondingly, we demonstrated that the 3'UTR of the major transcription factor IE3 in MCMV is targeted by miR-m01-2 and miR-M23-2. It is tempting to speculate that these viral miRNAs exert their repressive effects primarily during the establishment and maintenance of latency or reactivation thereof. Viral latency is associated with a suppressed transcription program that is critical to evade the host's immune system. Profound suppression of immediate early gene expression during latent carriage has been reported to prevent clearance by T-cells. In healthy HCMV-infected individuals, >10 % of CD8+ T-cells were shown to be IE72-specific [230], necessitating a robust control of IE72 expression during latency to prevent recognition and killing by CD8+ T-cells. Multiple viral suppressor proteins have been reported to downregulate IE expression in a concerted action during latency [231]. However, repression might still be leaky resulting in a low-level IE expression that requires additional repressive regulators, such as miRNAs. In this way, HCMV miR-UL112-1 was suggested to fine-tune IE72 expression during latency [232]. Correspondingly, robust suppression of the major transcription factor IE3 may be achieved by the two viral miRNAs miR-m01-2

and miR-M23-2, thereby effectively downregulating viral gene expression during latency and attenuating the immune system thereof. Furthermore, miRNA-mediated fine-tuning of IE3 gene expression may sufficiently inhibit MCMV reactivation upon weak stimuli. Expression of MCMV miR-m01-2 and miR-M23-2 may therefore necessitate stronger stimuli for MCMV reactivation.

Attenuating IE gene expression by miRNAs constitutes a conserved feature of many herpesviruses, suggesting its evolutionary relevance. No animal model has so far been available to evaluate this generalized characteristic *in vivo*. By demonstrating that MCMV miRNAs target IE3, future research on the role of miRNA-mediated IE regulation in herpesviruses can now be performed in a murine mouse model *in vivo*. This is of particular importance, as studies with viral deletion mutants indicated that a great number of CMV genes are dispensable for virus growth *in vitro*. Yet, many of these genes were proven to be pivotal for viral fitness *in vivo* as they affect the immune system of the infected hosts [175, 233, 234]. Such being the case, the importance of miRNA-regulated IE gene expression for controlling latent infection and reactivation can only be adequately addressed in a suitable *in vivo* model system.

Recently, we published data obtained by *in vivo* studies on IE3 expression during acute infection [198]. To summarize, we observed no difference in viral fitness between wild-type MCMV and its IE3 dual miRNA binding site mutant strain. Experiments with mice were conducted in a pathogen-free environment. This is of particular importance, as CMVs replicate particularly in the presence of other pathogens that induce an inflammatory response in the host. *In vivo* studies that are performed in a less sterile environment allowing for co-infections with other pathogens, might likely attribute a greater impact of IE3 on viral fitness [198].

4.5 Intercellular exchange of viral miRNAs

Curiously, miRNAs are exchanged between cells, potentially to mediate cell-cell communication [235, 236, 237]. The mechanism of horizontal transfer of mature miRNAs frequently involves exosomes, which are nanometer-sized, spheroid-shaped membrane vesicles that evolve from the endoplasmic reticulum and are secreted into the extracellular space by many eukaryotic cells [238, 239]. Interestingly, virus-infected cells not only cargo cellular but also viral miRNAs. Research on EBV and KSHV has revealed that both γ-herpesviruses exploit the cellular exosome-production machinery to actively secret their

own miRNAs [240, 237]. Since MCMV expresses several miRNAs at very high levels [172], it is tempting to speculate that miRNA abundance is aimed at functional miRNA transfer to prime the environment. As such, miR-m01-2 and miR-M23-2, which accumulate to great abundance at early times of MCMV infection, may well be secreted to modulate prospective infection circles in close recipient cells. Following the notion that naked DNA entering the cell gets initially transcribed until DNA silencing or degradation mechanisms are brought into action, pre-expression of miRNAs may help to robustly hamper viral DNA transcription immediately after infection. Correspondingly, we showed that pre-expression significantly delayed plaque formation supposedly by suppressing rather than eliminating the viral DNA. The establishment of latency might hence be greatly facilitated in cells permissive for latent infection that pre-express miRNAs as it may occur via horizontal transfer prior to infection. Elucidating the relevance of miRNAs in repressing IE3 transcripts in terms of establishing and maintaining latent carriage or virus reactivation, remains to be determined in an MCMV-latency model *in vivo*.

Chapter 5

Supplements

5.1 Oligonucleotides

All oligonucleotides listed below were ordered from Sigma Aldrich.

Table 5.1: Sequences of single-stranded oligonucleotides used to detect viral miRNAs (or U6 snRNA in the case of probe U6) through northern blot analysis

Name	Sequence (5'-3')
probe mcmv-miR-m01-2-3p	TCGAAGGAAACCGTGTCGAACG
probe mcmv-miR-M23-2-3p	CCGCTTGACCGAGGCCCCCAT
probe U6	CACGAATTTGCGTGTCATCCTT

Table 5.2: Sequences of oligonucleotides inserted into the pLenti-Blast-eGFPintron plasmid for constitutive miRNA expression

No.	Name	Sequence (5'-3')
1	**m01-2-NheI_for**	CAGACCCGCCTAAGGCTAGCGGTACGTTGCGGATGAAGAGAATCGG GTTGGAACGGTGTTTCTTAAGTACGAGCTACCGTTCGACACGGTTT CCTTCGACTGCGCTACCCAGCTAGCGGGGCCCATGATCA
2	**m01-2-NheI_rev**	TGATCATGGGCCCCGCTAGCTGGGTAGCGCAGTCGAAGGAAACCGT GTCGAACGGTAGCTCGTACTTAAGAAACACCGTTCCAACCCGATTC TCTTCATCCGCAACGTACCGCTAGCCTTAGGCGGGTCTG
3	**m01-2-NsiI_for**	CATCCCGGTTAATTAACGGATGCATGGTACGTTGCGGATGAAGAGA ATCGGGTTGGAACGGTGTTTCTTAAGTACGAGCTACCGTTCGACAC GGTTTCCTTCGACTGCGCTACCCAATGCATGATTTAAATGTGGCCG GCC
4	**m01-2-NsiI_rev**	GGCCGGCCACATTTAAATCATGCATTGGGTAGCGCAGTCGAAGGAA ACCGTGTCGAACGGTAGCTCGTACTTAAGAAACACCGTTCCAACCC GATTCTCTTCATCCGCAACGTACCATGCATCCGTTAATTAACCGGG ATG
5	**M23-2-NheI_for**	CAGACCCGCCTAAGGCTAGCCGAGGCGCTACCCCGGCTTGAACGTG TCCCCTATCGGTGGTAGTTTACTGCGTGTGCACGATGGGGGCCTCG GTCAAGCGGGGGGATGGCCGAGCTAGCGGGGCCCATGATCA
6	**M23-2-NheI_rev**	TGATCATGGGCCCCGCTAGCTCGGCCATCCCCCCGCTTGACCGAGG CCCCCATCGTGCACACGCAGTAAACTACCACCGATAGGGGACACGT TCAAGCCGGGGTAGCGCCTCGGCTAGCCTTAGGCGGGTCTG
7	**M23-2-NsiI_for**	CATCCCGGTTAATTAACGGATGCATCGAGGCGCTACCCCGGCTTGA ACGTGTCCCCTATCGGTGGTAGTTTACTGCGTGTGCACGATGGGGG CCTCGGTCAAGCGGGGGGATGGCCGAATGCATGATTTAAATGTGGC CGGCC
8	**M23-2-NsiI_rev**	GGCCGGCCACATTTAAATCATGCATTCGGCCATCCCCCCGCTTGAC CGAGGCCCCCATCGTGCACACGCAGTAAACTACCACCGATAGGGGA CACGTTCAAGCCGGGGTAGCGCCTCGATGCATCCGTTAATTAACCG GGATG

Bibliography

[1] J. A. Fishman. Overview: Cytomegalovirus and the herpesviruses in transplantation. *American Journal of Transplantation*, 13(s3):1–8, 2013. ISSN 16006135. doi: 10.1111/ajt.12002.

[2] Nicole L. Diggins and Meaghan H. Hancock. Hcmv mirna targets reveal important cellular pathways for viral replication, latency, and reactivation. *Non-coding RNA*, 4 (4), 2018. doi: 10.3390/ncrna4040029.

[3] Derek Gatherer, Sepehr Seirafian, Charles Cunningham, Mary Holton, Derrick J. Dargan, Katarina Baluchova, Ralph D. Hector, Julie Galbraith, Pawel Herzyk, Gavin W. G. Wilkinson, and Andrew J. Davison. High-resolution human cytomegalovirus transcriptome. *Proceedings of the National Academy of Sciences of the United States of America*, 108(49):19755–19760, 2011. ISSN 0027-8424. doi: 10.1073/pnas.1115861108.

[4] Santo Landolfo, Marisa Gariglio, Giorgio Gribaudo, and David Lembo. The human cytomegalovirus. *Pharmacology & Therapeutics*, 98(3):269–297, 2003. ISSN 01637258. doi: 10.1016/s0163-7258(03)00034-2.

[5] Marko Reschke. URL `http://www.virology.net/big_virology/bvdnaherpes.html`.

[6] Olivia Oswald. *Zytomegalievirus und Humanes Herpesvirus 6 nach allogener Stammzelltransplantation*. Dissertation, Medizinischen Fakultät Charité, Berlin, 30.10.2008. URL `https://refubium.fu-berlin.de/bitstream/handle/fub188/5970/oswald_diss_neu.pdf?sequence=1&isAllowed=y`.

[7] Thomas C. Mettenleiter, Barbara G. Klupp, and Harald Granzow. Herpesvirus as-

sembly: an update. *Virus research*, 143(2):222–234, 2009. doi: 10.1016/j.virusres.2009.03.018.

[8] Qiyi Tang and Gerd G. Maul. Mouse cytomegalovirus crosses the species barrier with help from a few human cytomegalovirus proteins. *Journal of Virology*, 80(15): 7510–7521, 2006. ISSN 0022-538X. doi: 10.1128/JVI.00684-06.

[9] Francisco Puerta Martínez, Ruth S. Cruz Cosme, and Qiyi Tang. Murine cytomegalovirus major immediate-early protein 3 interacts with cellular and viral proteins in viral dna replication compartments and is important for early gene activation. *The Journal of general virology*, 91(Pt 11):2664–2676, 2010. ISSN 0022-1317. doi: 10.1099/vir.0.022301-0.

[10] Michael J. Cannon, D. Scott Schmid, and Terri B. Hyde. Review of cytomegalovirus seroprevalence and demographic characteristics associated with infection. *Reviews in medical virology*, 20(4):202–213, 2010. doi: 10.1002/rmv.655.

[11] Pierre M. Jean Beltran and Ileana M. Cristea. The life cycle and pathogenesis of human cytomegalovirus infection: lessons from proteomics. *Expert review of proteomics*, 11(6):697–711, 2014. doi: 10.1586/14789450.2014.971116.

[12] Sheetal Manicklal, Vincent C. Emery, Tiziana Lazzarotto, Suresh B. Boppana, and Ravindra K. Gupta. The "silent" global burden of congenital cytomegalovirus. *Clinical microbiology reviews*, 26(1):86–102, 2013. doi: 10.1128/CMR.00062-12.

[13] Qiyi Tang and Gerd G. Maul. Mouse cytomegalovirus immediate-early protein 1 binds with host cell repressors to relieve suppressive effects on viral transcription and replication during lytic infection. *Journal of Virology*, 77(2):1357–1367, 2003. ISSN 0022-538X. doi: 10.1128/jvi.77.2.1357-1367.2003.

[14] Maria Waldhoer, Thomas N. Kledal, Helen Farrell, and Thue W. Schwartz. Murine cytomegalovirus (cmv) m33 and human cmv us28 receptors exhibit similar constitutive signaling activities. *Journal of Virology*, 76(16):8161–8168, 2002. ISSN 0022-538X. doi: 10.1128/JVI.76.16.8161-8168.2002.

[15] M. J. Reddehase, C. O. Simon, C. K. Seckert, N. Lemmermann, and N. K. A. Grzimek. Murine model of cytomegalovirus latency and reactivation. *Current topics in microbiology and immunology*, 325:315–331, 2008. ISSN 0070-217X. doi: 10.1007/978-3-540-77349-8{\textunderscore}18.

[16] M. Reeves and J. Sinclair. Aspects of human cytomegalovirus latency and reactivation. *Current topics in microbiology and immunology*, 325:297–313, 2008. ISSN 0070-217X. doi: 10.1007/978-3-540-77349-8{\textunderscore}17.

[17] Poornima Ramanan and Raymund R. Razonable. Cytomegalovirus infections in solid organ transplantation: a review. *Infection & chemotherapy*, 45(3):260–271, 2013. ISSN 2093-2340. doi: 10.3947/ic.2013.45.3.260.

[18] Justin Bo-Kai Hsu, Chih-Min Chiu, Sheng-Da Hsu, Wei-Yun Huang, Chia-Hung Chien, Tzong-Yi Lee, and Hsien-Da Huang. mirtar: an integrated system for identifying mirna-target interactions in human. *BMC bioinformatics*, 12:300, 2011. doi: 10.1186/1471-2105-12-300.

[19] Gang Li and Jeremy P. Kamil. Viral regulation of cell tropism in human cytomegalovirus. *Journal of Virology*, 90(2):626–629, 2016. ISSN 0022-538X. doi: 10.1128/JVI.01500-15.

[20] C. Sinzger, A. Grefte, B. Plachter, A. S. Gouw, T. H. The, and G. Jahn. Fibroblasts, epithelial cells, endothelial cells and smooth muscle cells are major targets of human cytomegalovirus infection in lung and gastrointestinal tissues. *The Journal of general virology*, 76 (Pt 4):741–750, 1995. ISSN 0022-1317. doi: 10.1099/0022-1317-76-4-741.

[21] Jiyeon Jeon, Marcia Victor, Stuart P. Adler, Abigail Arwady, Gail Demmler, Karen Fowler, Johanna Goldfarb, Harry Keyserling, Mehran Massoudi, Kristin Richards, Stephanie A. S. Staras, and Michael J. Cannon. Knowledge and awareness of congenital cytomegalovirus among women. *Infectious diseases in obstetrics and gynecology*, 2006:80383, 2006. doi: 10.1155/IDOG/2006/80383.

[22] Gail J. Demmler-Harrison. Congenital cytomegalovirus: Public health action towards awareness, prevention, and treatment. *Journal of clinical virology : the official publication of the Pan American Society for Clinical Virology*, 46 Suppl 4:S1–5, 2009. doi: 10.1016/j.jcv.2009.10.007.

[23] Elizabeth C. Swanson and Mark R. Schleiss. Congenital cytomegalovirus infection: new prospects for prevention and therapy. *Pediatric clinics of North America*, 60(2): 335–349, 2013. doi: 10.1016/j.pcl.2012.12.008.

[24] G. Ligat, R. Cazal, S. Hantz, and S. Alain. The human cytomegalovirus terminase complex as an antiviral target: a close-up view. *FEMS microbiology reviews*, 42(2): 137–145, 2018. ISSN 0168-6445. doi: 10.1093/femsre/fuy004.

[25] Thomas Goldner, Guy Hewlett, Nicole Ettischer, Helga Ruebsamen-Schaeff, Holger Zimmermann, and Peter Lischka. The novel anticytomegalovirus compound aic246 (letermovir) inhibits human cytomegalovirus replication through a specific antiviral mechanism that involves the viral terminase. *Journal of Virology*, 85(20):10884–10893, 2011. ISSN 0022-538X. doi: 10.1128/JVI.05265-11.

[26] K. Ogawa-Goto, K. Tanaka, W. Gibson, E. Moriishi, Y. Miura, T. Kurata, S. Irie, and T. Sata. Microtubule network facilitates nuclear targeting of human cytomegalovirus capsid. *Journal of Virology*, 77(15):8541–8547, 2003. ISSN 0022-538X. doi: 10.1128/jvi.77.15.8541-8547.2003.

[27] E. Gönczöl, P. W. Andrews, and S. A. Plotkin. Cytomegalovirus replicates in differentiated but not in undifferentiated human embryonal carcinoma cells. *Science (New York, N.Y.)*, 224(4645):159–161, 1984. doi: 10.1126/science.6322309.

[28] C. E. Ibanez, R. Schrier, P. Ghazal, C. Wiley, and J. A. Nelson. Human cytomegalovirus productively infects primary differentiated macrophages. *Journal of Virology*, 65(12):6581–6588, 1991. ISSN 0022-538X.

[29] M. Mendelson, S. Monard, P. Sissons, and J. Sinclair. Detection of endogenous human cytomegalovirus in cd34+ bone marrow progenitors. *The Journal of general virology*, 77 (Pt 12):3099–3102, 1996. ISSN 0022-1317. doi: 10.1099/0022-1317-77-12-3099.

[30] J. Taylor-Wiedeman, J. G. Sissons, L. K. Borysiewicz, and J. H. Sinclair. Monocytes are a major site of persistence of human cytomegalovirus in peripheral blood mononuclear cells. *The Journal of general virology*, 72 (Pt 9):2059–2064, 1991. ISSN 0022-1317. doi: 10.1099/0022-1317-72-9-2059.

[31] Felicia Goodrum. Human cytomegalovirus latency: Approaching the gordian knot. *Annual review of virology*, 3(1):333–357, 2016. doi: 10.1146/annurev-virology-110615-042422.

[32] Michael W. Wathen and Mark F. Stinski. Temporal patterns of human cytomegalovirus transcription: Mapping the viral rnas synthesized at immediate early, early,

and late times after infection. *Journal of Virology*, 41(2):462–477, 1982. ISSN 0022-538X.

[33] A. Angulo, P. Ghazal, and M. Messerle. The major immediate-early gene ie3 of mouse cytomegalovirus is essential for viral growth. *Journal of Virology*, 74(23): 11129–11136, 2000. ISSN 0022-538X. doi: 10.1128/jvi.74.23.11129-11136.2000.

[34] Mark F. Stinski and Hiroki Isomura. Role of the cytomegalovirus major immediate early enhancer in acute infection and reactivation from latency. *Medical microbiology and immunology*, 197(2):223–231, 2008. ISSN 0300-8584. doi: 10.1007/s00430-007-0069-7.

[35] Sita Awasthi, Jennifer A. Isler, and James C. Alwine. Analysis of splice variants of the immediate-early 1 region of human cytomegalovirus. *Journal of Virology*, 78(15): 8191–8200, 2004. ISSN 0022-538X. doi: 10.1128/JVI.78.15.8191-8200.2004.

[36] Andreas Busche, Ana Angulo, Penelope Kay-Jackson, Peter Ghazal, and Martin Messerle. Phenotypes of major immediate-early gene mutants of mouse cytomegalovirus. *Medical microbiology and immunology*, 197(2):233–240, 2008. ISSN 0300-8584. doi: 10.1007/s00430-008-0076-3.

[37] B. Bühler, G. M. Keil, F. Weiland, and U. H. Koszinowski. Characterization of the murine cytomegalovirus early transcription unit e1 that is induced by immediate-early proteins. *Journal of Virology*, 64(5):1907–1919, 1990. ISSN 0022-538X.

[38] M. Messerle, B. Bühler, G. M. Keil, and U. H. Koszinowski. Structural organization, expression, and functional characterization of the murine cytomegalovirus immediate-early gene 3. *Journal of Virology*, 66(1):27–36, 1992. ISSN 0022-538X.

[39] Elizabeth A. White and Deborah H. Spector. Exon 3 of the human cytomegalovirus major immediate-early region is required for efficient viral gene expression and for cellular cyclin modulation. *Journal of Virology*, 79(12):7438–7452, 2005. ISSN 0022-538X. doi: 10.1128/JVI.79.12.7438-7452.2005.

[40] Christina Paulus and Michael Nevels. The human cytomegalovirus major immediate-early proteins as antagonists of intrinsic and innate antiviral host responses. *Viruses*, 1(3):760–779, 2009. doi: 10.3390/v1030760.

[41] W. Gibson. Structure and formation of the cytomegalovirus virion. *Current topics in microbiology and immunology*, 325:187–204, 2008. ISSN 0070-217X. doi: 10.1007/978-3-540-77349-8{\textunderscore}11.

[42] James C. Alwine. The human cytomegalovirus assembly compartment: a masterpiece of viral manipulation of cellular processes that facilitates assembly and egress. *PLoS pathogens*, 8(9):e1002878, 2012. doi: 10.1371/journal.ppat.1002878.

[43] Subhendu Das and Philip E. Pellett. Spatial relationships between markers for secretory and endosomal machinery in human cytomegalovirus-infected cells versus those in uninfected cells. *Journal of Virology*, 85(12):5864–5879, 2011. ISSN 0022-538X. doi: 10.1128/JVI.00155-11.

[44] David P. Bartel. Micrornas. *Cell*, 116(2):281–297, 2004. ISSN 0092-8674. doi: 10.1016/S0092-8674(04)00045-5.

[45] Andrew Grimson, Mansi Srivastava, Bryony Fahey, Ben J. Woodcroft, H. Rosaria Chiang, Nicole King, Bernard M. Degnan, Daniel S. Rokhsar, and David P. Bartel. Early origins and evolution of micrornas and piwi-interacting rnas in animals. *Nature*, 455(7217):1193–1197, 2008. ISSN 0028-0836. doi: 10.1038/nature07415.

[46] Lisa Marcinowski, Mélanie Tanguy, Astrid Krmpotic, Bernd Rädle, Vanda J. Lisnić, Lee Tuddenham, Béatrice Chane-Woon-Ming, Zsolt Ruzsics, Florian Erhard, Corinna Benkartek, Marina Babic, Ralf Zimmer, Joanne Trgovcich, Ulrich H. Koszinowski, Stipan Jonjic, Sébastien Pfeffer, and Lars Dölken. Degradation of cellular mir-27 by a novel, highly abundant viral transcript is important for efficient virus replication in vivo. *PLoS pathogens*, 8(2):e1002510, 2012. doi: 10.1371/journal.ppat.1002510.

[47] M. Lagos-Quintana, R. Rauhut, W. Lendeckel, and T. Tuschl. Identification of novel genes coding for small expressed rnas. *Science (New York, N.Y.)*, 294(5543):853–858, 2001. doi: 10.1126/science.1064921.

[48] Rosalind C. Lee, Rhonda L. Feinbaum, and Victor Ambros. The c. elegans heterochronic gene lin-4 encodes small rnas with antisense complementarity to lin-14. *Cell*, 75(5):843–854, 1993. ISSN 0092-8674. doi: 10.1016/0092-8674(93)90529-y.

[49] Ana Kozomara, Maria Birgaoanu, and Sam Griffiths-Jones. mirbase: from microrna sequences to function. *Nucleic acids research*, 47(D1):D155–D162, 2019. doi: 10.1093/nar/gky1141.

[50] Witold Filipowicz, Suvendra N. Bhattacharyya, and Nahum Sonenberg. Mechanisms of post-transcriptional regulation by microrna: are the answers in sight? *Nature reviews. Genetics*, 9(2):102–114, 2008. doi: 10.1038/nrg2290.

[51] Natascha Bushati and Stephen M. Cohen. microrna functions. *Annual review of cell and developmental biology*, 23:175–205, 2007. ISSN 1081-0706. doi: 10.1146/annurev.cellbio.23.090506.123406.

[52] Harry L. A. Janssen, Hendrik W. Reesink, Eric J. Lawitz, Stefan Zeuzem, Maribel Rodriguez-Torres, Keyur Patel, Adriaan J. van der Meer, Amy K. Patick, Alice Chen, Yi Zhou, Robert Persson, Barney D. King, Sakari Kauppinen, Arthur A. Levin, and Michael R. Hodges. Treatment of hcv infection by targeting microrna. *The New England journal of medicine*, 368(18):1685–1694, 2013. doi: 10.1056/NEJMoa1209026.

[53] Daniel W. Thomson, Cameron P. Bracken, and Gregory J. Goodall. Experimental strategies for microrna target identification. *Nucleic acids research*, 39(16):6845–6853, 2011. doi: 10.1093/nar/gkr330.

[54] Victor Ambros. The functions of animal microrna. *Nature*, 431(7006):350–355, 2004. ISSN 0028-0836. doi: 10.1038/nature02871.

[55] Wigard P. Kloosterman and Ronald H. A. Plasterk. The diverse functions of microrna in animal development and disease. *Developmental cell*, 11(4):441–450, 2006. ISSN 1534-5807. doi: 10.1016/j.devcel.2006.09.009.

[56] Shuibin Lin and Richard I. Gregory. Microrna biogenesis pathways in cancer. *Nature reviews. Cancer*, 15(6):321–333, 2015. doi: 10.1038/nrc3932.

[57] Amaia Lujambio and Scott W. Lowe. The microcosmos of cancer. *Nature*, 482(7385):347–355, 2012. ISSN 0028-0836. doi: 10.1038/nature10888.

[58] Sébastien S. Hébert, Katrien Horré, Laura Nicolaï, Bruno Bergmans, Aikaterini S. Papadopoulou, André Delacourte, and Bart de Strooper. Microrna regulation of alzheimer's amyloid precursor protein expression. *Neurobiology of disease*, 33(3):422–428, 2009. doi: 10.1016/j.nbd.2008.11.009.

[59] Mathew B. Cox, Murray J. Cairns, Kaushal S. Gandhi, Adam P. Carroll, Sophia Moscovis, Graeme J. Stewart, Simon Broadley, Rodney J. Scott, David R. Booth,

and Jeannette Lechner-Scott. Micrornas mir-17 and mir-20a inhibit t cell activation genes and are under-expressed in ms whole blood. *PloS one*, 5(8):e12132, 2010. doi: 10.1371/journal.pone.0012132.

[60] V. Narry Kim. Microrna biogenesis: coordinated cropping and dicing. *Nature reviews. Molecular cell biology*, 6(5):376–385, 2005. ISSN 1471-0072. doi: 10.1038/nrm1644.

[61] N. C. Lau, L. P. Lim, E. G. Weinstein, and D. P. Bartel. An abundant class of tiny rnas with probable regulatory roles in caenorhabditis elegans. *Science (New York, N.Y.)*, 294(5543):858–862, 2001. doi: 10.1126/science.1065062.

[62] R. C. Lee and V. Ambros. An extensive class of small rnas in caenorhabditis elegans. *Science (New York, N.Y.)*, 294(5543):862–864, 2001. doi: 10.1126/science.1065329.

[63] Yoontae Lee, Kipyoung Jeon, Jun-Tae Lee, Sunyoung Kim, and V. Narry Kim. Microrna maturation: stepwise processing and subcellular localization. *The EMBO journal*, 21(17):4663–4670, 2002. ISSN 0261-4189. doi: 10.1093/emboj/cdf476.

[64] Clarissa P. C. Gomes, Ji-Hoon Cho, Leroy Hood, Octávio L. Franco, Rinaldo W. Pereira, and Kai Wang. A review of computational tools in microrna discovery. *Frontiers in genetics*, 4:81, 2013. ISSN 1664-8021. doi: 10.3389/fgene.2013.00081.

[65] Young-Kook Kim and V. Narry Kim. Processing of intronic micrornas. *The EMBO journal*, 26(3):775–783, 2007. ISSN 0261-4189. doi: 10.1038/sj.emboj.7601512.

[66] Antony Rodriguez, Sam Griffiths-Jones, Jennifer L. Ashurst, and Allan Bradley. Identification of mammalian microrna host genes and transcription units. *Genome research*, 14(10A):1902–1910, 2004. doi: 10.1101/gr.2722704.

[67] Zissimos Mourelatos, Josée Dostie, Sergey Paushkin, Anup Sharma, Bernard Charroux, Linda Abel, Juri Rappsilber, Matthias Mann, and Gideon Dreyfuss. mirnps: a novel class of ribonucleoproteins containing numerous micrornas. *Genes & development*, 16(6):720–728, 2002. ISSN 0890-9369. doi: 10.1101/gad.974702.

[68] Yoontae Lee, Minju Kim, Jinju Han, Kyu-Hyun Yeom, Sanghyuk Lee, Sung Hee Baek, and V. Narry Kim. Microrna genes are transcribed by rna polymerase ii. *The EMBO journal*, 23(20):4051–4060, 2004. ISSN 0261-4189. doi: 10.1038/sj.emboj.7600385.

[69] Xuezhong Cai, Curt H. Hagedorn, and Bryan R. Cullen. Human micrornas are processed from capped, polyadenylated transcripts that can also function as mrnas. *RNA (New York, N.Y.)*, 10(12):1957–1966, 2004. doi: 10.1261/rna.7135204.

[70] Glen M. Borchert, William Lanier, and Beverly L. Davidson. Rna polymerase iii transcribes human micrornas. *Nature structural & molecular biology*, 13(12):1097–1101, 2006. ISSN 1545-9993. doi: 10.1038/nsmb1167.

[71] Yukihide Tomari and Phillip D. Zamore. Microrna biogenesis: drosha can't cut it without a partner. *Current Biology*, 15(2):R61–4, 2005. ISSN 09609822. doi: 10.1016/j.cub.2004.12.057.

[72] Jinju Han, Yoontae Lee, Kyu-Hyeon Yeom, Jin-Wu Nam, Inha Heo, Je-Keun Rhee, Sun Young Sohn, Yunje Cho, Byoung-Tak Zhang, and V. Narry Kim. Molecular basis for the recognition of primary micrornas by the drosha-dgcr8 complex. *Cell*, 125(5):887–901, 2006. ISSN 0092-8674. doi: 10.1016/j.cell.2006.03.043.

[73] Wenwen Fang and David P. Bartel. The menu of features that define primary micrornas and enable de novo design of microrna genes. *Molecular cell*, 60(1):131–145, 2015. ISSN 1097-2765. doi: 10.1016/j.molcel.2015.08.015.

[74] Tuan Anh Nguyen, Myung Hyun Jo, Yeon-Gil Choi, Joha Park, S. Chul Kwon, Sungchul Hohng, V. Narry Kim, and Jae-Sung Woo. Functional anatomy of the human microprocessor. *Cell*, 161(6):1374–1387, 2015. ISSN 0092-8674. doi: 10.1016/j.cell.2015.05.010.

[75] Yoontae Lee, Chiyoung Ahn, Jinju Han, Hyounjeong Choi, Jaekwang Kim, Jeongbin Yim, Junho Lee, Patrick Provost, Olof Rådmark, Sunyoung Kim, and V. Narry Kim. The nuclear rnase iii drosha initiates microrna processing. *Nature*, 425(6956):415–419, 2003. ISSN 0028-0836. doi: 10.1038/nature01957.

[76] Jinju Han, Jakob S. Pedersen, S. Chul Kwon, Cassandra D. Belair, Young-Kook Kim, Kyu-Hyeon Yeom, Woo-Young Yang, David Haussler, Robert Blelloch, and V. Narry Kim. Posttranscriptional crossregulation between drosha and dgcr8. *Cell*, 136(1):75–84, 2009. ISSN 0092-8674. doi: 10.1016/j.cell.2008.10.053.

[77] V. Narry Kim, Jinju Han, and Mikiko C. Siomi. Biogenesis of small rnas in animals. *Nature reviews. Molecular cell biology*, 10(2):126–139, 2009. ISSN 1471-0072. doi: 10.1038/nrm2632.

[78] Eugene Berezikov, Wei-Jen Chung, Jason Willis, Edwin Cuppen, and Eric C. Lai. Mammalian mirtron genes. *Molecular cell*, 28(2):328–336, 2007. ISSN 1097-2765. doi: 10.1016/j.molcel.2007.09.028.

[79] Katsutomo Okamura, Joshua W. Hagen, Hong Duan, David M. Tyler, and Eric C. Lai. The mirtron pathway generates microrna-class regulatory rnas in drosophila. *Cell*, 130(1):89–100, 2007. ISSN 0092-8674. doi: 10.1016/j.cell.2007.06.028.

[80] J. Graham Ruby, Calvin H. Jan, and David P. Bartel. Intronic microrna precursors that bypass drosha processing. *Nature*, 448(7149):83–86, 2007. ISSN 0028-0836. doi: 10.1038/nature05983.

[81] Jakub O. Westholm and Eric C. Lai. Mirtrons: microrna biogenesis via splicing. *Biochimie*, 93(11):1897–1904, 2011. doi: 10.1016/j.biochi.2011.06.017.

[82] Yan Zeng and Bryan R. Cullen. Structural requirements for pre-microrna binding and nuclear export by exportin 5. *Nucleic acids research*, 32(16):4776–4785, 2004. doi: 10.1093/nar/gkh824.

[83] Markus T. Bohnsack, Kevin Czaplinski, and Dirk Gorlich. Exportin 5 is a rangtp-dependent dsrna-binding protein that mediates nuclear export of pre-mirnas. *RNA (New York, N.Y.)*, 10(2):185–191, 2004. doi: 10.1261/rna.5167604.

[84] V. Narry Kim. Microrna precursors in motion: exportin-5 mediates their nuclear export. *Trends in cell biology*, 14(4):156–159, 2004. ISSN 0962-8924. doi: 10.1016/j.tcb.2004.02.006.

[85] Elsebet Lund, Stephan Güttinger, Angelo Calado, James E. Dahlberg, and Ulrike Kutay. Nuclear export of microrna precursors. *Science (New York, N.Y.)*, 303(5654):95–98, 2004. doi: 10.1126/science.1090599.

[86] Rui Yi, Yi Qin, Ian G. Macara, and Bryan R. Cullen. Exportin-5 mediates the nuclear export of pre-microrna and short hairpin rnas. *Genes & development*, 17(24):3011–3016, 2003. ISSN 0890-9369. doi: 10.1101/gad.1158803.

[87] Jin-Biao Ma, Keqiong Ye, and Dinshaw J. Patel. Structural basis for overhang-specific small interfering rna recognition by the paz domain. *Nature*, 429(6989):318–322, 2004. ISSN 0028-0836. doi: 10.1038/nature02519.

[88] Eva Gottwein and Bryan R. Cullen. Viral and cellular micrornas as determinants of viral pathogenesis and immunity. *Cell host & microbe*, 3(6):375–387, 2008. doi: 10.1016/j.chom.2008.05.002.

[89] György Hutvágner and Phillip D. Zamore. A microrna in a multiple-turnover rnai enzyme complex. *Science (New York, N.Y.)*, 297(5589):2056–2060, 2002. doi: 10.1126/science.1073827.

[90] Zain Paroo, Qinghua Liu, and Xiaodong Wang. Biochemical mechanisms of the rna-induced silencing complex. *Cell research*, 17(3):187–194, 2007. doi: 10.1038/sj.cr.7310148.

[91] Anastasia Khvorova, Angela Reynolds, and Sumedha D. Jayasena. Functional sirnas and mirnas exhibit strand bias. *Cell*, 115(2):209–216, 2003. ISSN 0092-8674. doi: 10.1016/s0092-8674(03)00801-8.

[92] Dianne S. Schwarz, György Hutvágner, Tingting Du, Zuoshang Xu, Neil Aronin, and Phillip D. Zamore. Asymmetry in the assembly of the rnai enzyme complex. *Cell*, 115(2):199–208, 2003. ISSN 0092-8674. doi: 10.1016/S0092-8674(03)00759-1.

[93] Katsutomo Okamura, Nicolas Robine, Ying Liu, Qinghua Liu, and Eric C. Lai. R2d2 organizes small regulatory rna pathways in drosophila. *Molecular and cellular biology*, 31(4):884–896, 2011. doi: 10.1128/MCB.01141-10.

[94] Yukihide Tomari, Christian Matranga, Benjamin Haley, Natalia Martinez, and Phillip D. Zamore. A protein sensor for sirna asymmetry. *Science (New York, N.Y.)*, 306(5700):1377–1380, 2004. doi: 10.1126/science.1102755.

[95] Ligang Wu and Joel G. Belasco. Let me count the ways: mechanisms of gene regulation by mirnas and sirnas. *Molecular cell*, 29(1):1–7, 2008. ISSN 1097-2765. doi: 10.1016/j.molcel.2007.12.010.

[96] Jonathan B. Preall and Erik J. Sontheimer. Rnai: Risc gets loaded. *Cell*, 123(4):543–545, 2005. ISSN 0092-8674. doi: 10.1016/j.cell.2005.11.006.

[97] Asuka Azuma-Mukai, Hideo Oguri, Toutai Mituyama, Zhi Rong Qian, Kiyoshi Asai, Haruhiko Siomi, and Mikiko C. Siomi. Characterization of endogenous human argonautes and their mirna partners in rna silencing. *Proceedings of the National Academy*

of Sciences of the United States of America, 105(23):7964–7969, 2008. ISSN 0027-8424. doi: 10.1073/pnas.0800334105.

[98] Gunter Meister, Markus Landthaler, Agnieszka Patkaniowska, Yair Dorsett, Grace Teng, and Thomas Tuschl. Human argonaute2 mediates rna cleavage targeted by mirnas and sirnas. *Molecular cell*, 15(2):185–197, 2004. ISSN 1097-2765. doi: 10.1016/j.molcel.2004.07.007.

[99] Minju Ha and V. Narry Kim. Regulation of microrna biogenesis. *Nature reviews. Molecular cell biology*, 15(8):509–524, 2014. ISSN 1471-0072. doi: 10.1038/nrm3838.

[100] Nicole T. Schirle and Ian J. MacRae. The crystal structure of human argonaute2. *Science (New York, N.Y.)*, 336(6084):1037–1040, 2012. doi: 10.1126/science.1221551.

[101] Stanley D. Chandradoss, Nicole T. Schirle, Malwina Szczepaniak, Ian J. MacRae, and Chirlmin Joo. A dynamic search process underlies microrna targeting. *Cell*, 162 (1):96–107, 2015. ISSN 0092-8674. doi: 10.1016/j.cell.2015.06.032.

[102] Shannon M. Klum, Stanley D. Chandradoss, Nicole T. Schirle, Chirlmin Joo, and Ian J. MacRae. Helix-7 in argonaute2 shapes the microrna seed region for rapid target recognition. *The EMBO journal*, 37(1):75–88, 2018. ISSN 0261-4189. doi: 10.15252/embj.201796474.

[103] J. Robin Lytle, Therese A. Yario, and Joan A. Steitz. Target mrnas are repressed as efficiently by microrna-binding sites in the 5' utr as in the 3' utr. *Proceedings of the National Academy of Sciences of the United States of America*, 104(23):9667–9672, 2007. ISSN 0027-8424. doi: 10.1073/pnas.0703820104.

[104] Wigard P. Kloosterman, Erno Wienholds, René F. Ketting, and Ronald H. A. Plasterk. Substrate requirements for let-7 function in the developing zebrafish embryo. *Nucleic acids research*, 32(21):6284–6291, 2004. doi: 10.1093/nar/gkh968.

[105] Michael Schnall-Levin, Olivia S. Rissland, Wendy K. Johnston, Norbert Perrimon, David P. Bartel, and Bonnie Berger. Unusually effective microrna targeting within repeat-rich coding regions of mammalian mrnas. *Genome research*, 21(9):1395–1403, 2011. doi: 10.1101/gr.121210.111.

[106] David P. Bartel. Micrornas: target recognition and regulatory functions. *Cell*, 136 (2):215–233, 2009. ISSN 0092-8674. doi: 10.1016/j.cell.2009.01.002.

[107] Andrew Grimson, Kyle Kai-How Farh, Wendy K. Johnston, Philip Garrett-Engele, Lee P. Lim, and David P. Bartel. Microrna targeting specificity in mammals: determinants beyond seed pairing. *Molecular cell*, 27(1):91–105, 2007. ISSN 1097-2765. doi: 10.1016/j.molcel.2007.06.017.

[108] Shuo Gu, Lan Jin, Feijie Zhang, Peter Sarnow, and Mark A. Kay. Biological basis for restriction of microrna targets to the 3' untranslated region in mammalian mrnas. *Nature structural & molecular biology*, 16(2):144–150, 2009. ISSN 1545-9993. doi: 10.1038/nsmb.1552.

[109] Benjamin P. Lewis, Christopher B. Burge, and David P. Bartel. Conserved seed pairing, often flanked by adenosines, indicates that thousands of human genes are microrna targets. *Cell*, 120(1):15–20, 2005. ISSN 0092-8674. doi: 10.1016/j.cell.2004.12.035.

[110] Julius Brennecke, Alexander Stark, Robert B. Russell, and Stephen M. Cohen. Principles of microrna-target recognition. *PLoS biology*, 3(3):e85, 2005. doi: 10.1371/journal.pbio.0030085.

[111] Azra Krek, Dominic Grün, Matthew N. Poy, Rachel Wolf, Lauren Rosenberg, Eric J. Epstein, Philip MacMenamin, Isabelle da Piedade, Kristin C. Gunsalus, Markus Stoffel, and Nikolaus Rajewsky. Combinatorial microrna target predictions. *Nature genetics*, 37(5):495–500, 2005. ISSN 1061-4036. doi: 10.1038/ng1536.

[112] Marianthi Kiriakidou, Peter T. Nelson, Andrei Kouranov, Petko Fitziev, Costas Bouyioukos, Zissimos Mourelatos, and Artemis Hatzigeorgiou. A combined computational-experimental approach predicts human microrna targets. *Genes & development*, 18(10):1165–1178, 2004. ISSN 0890-9369. doi: 10.1101/gad.1184704.

[113] John G. Doench and Phillip A. Sharp. Specificity of microrna target selection in translational repression. *Genes & development*, 18(5):504–511, 2004. ISSN 0890-9369. doi: 10.1101/gad.1184404.

[114] Robin C. Friedman, Kyle Kai-How Farh, Christopher B. Burge, and David P. Bartel. Most mammalian mrnas are conserved targets of microrna. *Genome research*, 19 (1):92–105, 2009. doi: 10.1101/gr.082701.108.

[115] Ray M. Marín and Jirí Vanícek. Efficient use of accessibility in microrna target prediction. *Nucleic acids research*, 39(1):19–29, 2011. doi: 10.1093/nar/gkq768.

[116] Cydney B. Nielsen, Noam Shomron, Rickard Sandberg, Eran Hornstein, Jacob Kitzman, and Christopher B. Burge. Determinants of targeting by endogenous and exogenous microrna and sirnas. *RNA (New York, N.Y.)*, 13(11):1894–1910, 2007. doi: 10.1261/rna.768207.

[117] Marc Robert Fabian, Nahum Sonenberg, and Witold Filipowicz. Regulation of mrna translation and stability by microrna. *Annual review of biochemistry*, 79:351–379, 2010. doi: 10.1146/annurev-biochem-060308-103103.

[118] David T. Humphreys, Belinda J. Westman, David I. K. Martin, and Thomas Preiss. Microrna control translation initiation by inhibiting eukaryotic initiation factor 4e/cap and poly(a) tail function. *Proceedings of the National Academy of Sciences of the United States of America*, 102(47):16961–16966, 2005. ISSN 0027-8424. doi: 10.1073/pnas.0506482102.

[119] Géraldine Mathonnet, Marc R. Fabian, Yuri V. Svitkin, Armen Parsyan, Laurent Huck, Takayuki Murata, Stefano Biffo, William C. Merrick, Edward Darzynkiewicz, Ramesh S. Pillai, Witold Filipowicz, Thomas F. Duchaine, and Nahum Sonenberg. Microrna inhibition of translation initiation in vitro by targeting the cap-binding complex eif4f. *Science (New York, N.Y.)*, 317(5845):1764–1767, 2007. doi: 10.1126/science.1146067.

[120] Ramesh S. Pillai, Suvendra N. Bhattacharyya, Caroline G. Artus, Tabea Zoller, Nicolas Cougot, Eugenia Basyuk, Edouard Bertrand, and Witold Filipowicz. Inhibition of translational initiation by let-7 microrna in human cells. *Science (New York, N.Y.)*, 309(5740):1573–1576, 2005. doi: 10.1126/science.1115079.

[121] Patricia A. Maroney, Yang Yu, Jesse Fisher, and Timothy W. Nilsen. Evidence that microrna are associated with translating messenger rnas in human cells. *Nature structural & molecular biology*, 13(12):1102–1107, 2006. ISSN 1545-9993. doi: 10.1038/nsmb1174.

[122] Stephanie Nottrott, Martin J. Simard, and Joel D. Richter. Human let-7a mirna blocks protein production on actively translating polyribosomes. *Nature structural & molecular biology*, 13(12):1108–1114, 2006. ISSN 1545-9993. doi: 10.1038/nsmb1173.

[123] Huili Guo, Nicholas T. Ingolia, Jonathan S. Weissman, and David P. Bartel. Mam-

malian micrornas predominantly act to decrease target mrna levels. *Nature*, 466 (7308):835–840, 2010. ISSN 0028-0836. doi: 10.1038/nature09267.

[124] Bing Liu, Jiuyong Li, and Murray J. Cairns. Identifying mirnas, targets and functions. *Briefings in bioinformatics*, 15(1):1–19, 2014. doi: 10.1093/bib/bbs075.

[125] Ana Eulalio, Eric Huntzinger, Tadashi Nishihara, Jan Rehwinkel, Maria Fauser, and Elisa Izaurralde. Deadenylation is a widespread effect of mirna regulation. *RNA (New York, N.Y.)*, 15(1):21–32, 2009. doi: 10.1261/rna.1399509.

[126] Antonio J. Giraldez, Yuichiro Mishima, Jason Rihel, Russell J. Grocock, Stijn van Dongen, Kunio Inoue, Anton J. Enright, and Alexander F. Schier. Zebrafish mir-430 promotes deadenylation and clearance of maternal mrnas. *Science (New York, N.Y.)*, 312(5770):75–79, 2006. doi: 10.1126/science.1122689.

[127] Ligang Wu, Jihua Fan, and Joel G. Belasco. Micrornas direct rapid deadenylation of mrna. *Proceedings of the National Academy of Sciences of the United States of America*, 103(11):4034–4039, 2006. ISSN 0027-8424. doi: 10.1073/pnas.0510928103.

[128] Chyi-Ying A. Chen and Ann-Bin Shyu. Mechanisms of deadenylation-dependent decay. *Wiley interdisciplinary reviews. RNA*, 2(2):167–183, 2011. doi: 10.1002/wrna.40.

[129] Lasse Peters and Gunter Meister. Argonaute proteins: mediators of rna silencing. *Molecular cell*, 26(5):611–623, 2007. ISSN 1097-2765. doi: 10.1016/j.molcel.2007.05.001.

[130] Fabiola V. Rivas, Niraj H. Tolia, Ji-Joon Song, Juan P. Aragon, Jidong Liu, Gregory J. Hannon, and Leemor Joshua-Tor. Purified argonaute2 and an sirna form recombinant human risc. *Nature structural & molecular biology*, 12(4):340–349, 2005. ISSN 1545-9993. doi: 10.1038/nsmb918.

[131] Niraj H. Tolia and Leemor Joshua-Tor. Slicer and the argonautes. *Nature chemical biology*, 3(1):36–43, 2007. ISSN 1552-4450. doi: 10.1038/nchembio848.

[132] Yan Zeng, Rui Yi, and Bryan R. Cullen. Micrornas and small interfering rnas can inhibit mrna expression by similar mechanisms. *Proceedings of the National Academy of Sciences of the United States of America*, 100(17):9779–9784, 2003. ISSN 0027-8424. doi: 10.1073/pnas.1630797100.

[133] Matthew W. Jones-Rhoades, David P. Bartel, and Bonnie Bartel. Micrornas and their regulatory roles in plants. *Annual review of plant biology*, 57:19–53, 2006. ISSN 1543-5008. doi: 10.1146/annurev.arplant.57.032905.105218.

[134] Yehu Moran, David Fredman, Daniela Praher, Xin Z. Li, Liang Meng Wee, Fabian Rentzsch, Phillip D. Zamore, Ulrich Technau, and Hervé Seitz. Cnidarian micrornas frequently regulate targets by cleavage. *Genome research*, 24(4):651–663, 2014. doi: 10.1101/gr.162503.113.

[135] Maggie L. Bobbin and John J. Rossi. Rna interference (rnai)-based therapeutics: Delivering on the promise? *Annual review of pharmacology and toxicology*, 56:103–122, 2016. doi: 10.1146/annurev-pharmtox-010715-103633.

[136] Irina Haecker and Rolf Renne. Hits-clip and par-clip advance viral mirna targetome analysis. *Critical reviews in eukaryotic gene expression*, 24(2):101–116, 2014. ISSN 1045-4403.

[137] Daehyun Baek, Judit Villén, Chanseok Shin, Fernando D. Camargo, Steven P. Gygi, and David P. Bartel. The impact of micrornas on protein output. *Nature*, 455(7209): 64–71, 2008. ISSN 0028-0836. doi: 10.1038/nature07242.

[138] David P. Bartel. Metazoan micrornas. *Cell*, 173(1):20–51, 2018. ISSN 0092-8674. doi: 10.1016/j.cell.2018.03.006.

[139] Anton J. Enright, Bino John, Ulrike Gaul, Thomas Tuschl, Chris Sander, and Debora S. Marks. Microrna targets in drosophila. *Genome biology*, 5(1):R1, 2003. doi: 10.1186/gb-2003-5-1-r1.

[140] Michael Kertesz, Nicola Iovino, Ulrich Unnerstall, Ulrike Gaul, and Eran Segal. The role of site accessibility in microrna target recognition. *Nature genetics*, 39(10):1278–1284, 2007. ISSN 1061-4036. doi: 10.1038/ng2135.

[141] Ángela L. Riffo-Campos, Ismael Riquelme, and Priscilla Brebi-Mieville. Tools for sequence-based mirna target prediction: What to choose? *International journal of molecular sciences*, 17(12), 2016. doi: 10.3390/ijms17121987.

[142] Weijun Liu and Xiaowei Wang. Prediction of functional microrna targets by integrative modeling of microrna binding and target expression data. *Genome biology*, 20 (1):18, 2019. doi: 10.1186/s13059-019-1629-z.

[143] John G. Doench, Christian P. Petersen, and Phillip A. Sharp. sirnas can function as mirnas. *Genes & development*, 17(4):438–442, 2003. ISSN 0890-9369. doi: 10.1101/gad.1064703.

[144] Pierre Mazière and Anton J. Enright. Prediction of microrna targets. *Drug discovery today*, 12(11-12):452–458, 2007. ISSN 1359-6446. doi: 10.1016/j.drudis.2007.04.002.

[145] Ivo L. Hofacker. Vienna rna secondary structure server. *Nucleic acids research*, 31 (13):3429–3431, 2003. doi: 10.1093/nar/gkg599.

[146] Yuka Watanabe, Masaru Tomita, and Akio Kanai. Computational methods for microrna target prediction. In *MicroRNA Methods*, volume 427 of *Methods in Enzymology*, pages 65–86. Elsevier, 2007. ISBN 9780123739179. doi: 10.1016/S0076-6879(07)27004-1.

[147] Stefan Wuchty, Walter Fontana, Ivo L. Hofacker, and Peter Schuster. Complete suboptimal folding of rna and the stability of secondary structures. *Biopolymers*, 49(2):145–165, 1999. ISSN 0006-3525. doi: 10.1002/(SICI)1097-0282(199902)49:2{\textless}145::AID-BIP4{\textgreater}3.0.CO;2-G.

[148] Benjamin P. Lewis, I-hung Shih, Matthew W. Jones-Rhoades, David P. Bartel, and Christopher B. Burge. Prediction of mammalian microrna targets. *Cell*, 115(7):787–798, 2003. ISSN 0092-8674. doi: 10.1016/S0092-8674(03)01018-3.

[149] Kevin C. Miranda, Tien Huynh, Yvonne Tay, Yen-Sin Ang, Wai-Leong Tam, Andrew M. Thomson, Bing Lim, and Isidore Rigoutsos. A pattern-based method for the identification of microrna binding sites and their corresponding heteroduplexes. *Cell*, 126(6):1203–1217, 2006. ISSN 0092-8674. doi: 10.1016/j.cell.2006.07.031.

[150] D. H. Mathews, J. Sabina, M. Zuker, and D. H. Turner. Expanded sequence dependence of thermodynamic parameters improves prediction of rna secondary structure. *Journal of molecular biology*, 288(5):911–940, 1999. ISSN 0022-2836. doi: 10.1006/jmbi.1999.2700.

[151] Ronny Lorenz, Stephan H. Bernhart, Christian Höner Zu Siederdissen, Hakim Tafer, Christoph Flamm, Peter F. Stadler, and Ivo L. Hofacker. Viennarna package 2.0. *Algorithms for molecular biology : AMB*, 6:26, 2011. doi: 10.1186/1748-7188-6-26.

[152] Hyeyoung Min and Sungroh Yoon. Got target? computational methods for microrna target prediction and their extension. *Experimental & molecular medicine*, 42(4): 233–244, 2010. doi: 10.3858/emm.2010.42.4.032.

[153] William Ritchie, Stephane Flamant, and John E. J. Rasko. Predicting microrna targets and functions: traps for the unwary. *Nature methods*, 6(6):397–398, 2009. ISSN 1548-7091. doi: 10.1038/nmeth0609-397.

[154] Donald E. Kuhn, Mickey M. Martin, David S. Feldman, Alvin V. Terry, Gerard J. Nuovo, and Terry S. Elton. Experimental validation of mirna targets. *Methods (San Diego, Calif.)*, 44(1):47–54, 2008. ISSN 1046-2023. doi: 10.1016/j.ymeth.2007.09.005.

[155] Dimitra Karagkouni, Maria D. Paraskevopoulou, Serafeim Chatzopoulos, Ioannis S. Vlachos, Spyros Tastsoglou, Ilias Kanellos, Dimitris Papadimitriou, Ioannis Kavakiotis, Sofia Maniou, Giorgos Skoufos, Thanasis Vergoulis, Theodore Dalamagas, and Artemis G. Hatzigeorgiou. Diana-tarbase v8: a decade-long collection of experimentally supported mirna-gene interactions. *Nucleic acids research*, 46(D1):D239–D245, 2018. doi: 10.1093/nar/gkx1141.

[156] Emmanuel Beillard, Siau Chi Ong, Antonis Giannakakis, Ernesto Guccione, Leah A. Vardy, and P. Mathijs Voorhoeve. mir-sens–a retroviral dual-luciferase reporter to detect microrna activity in primary cells. *RNA (New York, N.Y.)*, 18(5):1091–1100, 2012. doi: 10.1261/rna.031831.111.

[157] Yi Jin, Zujian Chen, Xiqiang Liu, and Xiaofeng Zhou. Evaluating the microrna targeting sites by luciferase reporter gene assay. *Methods in molecular biology (Clifton, N.J.)*, 936:117–127, 2013. doi: 10.1007/978-1-62703-083-0{\textunderscore}10.

[158] Sung Wook Chi, Julie B. Zang, Aldo Mele, and Robert B. Darnell. Argonaute hits-clip decodes microrna-mrna interaction maps. *Nature*, 460(7254):479–486, 2009. ISSN 0028-0836. doi: 10.1038/nature08170.

[159] George Easow, Aurelio A. Teleman, and Stephen M. Cohen. Isolation of microrna targets by mirnp immunopurification. *RNA (New York, N.Y.)*, 13(8):1198–1204, 2007. doi: 10.1261/rna.563707.

[160] David G. Hendrickson, Daniel J. Hogan, Daniel Herschlag, James E. Ferrell, and Patrick O. Brown. Systematic identification of mrnas recruited to argonaute 2 by

specific microrna s and corresponding changes in transcript abundance. *PloS one*, 3 (5):e2126, 2008. doi: 10.1371/journal.pone.0002126.

[161] Stavroula Mili and Joan A. Steitz. Evidence for reassociation of rna-binding proteins after cell lysis: implications for the interpretation of immunoprecipitation analyses. *RNA (New York, N.Y.)*, 10(11):1692–1694, 2004. doi: 10.1261/rna.7151404.

[162] Markus Hafner, Markus Landthaler, Lukas Burger, Mohsen Khorshid, Jean Hausser, Philipp Berninger, Andrea Rothballer, Manuel Ascano, Anna-Carina Jungkamp, Mathias Munschauer, Alexander Ulrich, Greg S. Wardle, Scott Dewell, Mihaela Zavolan, and Thomas Tuschl. Transcriptome-wide identification of rna-binding protein and microrna target sites by par-clip. *Cell*, 141(1):129–141, 2010. ISSN 0092-8674. doi: 10.1016/j.cell.2010.03.009.

[163] Maria D. Paraskevopoulou, Dimitra Karagkouni, Ioannis S. Vlachos, Spyros Tastsoglou, and Artemis G. Hatzigeorgiou. microclip super learning framework uncovers functional transcriptome-wide mirna interactions. *Nature communications*, 9(1):3601, 2018. doi: 10.1038/s41467-018-06046-y.

[164] Sébastien Pfeffer, Mihaela Zavolan, Friedrich A. Grässer, Minchen Chien, James J. Russo, Jingyue Ju, Bino John, Anton J. Enright, Debora Marks, Chris Sander, and Thomas Tuschl. Identification of virus-encoded microrna s. *Science (New York, N.Y.)*, 304(5671):734–736, 2004. doi: 10.1126/science.1096781.

[165] Rodney P. Kincaid and Christopher S. Sullivan. Virus-encoded microrna s: an overview and a look to the future. *PLoS pathogens*, 8(12):e1003018, 2012. doi: 10.1371/journal.ppat.1003018.

[166] Daqian Sun, Margherita Melegari, Sunandini Sridhar, Charles E. Rogler, and Liang Zhu. Multi-mirna hairpin method that improves gene knockdown efficiency and provides linked multi-gene knockdown. *BioTechniques*, 41(1):59–63, 2006. ISSN 0736-6205. doi: 10.2144/000112203.

[167] Lauren Hook, Meaghan Hancock, Igor Landais, Robert Grabski, William Britt, and Jay A. Nelson. Cytomegalovirus microrna s. *Current opinion in virology*, 7:40–46, 2014. doi: 10.1016/j.coviro.2014.03.015.

[168] Stephanie Barth, Gunter Meister, and Friedrich A. Grässer. Ebv-encoded mirnas. *Biochimica et biophysica acta*, 1809(11-12):631–640, 2011. ISSN 0006-3002. doi: 10.1016/j.bbagrm.2011.05.010.

[169] Eva Gottwein. Kaposi's sarcoma-associated herpesvirus micrornas. *Frontiers in microbiology*, 3:165, 2012. doi: 10.3389/fmicb.2012.00165.

[170] Amos Markus, Linoy Golani, Nishant Kumar Ojha, Tatiana Borodiansky-Shteinberg, Paul R. Kinchington, and Ronald S. Goldstein. Varicella-zoster virus expresses multiple small noncoding rnas. *Journal of Virology*, 91(24), 2017. ISSN 0022-538X. doi: 10.1128/JVI.01710-17.

[171] Sébastien Pfeffer, Alain Sewer, Mariana Lagos-Quintana, Robert Sheridan, Chris Sander, Friedrich A. Grässer, Linda F. van Dyk, C. Kiong Ho, Stewart Shuman, Minchen Chien, James J. Russo, Jingyue Ju, Glenn Randall, Brett D. Lindenbach, Charles M. Rice, Viviana Simon, David D. Ho, Mihaela Zavolan, and Thomas Tuschl. Identification of micrornas of the herpesvirus family. *Nature methods*, 2(4):269–276, 2005. ISSN 1548-7091. doi: 10.1038/nmeth746.

[172] Lars Dölken, Jonathan Perot, Valérie Cognat, Abdelmalek Alioua, Matthias John, Jürgen Soutschek, Zsolt Ruzsics, Ulrich Koszinowski, Olivier Voinnet, and Sébastien Pfeffer. Mouse cytomegalovirus micrornas dominate the cellular small rna profile during lytic infection and show features of posttranscriptional regulation. *Journal of Virology*, 81(24):13771–13782, 2007. ISSN 0022-538X. doi: 10.1128/JVI.01313-07.

[173] Walter Dunn, Phong Trang, Qiu Zhong, Edward Yang, Christopher van Belle, and Fenyong Liu. Human cytomegalovirus expresses novel micrornas during productive viral infection. *Cellular microbiology*, 7(11):1684–1695, 2005. ISSN 1462-5814. doi: 10.1111/j.1462-5822.2005.00598.x.

[174] Thomas J. Stark, Justin D. Arnold, Deborah H. Spector, and Gene W. Yeo. High-resolution profiling and analysis of viral and host small rnas during human cytomegalovirus infection. *Journal of Virology*, 86(1):226–235, 2012. ISSN 0022-538X. doi: 10.1128/JVI.05903-11.

[175] Lars Dölken, Sébastien Pfeffer, and Ulrich H. Koszinowski. Cytomegalovirus micrornas. *Virus genes*, 38(3):355–364, 2009. doi: 10.1007/s11262-009-0347-0.

[176] Isaac W. Boss, Karlie B. Plaisance, and Rolf Renne. Role of virus-encoded micrornas in herpesvirus biology. *Trends in microbiology*, 17(12):544–553, 2009. doi: 10.1016/j.tim.2009.09.002.

[177] Jiang Deng, Jun Xiao, Ping Ma, Bo Gao, Feng Gong, Liping Lv, Yanyu Zhang, and Jinbo Xu. Manipulation of viral micrornas as a potential antiviral strategy for the treatment of cytomegalovirus infection. *Viruses*, 9(5), 2017. doi: 10.3390/v9050118.

[178] Finn Grey, Heather Meyers, Elizabeth A. White, Deborah H. Spector, and Jay Nelson. A human cytomegalovirus-encoded microrna regulates expression of multiple viral genes involved in replication. *PLoS pathogens*, 3(11):e163, 2007. doi: 10.1371/journal.ppat.0030163.

[179] Xin Guo, Ying Qi, Yujing Huang, Zhongyang Liu, Yanping Ma, Yaozhong Shao, Shujuan Jiang, Zhengrong Sun, and Qiang Ruan. Human cytomegalovirus mir-us33-5p inhibits viral dna synthesis and viral replication by down-regulating expression of the host syntaxin3. *FEBS letters*, 589(4):440–446, 2015. doi: 10.1016/j.febslet.2014.12.030.

[180] Yujing Huang, Ying Qi, Yanping Ma, Rong He, Yaohua Ji, Zhengrong Sun, and Qiang Ruan. Down-regulation of human cytomegalovirus ul138, a novel latency-associated determinant, by hcmv-mir-ul36. *Journal of biosciences*, 38(3):479–485, 2013. doi: 10.1007/s12038-013-9353-4.

[181] Shujuan Jiang, Ying Qi, Rong He, Yujing Huang, Zhongyang Liu, Yanping Ma, Xin Guo, Yaozhong Shao, Zhengrong Sun, and Qiang Ruan. Human cytomegalovirus microrna mir-us25-1-5p inhibits viral replication by targeting multiple cellular genes during infection. *Gene*, 570(1):108–114, 2015. doi: 10.1016/j.gene.2015.06.009.

[182] Jon Pavelin, Natalie Reynolds, Stephen Chiweshe, Guanming Wu, Rebecca Tiribassi, and Finn Grey. Systematic microrna analysis identifies atp6v0c as an essential host factor for human cytomegalovirus replication. *PLoS pathogens*, 9(12):e1003820, 2013. doi: 10.1371/journal.ppat.1003820.

[183] Noam Stern-Ginossar, Niveen Saleh, Miri D. Goldberg, Mark Prichard, Dana G. Wolf, and Ofer Mandelboim. Analysis of human cytomegalovirus-encoded microrna activity during infection. *Journal of Virology*, 83(20):10684–10693, 2009. ISSN 0022-538X. doi: 10.1128/JVI.01292-09.

[184] Sungchul Kim, Sanghyun Lee, Jinwook Shin, Youngkyun Kim, Irini Evnouchidou, Donghyun Kim, Young-Kook Kim, Young-Eui Kim, Jin-Hyun Ahn, Stanley R. Riddell, Efstratios Stratikos, V. Narry Kim, and Kwangseog Ahn. Human cytomegalovirus microrna mir-us4-1 inhibits cd8(+) t cell responses by targeting the aminopeptidase erap1. *Nature immunology*, 12(10):984–991, 2011. doi: 10.1038/ni.2097.

[185] Youngkyun Kim, Sanghyun Lee, Sungchul Kim, Donghyun Kim, Jin-Hyun Ahn, and Kwangseog Ahn. Human cytomegalovirus clinical strain-specific microrna mir-ul148d targets the human chemokine rantes during infection. *PLoS pathogens*, 8(3): e1002577, 2012. doi: 10.1371/journal.ppat.1002577.

[186] Daphna Nachmani, Dikla Lankry, Dana G. Wolf, and Ofer Mandelboim. The human cytomegalovirus microrna mir-ul112 acts synergistically with a cellular microrna to escape immune elimination. *Nature immunology*, 11(9):806–813, 2010. doi: 10.1038/ni.1916.

[187] Adam Grundhoff and Christopher S. Sullivan. Virus-encoded micrornas. *Virology*, 411(2):325–343, 2011. ISSN 0042-6822. doi: 10.1016/j.virol.2011.01.002.

[188] Shankar Mukherji, Margaret S. Ebert, Grace X. Y. Zheng, John S. Tsang, Phillip A. Sharp, and Alexander van Oudenaarden. Micrornas can generate thresholds in target gene expression. *Nature genetics*, 43(9):854–859, 2011. ISSN 1061-4036. doi: 10.1038/ng.905.

[189] Rebecca L. Skalsky and Bryan R. Cullen. Viruses, micrornas, and host interactions. *Annual review of microbiology*, 64:123–141, 2010. doi: 10.1146/annurev.micro.112408.134243.

[190] Diogo Piedade and José Miguel Azevedo-Pereira. The role of micrornas in the pathogenesis of herpesvirus infection. *Viruses*, 8(6), 2016. doi: 10.3390/v8060156.

[191] Isaac W. Boss and Rolf Renne. Viral mirnas and immune evasion. *Biochimica et biophysica acta*, 1809(11-12):708–714, 2011. ISSN 0006-3002. doi: 10.1016/j.bbagrm.2011.06.012.

[192] Bryan R. Cullen. Herpesvirus micrornas: phenotypes and functions. *Current opinion in virology*, 1(3):211–215, 2011. doi: 10.1016/j.coviro.2011.04.003.

[193] Mesfin K. Meshesha, Zvi Bentwich, Semaria A. Solomon, and Yonat Shemer Avni. In vivo expression of human cytomegalovirus (hcmv) micrornas during latency. *Gene*, 575(1):101–107, 2016. doi: 10.1016/j.gene.2015.08.040.

[194] Eain Murphy, Jirí Vanícek, Harlan Robins, Thomas Shenk, and Arnold J. Levine. Suppression of immediate-early viral gene expression by herpesvirus-coded micrornas: implications for latency. *Proceedings of the National Academy of Sciences of the United States of America*, 105(14):5453–5458, 2008. ISSN 0027-8424. doi: 10.1073/pnas.0711910105.

[195] Priya Bellare and Don Ganem. Regulation of kshv lytic switch protein expression by a virus-encoded microrna: an evolutionary adaptation that fine-tunes lytic reactivation. *Cell host & microbe*, 6(6):570–575, 2009. doi: 10.1016/j.chom.2009.11.008.

[196] Fang Lu, William Stedman, Malik Yousef, Rolf Renne, and Paul M. Lieberman. Epigenetic regulation of kaposi's sarcoma-associated herpesvirus latency by virus-encoded micrornas that target rta and the cellular rbl2-dnmt pathway. *Journal of Virology*, 84(6):2697–2706, 2010. ISSN 0022-538X. doi: 10.1128/JVI.01997-09.

[197] Jennifer Lin Umbach, Martha F. Kramer, Igor Jurak, Heather W. Karnowski, Donald M. Coen, and Bryan R. Cullen. Micrornas expressed by herpes simplex virus 1 during latent infection regulate viral mrnas. *Nature*, 454(7205):780–783, 2008. ISSN 0028-0836. doi: 10.1038/nature07103.

[198] Stefanie Herb, Jelena Zeleznjak, Thomas Hennig, Anne L'Hernault, Manivel Lodha, Christopher Jürges, Tihana Trsan, Vanda Juranic Lisnic, Stipan Jonjic, Florian Erhard, Astrid Krmpotic, and Lars Dölken. Two murine cytomegalovirus micrornas target the major viral immediate early 3 gene. *The Journal of general virology*, 103 (11), 2022. ISSN 0022-1317. doi: 10.1099/jgv.0.001804.

[199] Matthias J. Reddehase and Niels A. W. Lemmermann. Mouse model of cytomegalovirus disease and immunotherapy in the immunocompromised host: Predictions for medical translation that survived the "test of time". *Viruses*, 10(12), 2018. doi: 10.3390/v10120693.

[200] Colin Powers and Klaus Früh. Rhesus cmv: an emerging animal model for human cmv. *Medical microbiology and immunology*, 197(2):109–115, 2008. ISSN 0300-8584. doi: 10.1007/s00430-007-0073-y.

[201] Meaghan H. Hancock, Rebecca S. Tirabassi, and Jay A. Nelson. Rhesus cytomegalovirus encodes seventeen micrornas that are differentially expressed in vitro and in vivo. *Virology*, 425(2):133–142, 2012. ISSN 0042-6822. doi: 10.1016/j.virol.2012.01.009.

[202] Astrid Krmpotic, Ivan Bubic, Bojan Polic, Pero Lucin, and Stipan Jonjic. Pathogenesis of murine cytomegalovirus infection. *Microbes and infection*, 5(13):1263–1277, 2003. ISSN 1286-4579. doi: 10.1016/j.micinf.2003.09.007.

[203] Geoffrey R. Shellam, Redwood, Smith, Lee M., and Shelley Gorman. Murine cytomegalovirus and other herpesviruses. In *The Mouse in Biomedical Research*, volume II, pages 1–48. Elsevier, 2007. ISBN 978-0-12-369454-6. doi: 10.1016/B978-012369454-6/50029-7.

[204] Marielle Maurice, Els Verhoeyen, Patrick Salmon, Didier Trono, Stephen J. Russell, and François-Loïc Cosset. Efficient gene transfer into human primary blood lymphocytes by surface-engineered lentiviral vectors that display a t cell-activating polypeptide. *Blood*, 99(7):2342–2350, 2002. ISSN 0006-4971. doi: 10.1182/blood.v99.7.2342.

[205] Marjolein J. G. Hooykaas, Michiel van Gent, Jasper A. Soppe, Elisabeth Kruse, Ingrid G. J. Boer, Dik van Leenen, Marian J. A. Groot Koerkamp, Frank C. P. Holstege, Maaike E. Ressing, Emmanuel J. H. J. Wiertz, and Robert Jan Lebbink. Ebv microrna bart16 suppresses type i ifn signaling. *Journal of immunology (Baltimore, Md. : 1950)*, 198(10):4062–4073, 2017. doi: 10.4049/jimmunol.1501605.

[206] Danae Campos-Melo, Cristian Droppelmann, Kathryn Volkening, and Michael Strong. Comprehensive luciferase-based reporter gene assay reveals previously masked up-regulatory effects of mirnas. *International journal of molecular sciences*, 15(9):15592–15602, 2014. doi: 10.3390/ijms150915592.

[207] R. H. Don, P. T. Cox, B. J. Wainwright, K. Baker, and J. S. Mattick. 'touchdown' pcr to circumvent spurious priming during gene amplification. *Nucleic acids research*, 19(14):4008, 1991.

[208] Block-it™ fluorescent oligo as rnai transfection control: Protocol: Handling the block-it™ fluorescent oligo. URL `https://www.thermofisher.com/de/en/home/refere`

nces/protocols/rnai-epigenetics-and-gene-regulation/rnai-protocol/use-of-block-it-fluorescent-oligo-as-rna-transfection-control.html.

[209] Ketaki Pradhan and Mugdha Gadgil. Effect of addition of 'carrier' dna during transient protein expression in suspension cho culture. *Cytotechnology*, 64(6):613–622, 2012. ISSN 0920-9069. doi: 10.1007/s10616-012-9435-4.

[210] Xin Lai, Ulf Schmitz, Shailendra K. Gupta, Animesh Bhattacharya, Manfred Kunz, Olaf Wolkenhauer, and Julio Vera. Computational analysis of target hub gene repression regulated by multiple and cooperative mirnas. *Nucleic acids research*, 40 (18):8818–8834, 2012. doi: 10.1093/nar/gks657.

[211] Pål Saetrom, Bret S. E. Heale, Ola Snøve, Lars Aagaard, Jessica Alluin, and John J. Rossi. Distance constraints between microrna target sites dictate efficacy and cooperativity. *Nucleic acids research*, 35(7):2333–2342, 2007. doi: 10.1093/nar/gkm133.

[212] Dominic Didiano and Oliver Hobert. Perfect seed pairing is not a generally reliable predictor for mirna-target interactions. *Nature structural & molecular biology*, 13(9): 849–851, 2006. ISSN 1545-9993. doi: 10.1038/nsmb1138.

[213] Patrick Sieber, Frank Wellmer, Jacqueline Gheyselinck, José Luis Riechmann, and Elliot M. Meyerowitz. Redundancy and specialization among plant microrna: role of the mir164 family in developmental robustness. *Development (Cambridge, England)*, 134(6):1051–1060, 2007. ISSN 0950-1991. doi: 10.1242/dev.02817.

[214] Simon Fischer, René Handrick, Armaz Aschrafi, and Kerstin Otte. Unveiling the principle of microrna-mediated redundancy in cellular pathway regulation. *RNA biology*, 12(3):238–247, 2015. doi: 10.1080/15476286.2015.1017238.

[215] Elena Herrera-Carrillo, Ying Poi Liu, and Ben Berkhout. Improving mirna delivery by optimizing mirna expression cassettes in diverse virus vectors. *Human gene therapy methods*, 28(4):177–190, 2017. doi: 10.1089/hgtb.2017.036.

[216] Susanne M. Bailer and Diana Lieber. *Virus-Host Interactions*, volume 1064. Humana Press, Totowa, NJ, 2013. ISBN 978-1-62703-600-9. doi: 10.1007/978-1-62703-601-6.

[217] Tao Wang, Leon M. Larcher, Lixia Ma, and Rakesh N. Veedu. Systematic screening of commonly used commercial transfection reagents towards efficient transfection of

single-stranded oligonucleotides. *Molecules (Basel, Switzerland)*, 23(10), 2018. doi: 10.3390/molecules23102564.

[218] Catherine Shaffer. In dna transfection, efficiency and cytotoxicity are two sides of the same coin, 2011. URL `https://www.biocompare.com/Editorial-Articles/41821-In-DNA-Transfection-Efficiency-and-Cytotoxicity-Are-Two-Sides-of-the-Same-Coin/`.

[219] Christoffer Tamm, Sandeep Kadekar, Sara Pijuan-Galitó, and Cecilia Annerén. Fast and efficient transfection of mouse embryonic stem cells using non-viral reagents. *Stem cell reviews and reports*, 12(5):584–591, 2016. doi: 10.1007/s12015-016-9673-5.

[220] Hsiao-yin Yang, Lucienne A. Vonk, Ruud Licht, Antonetta M. G. van Boxtel, Joris E. J. Bekkers, Angela H. M. Kragten, San Hein, Oommen P. Varghese, Kenneth A. Howard, F. Cumhur Öner, Wouter J. A. Dhert, and Laura B. Creemers. Cell type and transfection reagent-dependent effects on viability, cell content, cell cycle and inflammation of rnai in human primary mesenchymal cells. *European journal of pharmaceutical sciences : official journal of the European Federation for Pharmaceutical Sciences*, 53:35–44, 2014. doi: 10.1016/j.ejps.2013.12.006.

[221] Xing Li, Shihai Liu, Dongyang Wang, Hao Chen, and Haibin Xia. Adenoviral delivered egfp-intron splicing system for multiple gene rnai. *Biotechnology letters*, 33 (9):1723–1728, 2011. doi: 10.1007/s10529-011-0633-5.

[222] Frank Stegmeier, Guang Hu, Richard J. Rickles, Gregory J. Hannon, and Stephen J. Elledge. A lentiviral microrna-based system for single-copy polymerase ii-regulated rna interference in mammalian cells. *Proceedings of the National Academy of Sciences of the United States of America*, 102(37):13212–13217, 2005. ISSN 0027-8424. doi: 10.1073/pnas.0506306102.

[223] Tao Hu, Ping Chen, Qiong Fu, Ye Liu, Musarat Ishaq, Junwei Li, Li Ma, and Deyin Guo. Comparative studies of various artificial microrna expression vectors for rnai in mammalian cells. *Molecular biotechnology*, 46(1):34–40, 2010. doi: 10.1007/s12033-010-9264-7.

[224] Yan Zeng and Bryan R. Cullen. Efficient processing of primary microrna hairpins by drosha requires flanking nonstructured rna sequences. *The Journal of biological*

chemistry, 280(30):27595–27603, 2005. ISSN 0021-9258. doi: 10.1074/jbc.M504714200.

[225] Hongxia Zhou, Xu Gang Xia, and Zuoshang Xu. An rna polymerase ii construct synthesizes short-hairpin rna with a quantitative indicator and mediates highly efficient rnai. *Nucleic acids research*, 33(6):e62, 2005. doi: 10.1093/nar/gni061.

[226] Chang-Zheng Chen, Ling Li, Harvey F. Lodish, and David P. Bartel. Microrna modulate hematopoietic lineage differentiation. *Science (New York, N.Y.)*, 303(5654): 83–86, 2004. doi: 10.1126/science.1091903.

[227] Tao Hu, Qiong Fu, Ping Chen, Li Ma, Onsam Sin, and Deyin Guo. Construction of an artificial microrna expression vector for simultaneous inhibition of multiple genes in mammalian cells. *International journal of molecular sciences*, 10(5):2158–2168, 2009. doi: 10.3390/ijms10052158.

[228] Aaron R. Cooper, Georgia R. Lill, Eric H. Gschweng, and Donald B. Kohn. Rescue of splicing-mediated intron loss maximizes expression in lentiviral vectors containing the human ubiquitin c promoter. *Nucleic acids research*, 43(1):682–690, 2015. doi: 10.1093/nar/gku1312.

[229] Takuya Mishima, Elena Sadovsky, Margaret E. Gegick, and Yoel Sadovsky. Determinants of effective lentivirus-driven microrna expression in vivo. *Scientific Reports*, 6 (1):844, 2016. doi: 10.1038/srep33345.

[230] G. M. Gillespie, M. R. Wills, V. Appay, C. O'Callaghan, M. Murphy, N. Smith, P. Sissons, S. Rowland-Jones, J. I. Bell, and P. A. Moss. Functional heterogeneity and high frequencies of cytomegalovirus-specific cd8(+) t lymphocytes in healthy seropositive donors. *Journal of Virology*, 74(17):8140–8150, 2000. ISSN 0022-538X. doi: 10.1128/jvi.74.17.8140-8150.2000.

[231] Benjamin Rauwel, Suk Min Jang, Marco Cassano, Adamandia Kapopoulou, Isabelle Barde, and Didier Trono. Release of human cytomegalovirus from latency by a kap1/trim28 phosphorylation switch. *eLife*, 4, 2015. doi: 10.7554/eLife.06068.

[232] Betty Lau, Emma Poole, Ellen van Damme, Lieve Bunkens, Madeleine Sowash, Harry King, Eain Murphy, Mark Wills, Marnix van Loock, and John Sinclair. Human

cytomegalovirus mir-ul112-1 promotes the down-regulation of viral immediate early-gene expression during latency to prevent t-cell recognition of latently infected cells. *The Journal of general virology*, 97(9):2387–2398, 2016. ISSN 0022-1317. doi: 10.1099/jgv.0.000546.

[233] C. Sweet. The pathogenicity of cytomegalovirus. *FEMS microbiology reviews*, 23(4):457–482, 1999. ISSN 0168-6445. doi: 10.1111/j.1574-6976.1999.tb00408.x.

[234] J. Xiao, T. Tong, X. Zhan, E. Haghjoo, and F. Liu. In vitro and in vivo characterization of a murine cytomegalovirus with a transposon insertional mutation at open reading frame m43. *Journal of Virology*, 74(20):9488–9497, 2000. ISSN 0022-538X. doi: 10.1128/jvi.74.20.9488-9497.2000.

[235] Mattias Belting and Anders Wittrup. Nanotubes, exosomes, and nucleic acid-binding peptides provide novel mechanisms of intercellular communication in eukaryotic cells: implications in health and disease. *The Journal of cell biology*, 183(7):1187–1191, 2008. doi: 10.1083/jcb.200810038.

[236] Maria Mittelbrunn and Francisco Sánchez-Madrid. Intercellular communication: diverse structures for exchange of genetic information. *Nature reviews. Molecular cell biology*, 13(5):328–335, 2012. ISSN 1471-0072. doi: 10.1038/nrm3335.

[237] D. Michiel Pegtel, Katherine Cosmopoulos, David A. Thorley-Lawson, Monique A. J. van Eijndhoven, Erik S. Hopmans, Jelle L. Lindenberg, Tanja D. de Gruijl, Thomas Würdinger, and Jaap M. Middeldorp. Functional delivery of viral mirnas via exosomes. *Proceedings of the National Academy of Sciences of the United States of America*, 107(14):6328–6333, 2010. ISSN 0027-8424. doi: 10.1073/pnas.0914843107.

[238] Isaku Kohama, Nobuyoshi Kosaka, Hirotaka Chikuda, and Takahiro Ochiya. An insight into the roles of micrornas and exosomes in sarcoma. *Cancers*, 11(3), 2019. ISSN 2072-6694. doi: 10.3390/cancers11030428.

[239] Hadi Valadi, Karin Ekström, Apostolos Bossios, Margareta Sjöstrand, James J. Lee, and Jan O. Lötvall. Exosome-mediated transfer of mrnas and micrornas is a novel mechanism of genetic exchange between cells. *Nature cell biology*, 9(6):654–659, 2007. ISSN 1465-7392. doi: 10.1038/ncb1596.

[240] Shiho Hoshina, Tsuyoshi Sekizuka, Michiyo Kataoka, Hideki Hasegawa, Hiromichi Hamada, Makoto Kuroda, and Harutaka Katano. Profile of exosomal and intracellular microrna in gamma-herpesvirus-infected lymphoma cell lines. *PloS one*, 11(9): e0162574, 2016. doi: 10.1371/journal.pone.0162574.

Danksagung

An dieser Stelle möchte ich mich bei allen lieben Menschen bedanken, die mich auf meinem Weg, der mich zum Gelingen dieser Arbeit geführt hat, begleitetet haben.
Allen Voran gilt mein Dank Prof. Dr. med. Lars Dölken, meinem Doktorvater, zum einen für die Vergabe des Themas, zum anderen für die spitzen Betreuung, die mir erst die reibungsfreie Ausarbeitung möglich machte. Ein weiteres riesengroßes Dankeschön möchte ich Dr. Thomas Hennig aussprechen. Einen besseren Betreuer im Labor kann man sich nicht vorstellen! Prof. Dr. Florian Erhard danke ich für die spannenden Einblicke in die Bioinformatik, die ich während meiner Zeit am virologischen Institut erhalten durfte. Eine großes Dankeschön gilt auch meinen weiteren Betreuern, Frau Prof. Dr. med. Üceyler und Herrn Dr. med. Beyersdorf. Vielen lieben Dank Manivel Lodha und Adam Whisnant für Eure Unterstützung im Labor.
Zu guter Letzt möchte ich meiner Familie und meinen Freunden danken.
Chris an erster Stelle: Danke, mein Schatz, dass du immer für mich da bist, mir zur Seite stehst und an mich glaubst! Es ist mein aller-aller-größtes Glück dich zu haben.
Danke allerliebste Mama, allerliebster Papa, liebste Omas, liebster Domi, Fabi und Joni. So viel Liebe und Kraft, wie ihr mir gebt, ist unbeschreiblich. Nie hätte ich es ohne euch so weit geschafft!